AN ELECTRON PROBE FOR LOCAL ANALYSIS

BY MEANS OF X-RAYS

Thesis by

David B. Wittry

In Partial Fulfillment of the Requirements

For the Degree of

Doctor of Philosophy

California Institute of Technology

Pasadena, California

1957

Acknowledgments

It is a pleasure to acknowledge the advice and suggestions of Dr. Jesse W. M. DuMond who encouraged me to undertake this work and of Dr. Pol Duwez whose efforts in securing facilities and continued financial support of the project made its completion possible.

I would also like to acknowledge the assistance of the students and employees of Caltech who worked on this project. Valuable contributions to the design and construction of the instrument were made by the following students: William Dibble, William Steyert, Ronald Fuchs, Robert Phelan, David Ackley, Tom Noonan, Charles Mosher, Richard Van de Houten, and Joel Lifter. The precision of the specimen stage is due to the skill of Mr. Ernst Keil, machinist. The work on field emission was aided by investigations on the fabrication of emitters by Mr. Han Ying Ku.

Acknowledgments are also due the Physics Shop and the Mechanical Engineering Shop for the use of their facilities and the Astrophysics Shop for the excellent machine work which was done by Mr. Frank Tennant.

This work was supported initially by Watertown Arsenal and is now under the sponsorship of the Office of Ordnance Research.

TABLE OF CONTENTS

	page
I. Electron Beam Devices for the Study of Matter	1
II. Microanalysis by Means of Electron Probes	
A. The physical basis of Castaing's method	12
B. Verification and extension of the method	17
C. Corrections for accurate quantitative analysis and limitations on the accuracy of the method	29
1. Intrinsic corrections	
a. Self-absorption of the x-rays	30
b. Fluorescence excitation	38
c. Effect of fluorescence excitation in the analysis of small regions	63
2. Instrumental corrections	
a. Contamination deposits	68
b. Detector dead time	74
c. Drift of the beam current	79
III. Design and Construction of an Electron Probe for Local X-Ray Analysis	
A. Thermionic vs. field emission sources	88
1. Temperature effects in the target	91
2. Effect of using a pulsed electron source on the detection of the x-rays	95
3. Stability	96
4. Cathode life	98
5. Alignment requirements	98
6. Currents possible in the focal spot	99
B. Realization of an Electron Probe Microanalyzer using thermionic emission	106
1. The electron probe system	109
2. The vacuum system	128
3. The sample traverse mechanism and viewing system	133
4. The spectrometer and associated equipment	142
IV. A Preliminary Application of the Electron Probe Microanalyzer	153
Appendix	
A. An experimental field emission cathode assembly	166
B. Heating of the specimen for a pulsed electron source	177
References	184

I. Electron Beam Devices for the Study of Matter

When a beam of charged particles impinges on matter, the various scattering, absorption, and excitation processes which take place can be used to obtain information about the matter which is bombarded. Proton or electron beams are used in a large variety of scientific instruments for the study of local properties, such as crystal structure, density, work function, and composition of matter. It is useful to review the existing types of such instruments as an introduction to this thesis in which the construction and method of application of one such beam device is described.

The source of information in the instruments which will be considered may be the spatial distribution of the scattered particles, the spatial distribution of the unscattered particles, the energy loss of the transmitted particles, or the energies of electrons and photons emitted as a result of absorption of energy from the particles of the incident beam. The kind of matter to be studied, the information desired, and the ease of interpretation of the results are the primary factors in determining which of these sources of information is to be preferred as a physical basis for an analysis.

The *electron microscope*, for example, has found numerous applications in the study of biological materials, such as bacteria, viruses, colloidal particles, and large molecules, but the opacity of many materials is too great to permit direct observation. In those cases in which the material is transparent to electrons, contrast in

the image depends chiefly on the differential scattering in the specimen. Specimens which are sufficiently thick for absorption to be important are usually avoided because of the chromatic aberration which is present in the electron lenses of electron microscopes. Since the electron scattering depends chiefly on density and object thickness, the interpretation of the results is simple except for undesirable effects such as diffraction, distortion of the specimen due to desiccation or heating, or distortion of the image due to aberrations present in the electron lenses. Limited study of opaque materials is possible in conventional transmission electron microscopes but only at the expense of an easy interpretation. In this case, a replica of the surface is made of collodion or carbon which reveals the profile of the surface when observed in the electron microscope. However, the correlation of this profile with the structure of the specimen requires knowledge or assumptions about the phases present and their properties with respect to preferential etching or polishing. Special electron microscopes have only recently been devised which enable the study of opaque materials by electron reflection (1).

Of the many forms of the electron microscope in existence, the RCA, Siemens, Von Ardenne, Metropolitan Vickers, General Electric, and Phillips are the most well known. All of these employ some form of triode electron gun, a condensing lens, movable sample holder, objective lens, projector lens, and either a fluorescent screen or photographic plate for detecting the image.

Electron diffraction instruments have found application in determining the size, shape, and structure of small particles and have also been used to study thin metallic films. The study of molecular structures is difficult because the phase of the diffracted electrons cannot be determined exactly.

The experimental arrangement for electron diffraction is quite simple and most electron microscopes can be readily modified for this purpose. Usually, the condenser and objective lens are used to form a demagnified image of the electron source which then serves a point source of electrons. The sample is arranged at a convenient distance from this source and the diffraction pattern recorded with the same screen or plate as is used to view the electron microscope image. Often, special lenses are provided to form the electron source in such a way that the normal specimen holder can be used. Additional lenses may be provided to focus the diffraction pattern at the screen.

The electron shadow microscope is analogous to the ordinary electron microscope in that the contrast in the image is the result of scattering, diffraction, or partial absorption of the incident beam of electrons. In this case, however, the specimen is not followed by electron lenses but casts a shadow picture in which the magnification is obtained by conical projection. A point source of electrons is used, but unlike electron diffraction units, this is in close proximity to the specimen to achieve maximum magnification in the projected shadow.

The simplest form of electron shadow microscope is the field emission microscope. In this device, the point source of electrons is a tungsten wire which has been sharpened by electrolytically etching in sodium or potassium hydroxide solution. The tip of a wire etched in this way can be a fraction of a micron in radius, and, consequently, if the wire is maintained at a negative potential of several kilovolts relative to an anode at a distance of a few centimeters, the field at the tip is of the order of 10^8 volts/cm. and results in drawing conduction electrons through the potential barrier at the surface of the metal. Also because of the high field at the emitter tip, the electrons so emitted attain about 90% of their ultimate kinetic energy within a distance of a few radii from the emitter and thereafter move in nearly straight lines if the anode is a portion of a sphere. A hemispherical fluorescent screen, partially metallized, is often used as an anode.

The small size of the electron source results in magnifications of up to a million if the object is located near the tip or adsorbed on its surface. Theoretically it should be possible to see individual molecules at this magnification, and some workers in this field believe that they have observed them (2). However, the combined effects of (a) irregularities in the emitter itself, (b) distortions of the electrostatic field by the object being measured, and (c) absorption or emission from the object itself render interpretation difficult. For this reason, and also because of instability and changes in the work function of the emitter due to contamination, the field emission

microscope has been more useful in studying the properties of the metals used as emitters than as a tool for studying other matter.

Proton shadow microscopes have also been devised. One form of this, called a field ion emission microscope, utilizes the same geometry as the electron field emission microscope but the polarity is reversed and a small quantity of hydrogen is admitted. The hydrogen becomes ionized by collision with the emitter tip or by auto-ionization due to the high field near the tip and the resulting protons behave in a manner similar to electrons, but result in an image of greater resolution because of the greater mass of the particles.

In the field emission microscope used as an electron shadow microscope the difficulties of contamination of the emitters can be avoided by using as an electron source an image of the source formed by focusing the electrons through an electron optical system. Such a system is called an electron probe. In most electron probes, however, due to practical limitations of field emission sources a thermionic electron source is used instead. In this case, the electron lenses are used to form a demagnified image of the virtual source which is a crossover point located in the vicinity of the cathode. A stationary electron probe can be used as an electron shadow microscope, but its utility is quite limited and consequently there has been little interest in electron probes with this application. The electron probe, however, constitutes the principal component of many other electron beam devices such as the various scanning microscopes, the x-ray shadow microscope, and the microanalyzer of Castaing.

The scanning microscope utilizes an electron microprobe in which the electron focal spot is caused to scan a surface, and the resulting interaction of the electron beam with the matter constituting the target results in a signal which may be used to modulate the intensity of the spot of a cathode ray tube which is caused to scan with the same frequency but larger amplitude. The signal which is obtained from the target may be in the form of secondary electrons, reflected electrons, transmitted electrons from the primary beam, or x-rays produced in the target.

Zworykin has devised a scanning microscope in which the signal consists of the secondary electrons from the target (3). Interpretation of the image in this case is difficult because the electrons ejected may include primary electrons scattered at large angles in addition to true secondary electrons. The low energy secondaries, moreover, are sensitive to the condition of the surface of the specimen. In this device, the probe is formed by a triode gun followed by two electrostatic unipotential lenses and the electrons are detected by a scintillation counter after passing back through the second lens.

McMullen and Oatley have constructed an improved secondary emission scanning microscope in which the signal consists of "reflected" electrons (4). The energy of the primary beam is much greater than that of Zworykin's microscope and, as a result, the effect of surface condition of the specimen is reduced. Furthermore, the angle of incidence of the primary beam is selected so that the effect of variations with the composition of the target is minimized. As a result, the image is more or less directly related to the surface

profile of the specimen, thus simplifying the interpretation. The electron probe is formed by a triode gun and two electrostatic reducing lenses, and the detection is accomplished by an electron multiplier.

Von Ardenne's scanning electron microscope uses the transmitted electrons as a signal (5). In this case, the recording is done photographically on a revolving drum; the movement of the drum accomplishes the magnification. While this instrument is restricted to the use of transparent samples, it overcomes the disadvantage of the conventional electron microscope in the study of relatively thick samples where aberration results from the energy losses of the electrons and the chromatic aberration of the electron lenses. Von Ardenne's probe is formed by an electron gun and two magnetic lenses.

In the scanning microscopes which are being constructed at Cambridge by Peter Duncumb (6) and at Imperial Chemical Industries, Ltd. by Martin Bloom (7), the signal is the x-rays produced in the specimen itself. Interpretation of the results is very straightforward and can be made quantitative by the use of proportional counters or an x-ray spectrometer. Thus, one has in effect a combination of a scanning microscope and a microanalyzer of the type devised by Castaing (see p. 11).

Mention should be made of the x-ray shadow microscope which can make use of either a stationary electron probe or a scanning electron probe although this device does not give information directly

from the interaction of the probe with matter, and hence does not constitute a beam device in the same sense as the others. In this instrument the electron probe is merely an accessory to the production of a point source of x-rays which then interact with the matter being studied. The scanning x-ray microscope of Pattee at Stanford utilizes an electron probe formed by focusing electrons from a field emitter through an electrostatic lens on a thin foil target (8). The probe is scanned over the target and the x-rays produced pass through the foil and the specimen. The image is reproduced on a cathode ray tube with the contrast resulting from the variations of x-ray transmission in the specimen.

The x-ray shadow microscope with stationary electron probe was pioneered by Cosslett and Nixon at Cambridge (9). This utilizes a thermionic source and two magnetic lenses of which only one is normally used for demagnifying the source, the other being used to vary the effective source distance. Marton and his co-workers have experimented with x-ray shadow microscopes using field emission and electrostatic focusing (10). Newberry, at General Electric, has developed the prototype of an electrostatic x-ray shadow microscope which is now commercially available (11). Finally, attempts have been made to modify commercial electron microscopes for use as an x-ray shadow microscope (12).

The information which may be obtained from the beam devices discussed up to this point is mainly qualitative and is subject to some ambiguities in interpretation. If quantitative information is desired,

it is necessary to use effects which are not only more susceptible to measurement than is the brightness of a fluorescent screen, but which can also be correlated with the nature of the target material to a greater degree than is possible on the basis of the number of electrons scattered or absorbed from an electron beam.

One method of obtaining more quantitative information about the chemical constitution of matter has been used by Hillier and Baker (13). This consists in measuring the energy distribution of electrons transmitted by a thin target. The discrete energy losses suffered by the electrons in traversing the thin layer can, it is asserted, be correlated with energy levels of the elements present in the target. A similar method based on the elastic scattering of protons has been used at the Stanford Research Institute for trace analysis of surfaces (14). The Kellogg Radiation Laboratory at Caltech and many other laboratories engaged in measuring nuclear energy levels are also performing, in a sense, chemical analyses of the target materials. However, with the exception of the Stanford project, the emphasis is usually on determining energy levels or scattering properties in a known target material, rather than making use of known energy levels or scattering properties to obtain information about the chemical constitution of the target. The instrumentation required for these methods of analysis is complicated and costly. The Stanford equipment consisted of a Van de Graaf generator followed by a system of alternating gradient lenses which resulted in a proton focal spot of

several square millimeters in area. Analysis of the elastically scattered protons was accomplished by a magnetic analyzer.

The last type of instrument for local analysis of matter by electron beams which will be described makes use of the only effect which has not yet been fully exploited, and this type of instrument is the subject of this thesis. The effect which is used in this instrument is the emission of characteristic x-radiation when an electron beam strikes matter. Fluorescence analysis by means of x-rays has, for the most part, supplanted the use of demountable target tubes for studying matter by means of the primary x-radiation because of the great convenience of not requiring evacuation of the specimen chamber. Only recently, however, have attempts been made to utilize one of the great advantages of analysis by means of the primary x-radiation, namely that it can be localized to a very high degree by focusing the electrons on the target.

It is interesting to note that analogous attempts at localizing the analysis have been made in the case of optical emission spectroscopy. This has been done by localizing the spark excitation of the sample with the use of apertures or tubes. However, the destructive nature of the spark and the reduction of intensity with decrease in source area makes it impractical to localize the analysis below one tenth millimeter. The method of local analysis by means of x-rays which was developed by Castaing (15), on the other hand, is non-destructive and limited in spatial resolution only by the diffusion of the electrons in the target.

Castaing's original work on this method demonstrated that it was capable of quantitative analysis of regions of the surface of a sample of several cubic microns in size and with an accuracy which is limited, in most cases, chiefly by statistical fluctuations of the x-ray emission lines. The first instrument which Castaing constructed was made from an electron microscope and used a triode gun, two electrostatic lenses, and a curved crystal x-ray spectrometer operating in air. In a later version, the final electrostatic lens is replaced with a magnetic lens and has a more refined viewing system for observing the surface of the specimen so that the point of impact of the electron probe can be determined.

The principle of Castaing's x-ray microanalyzer is now being exploited in several analogous instruments under development in the United States and England. We have already mentioned the scanning x-ray microanalyzers which are being developed in England (see p. 7) by Duncumb and Bloom. Three microanalyzers are in operation or under construction in the United States. One of these was constructed by Fisher and Swartz at the United States Steel Company by modifying an RCA EMU electron microscope (16). Another is being built at the U.S. Naval Research Laboratories in Washington by Birks and Brooks (17). Finally, there is the microanalyzer at Caltech which is the subject of this thesis.

II. Microanalysis by Means of Electron Probes

A. The Physical Basis of Castaing's Method

Let us investigate the methods by which quantitative information can be obtained about the composition of matter from the characteristic radiation produced under bombardment by electrons. The procedure will differ in certain fundamental respects from that used in optical spectroscopy and in ordinary macroscopic x-ray analysis (as, for example, fluorescence analysis) because of the requirement that the analysis give the location of the chemical elements which constitute the target.

In the case of optical spectroscopy, thermal equilibrium conditions can be brought about either in the unknown or in reference samples, and this provides important theoretical information for the evaluation of relative intensities of the spectral lines. In the case of x-ray analysis, however, the conditions of thermal equilibrium are seldom attained and as a result, the theoretical calculation of the x-ray line intensities is more difficult. As a result, one is usually restricted in x-ray analysis to a comparison of the intensities of the lines from neighboring elements in the periodic table so that the effects of different electronic configurations on the intensities of the lines being compared will not be too great. The common procedure in the latter case consists of determining the emission spectrum of a mixture containing an unknown amount of the element for which the determination is being made and a known amount of the reference element which

is selected to be near in atomic number to the element being measured. In both optical emission spectroscopy and x-ray analysis it is possible to resort to the use of standards whose composition can be determined by chemical analysis.

In the case of x-ray microanalysis, however, it is not feasible to compare relative intensities of different spectral lines for the following reasons:

(1) the theoretical intensities cannot be calculated,

(2) experimental measurement of the line intensities is subject to large errors because of the variation of spectrometer and detector sensitivity with wavelength,

(3) standards of known composition cannot always be prepared which are homogeneous.

Hence, in x-ray microanalysis, it is necessary to compare the intensities of the same spectral line obtained from an alloy containing an unknown quantity of an element with that obtained from a target consisting exclusively of this element.

It would be expected that in the first approximation the ratio of these intensities will be directly proportional to the mass concentration of the element in the alloy. It can be demonstrated both theoretically and experimentally that this approximation is valid under certain conditions, namely that the elements making up the target are sufficiently close in atomic number that their properties are similar with respect to the retardation and scattering of electrons and the self-absorption of the x-rays, and that there is no selective absorption of the x-ray line emitted by one element by the atoms of another element. The utility

of the analysis would be extremely limited by these conditions, but we will see later that it is possible to derive correction formulae which permit the extension of the method of analysis to elements of widely different atomic number.

The theoretical arguments for the approximation that the intensity of the x-ray emission line is proportional to the concentration have been given by Castaing, first in his thesis (15) and later in a more refined form in a paper with Descamps (18). We will review this latter argument for the sake of completeness.

Let us assume that a homogeneous region of an alloy containing n_j elements of atomic number Z_j is placed under the focal spot of an electron probe. Let c_j be the mass concentration of element j and let I_Z be the intensity of the $K_{\alpha 1}$ line from the alloy. Let I(Z) be the intensity of the $K_{\alpha 1}$ line from a target of pure Z. Furthermore, let us assume that the constituents of the target have been chosen so that they satisfy the conditions mentioned in the preceding paragraphs.

The number of K(Z) ionizations in a length dx of an electron's trajectory is:

$$dn = \Phi\,(E, E_k, n_k)\,dx \tag{1.1}$$

where Φ is the ionization function, $E_k = eV_k$ is the energy of excitation of an atom in its K shell, and n_k is the number of K(Z) electrons per cubic centimeter. Clearly, dn contains n_k as a factor, and letting ρ be the density of the alloy in the region bombarded we have

$$dn = \rho \frac{c_Z}{A_Z} \frac{\psi_Z(E)}{\frac{dE}{dx}}\,dE \tag{1.2}$$

where $\psi(E)$ is a function which depends only on the element Z, A_Z is the atomic weight of this element, and dE/dx is the energy loss per unit length of the electron's trajectory.

In order to evaluate this, we may use, as a first approximation to dE/dx, the Williams retardation law (19):

$$\frac{dE}{dx} = 1.06 \cdot 10^3 \rho \beta^{-1.4} \tag{1.3}$$

where dE/dx is expressed in electron-kilovolts per cm. and β is the ratio of the velocity of the electrons to the velocity of light.

With this substitution we would have

$$dn = \frac{c_Z}{A_Z} F_Z(E)\, dE \tag{1.4}$$

where F_Z depends only on the element Z.

The total number of K(Z) ionizations produced by a single electron along its trajectory, assuming that this trajectory lies entirely within the sample for the energy range which can result in K ionization is then

$$n = \frac{c_Z}{A_Z} \int_{E_o}^{E_k} F_Z(E)\, dE \tag{1.5}$$

where E_o is the initial energy of the electron.

Similarly, for the ionization produced in the target of pure Z, we have

$$n' = \frac{1}{A_Z} \int_{E_o}^{E_k} F_Z(E)\, dE \tag{1.6}$$

If the absorption of the x-ray is negligible and if the integral of $F_Z(E)$ is independent of the path of the electron, this gives

$$\frac{I_Z}{I(Z)} = \frac{n}{n'} = c_j \qquad (1.7)$$

A second approximation could be made by taking for dE/dx Webster's modified form of the Williams retardation law (19)

$$\frac{dE}{dx} = 1.06 \cdot 10^3 \rho \beta^{-1.4} \frac{Z}{A_Z} \qquad (1.8)$$

where Z is the atomic number of element Z and the other quantities are as defined before. For a complex cathode this becomes

$$\frac{dE}{dx} = 1.06 \cdot 10^3 \rho \beta^{-1.4} \sum_j \frac{c_j Z_j}{A_j} \qquad (1.9)$$

Substituting formulae 1.8 and 1.9 in equation 1.2 and repeating the same steps, we find

$$\frac{I_Z}{I(Z)} = c_Z \frac{Z}{A_Z} \left(\sum_j c_j \frac{Z_j}{A_j} \right)^{-1} \qquad (1.10)$$

We have assumed that the properties of the alloy with respect to scattering of the electrons is independent of its composition. This is not strictly true, however, for two reasons. In the first place, some of the electrons of energy sufficient to cause K(A) ionization will be scattered out of the target, and this number will in general be greater for targets composed of heavy elements. In the second place, the diffusion of electrons in the target will also be different for targets

of different composition. Since the x-ray excitation occurring at a given depth will depend on the scattering of the electrons, it will not be possible, when account is taken of the x-ray self-absorption, to distinguish by external measurement of intensity a lower production of the x-rays from a lower intensity due to a greater depth of production.

The corrections for self-absorption of the x-rays and for fluorescence excitation will require a knowledge of the distribution of excitation as a function of depth in the target. Thus, although the simple treatment which has been given furnishes a basis for a first approximation it is not a useful formulation from which to derive the necessary corrections for extending the method of analysis to other cases of interest because it has eliminated all dependence of the excitation on depth in the sample.

B. Verification of the Method

Following Castaing and Descamps (18) we will introduce an excitation distribution function defined by the following equation:

$$dI = I_o \, \phi_Z (\rho z) \, d\rho z \qquad (2.1)$$

where dI is the intensity of a particular x-ray emission line of element Z emitted by an infinitely thin layer of thickness dz at depth z in a target which is subjected to bombardment by an electron probe normal to its surface. I_o is the intensity from an isolated layer of thickness dz and $\phi(\rho z)$ is a function which takes account of the diffusion and retardation of electrons in the thick target. The function $\phi(\rho z)$ will not

necessarily be unity at $\rho z = 0$ because of back-scattering from the deeper layers, and its form will in general depend on the nature of the target. We will distinguish between this function for targets consisting of element A, element B, and an alloy of A and B using the subscripts $_A$, $_B$, and $_{AB}$.

It should also be noted that the form of the function $\phi(\rho z)$ will depend on the accelerating voltage of the electron beam. However, since it is not usually necessary for the purposes of a chemical analysis to vary this voltage, we shall assume that it remains fixed in all the derivations which follow.

If the self-absorption of the x-rays and the excitation of fluorescence radiation is neglected, the intensity observed from a target of pure A would be

$$I(A) = \frac{k\rho N}{A} \int_0^{\infty} \phi_A(\rho z) dz \qquad (2.2)$$

where k is a constant which depends on the current in the electron probe, N is Avogadro's constant, and A is the atomic weight of element A.

The intensity of the same emission line of element A which is observed when an alloy AB is subjected to identical electron bombardment would be

$$I_A = \frac{k c_A \rho N}{A} \int_0^{\infty} \phi_A(\rho z)\, dz \qquad (2.3)$$

The ratio of these intensities is therefore

$$\frac{I_A}{I(A)} = c_A \frac{\int_0^{\infty} \phi_{AB}(\rho z)\, d(\rho z)}{\int_0^{\infty} \phi_A(\rho z)\, d(\rho z)} \qquad (2.4)$$

In the case of an alloy infinitely dilute in A, we see that the proportionality of emission and concentration has the same relative error as is made in equating the two integrals

$$S_A = \int_0^{\infty} \phi_A(\rho z)\, d(\rho z)$$

and

$$S_B = \int_0^{\infty} \phi_B(\rho z)\, d(\rho z) \qquad (2.5)$$

Now it is possible, in principle, to deduce the functions $\phi_A(\rho z)$ and $\phi_B(\rho z)$ from theory. One might hope to do this by assuming that the density of scattered electrons in the target obeys the diffusion equation with a source term such that the point of "creation" of the electrons is the point at which the first scattering occurs (20). In order to make use of the diffusion equations one must artificially assume that the electrons are absorbed in a single collision with a probability which is inversely proportional to the number of collisions (or close encounters) which are required on the average to reduce its energy below the ionization energy of the x-ray level. The excitation function would be proportional to the rate of absorption of the total electron

density comprising diffuse electrons plus incident electrons. The diffusion equation, however, is valid only if the electrons are near enough alike in speed and heterogeneous enough in direction of motion so that they all behave not too differently from the mean behavior. For the case of 30 kv electrons in metals, the velocities which must be considered range all the way from $E_o/2m$ to $E_k/2m$ and, as a result, the mean free path depends greatly on particle energy. Therefore, the approximation that the electrons obey the diffusion equation is not sufficient. (We shall see later that the experimental determination of the excitation distribution function gives functions which vary considerably within distances of the order of one mean free path and the diffusion equation is insufficient to describe this behavior.)

Thus, the theoretical prediction of the excitation distribution function $\phi(\rho z)$ would require a solution of the transport equation (a form of Boltzmann's integro-differential equation). This equation is (21):

$$\frac{\lambda(u)}{v}\frac{\partial\psi(\underline{r},u,\underline{a}_u)}{\partial t} + \lambda(u)\underline{a}_u \cdot \operatorname{grad}\psi(\underline{r},u,\underline{a}_u) + \psi(\underline{r},u,\underline{a}_u)$$

$$= \int_0^u k(u')du' \iint d\Omega\, \alpha(\theta, u-u')\, \psi(\underline{r},u',\underline{a}_u') + S(\underline{r},u,\underline{a}_u) \qquad (2.6)$$

where $S(\underline{r},u,\underline{a}_u)$ is the number of particles "created" per second per unit volume with energy corresponding to $u = \ln E_o/E$ and with direction of motion given by $\underline{a}_u$,

$\psi(\underline{r}, u, \underline{a}_u)$ is the number of collisions per second per unit volume made by particles in the energy range du with velocities directed in the solid angle $d\Omega$,

$\lambda(u)$ is the mean free path for particles of energy corresponding to u,

α is the probability that a particle whose incident direction is $\underline{a}_u'$ will be scattered in the direction $\underline{a}_u$,

θ' is the scattering angle,

$k(u)$ is the ratio of the cross-section for scattering to the total cross-section .

The solution of this equation is beyond the scope of this thesis. We must be content for the present with experimental determinations of the excitation distribution functions $\phi(\rho z)$. These functions have been determined by Castaing and Descamps by the method of "tracers" (18). In this method, to determine $\phi_A(\rho z)$ a pure block of element A is coated by vacuum evaporation with a thin layer of another element, C (the tracer). The layer of C is then coated with layers of varying thickness of A. The intensity of the $K_{\alpha 1}$ radiation from C is investigated as a function of the known thickness of the overlying layer of A. Correction for the absorption of the x-rays in the layers of A can be made accurately since the absorption path is known. The ratio of this corrected intensity to the intensity of an isolated layer of C of identical thickness with that layer used as the tracer gives $\phi_A(\rho z)$. In the ideal case, the tracer, C, should be close to A in the periodic table, have a small absorption of its $K_{\alpha 1}$ line in A, and not be strongly fluorescence-excited by the radiation from A.

Castaing and Descamps determined the function $\phi(\rho z)$ for aluminum (Cu tracer), copper (Zn tracer), and gold (Bi tracer) at an accelerating voltage of 29 kv. Because of the importance of these functions relative to the theory of the method of analysis and in the calculation of correction for self-absorption and fluorescence excitation, we have reproduced in fig. 1 the curves which they obtained.

One should remark that the accuracy of the curve for aluminum is much less than the curves for copper and gold because of greater deviations from the conditions of an ideal tracer. One of these conditions is that the excitation potential of the tracer be nearly the same as that of the target element studied. For the case of copper, using a zinc tracer ($V_k(Zn)/V_k(Cu) = 1.079$), and for gold, using a bismuth tracer ($V_{LIII}(Bi)/V_{LIII}(Au) = 1.125$) this condition is satisfied. For aluminum, however, which was investigated with a tracer of copper ($V_k(Cu)/V_k(Al) = 5.75$) the condition is not satisfied. Hence, one would expect the experimental curve for aluminum to be more sharply peaked than the true curve due to the effective elimination of electrons whose energy lies between $V_k(Cu)$ and $V_k(Al)$.

In the case of copper and gold, where this limitation is of small importance, the accuracy of determining the functions $\phi(\rho z)$ is limited chiefly by the counting statistics and is about 5%.

Using the experimentally determined curves for $\phi(\rho z)$, Castaing and Descamps attempted to verify the equality of the integrals of equation 2.5. For aluminum, copper, and gold the integrals were found to be equal to within the accuracy of determining $\phi(\rho z)$ provided

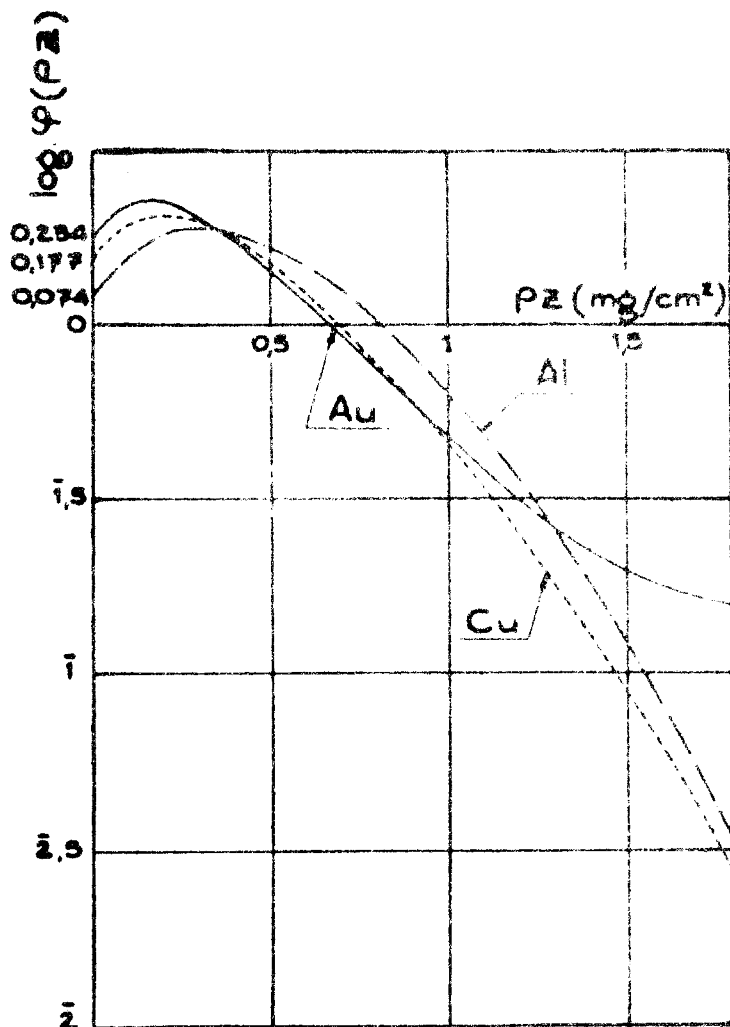

FIG. 1 $\phi(\rho z)$ obtained by Castaing and Descamps (18) for aluminum (Cu tracer), copper (Zn tracer), and gold (Bi tracer) using an accelerating voltage of 29 kv.

the integration was not carried to infinite depths but was terminated at a finite depth where the electronic intensity was negligible ($\rho z \approx 1.6$ mg/cm^2). This procedure partially eliminated the effects of fluorescence radiation, which comes mainly from greater depths in the target than the primary radiation.

We can see from the form of the curves that scattering of the electrons in the target plays a very important role, since, in the absence of scattering, the functions $\phi(\rho z)$ would start at the origin and decay more or less exponentially according to the Lenard law. The increase in the value of $\phi(0)$ with increasing atomic number indicates that there is relatively more back-scattering from the heavier elements. This effect deserves more than a passing comment because the number of back-scattered primary electrons will affect the determination of the functions $\phi(\rho z)$.

It has been shown by Wagner (22) that the number of high speed secondary electrons ejected from a thick target bombarded with primary electrons of energy eV_o = 30 kev. has a maximum at energies of about 0.94 eV_o for gold or silver, 0.92 eV_o for copper, and 0.85 eV_o for aluminum. More quantitative measurements on the number of high speed secondaries emitted per bombarding primary electron have been made by Brand (23) for primary electrons having an energy of 32 kev. While we must admit that the distribution of energy in the high speed secondaries may be a function of angle of primary incidence, the work of both Brand and Wagner serves to indicate that the back-reflected electrons for the most part have caused less excitation of the target

atoms in their inner shells than an equal number of the primary electrons which are not back-reflected.* Moreover, as Palluel (24) and Schonland (25) have demonstrated, the number of high speed secondaries can be a substantial fraction of the number of incident electrons. Thus, there is a reduction in the effective number of bombarding electrons for thick targets, the reduction being greater for heavier elements. This reduction in effective bombarding intensity is included in the functions $\phi(\rho z)$ as determined by Castaing and Descamps, because these functions were normalized with reference to the intensity from an isolated layer which is so thin that back-scattering is negligible; the thickness of the zinc tracer used for $\phi_{Cu}(\rho z)$ was 0.03 mg/cm^2.

This reduction in effective bombarding intensity also occurs in the analysis if the x-ray intensity is measured for a fixed period of time with constant current in the electron probe. Thus, we can conclude that the proportionality of emission and concentration depends on the fortuitous balance between the scattering and retardation of electrons in matter which leads to a nearly constant value of $\int \phi(\rho z) dz$ for all elements.

---

* This is supported by investigations made by Sternglass (Phys. Rev. (1954) Vol. 95, pp. 345-358), who found that the dominant mechanism in the back-scattering of kilovolt electrons is inelastic collisions with atomic electrons. Sternglass attempted to confirm, in part, the theory of inelastic collisions worked out by Bohr and Bothe which predicts that the maximum effectiveness as scattering agents is reached only for those atomic electrons which have energies of 1/e times the energy of the incident particle. The elastic scattering by the Coulomb field of the nucleus is important only at high energies because of the strong screening of the scattering field by the atomic electrons. Although back-scattered electrons will consist in part of incident electrons suffering inelastic collisions with K electrons, the major contribution will be due to multiple scattering by outer-shell electrons.

The value of this integral is not strictly constant for all elements, and the experimental verification of its constancy was insufficient to assure an accuracy of better than about 5 % if the analysis is based on the proportionality of emission and concentration. In the analysis of samples containing elements widely separated in atomic number it is therefore necessary to make allowance for possible variations in $\phi(\rho z)$ by a procedure which will require some comparison to reference alloys of known composition. In any given alloy system, it is usually possible to prepare a few alloys or intermetallic compounds which will satisfy the requirement of homogeneity.

As an introduction to the method of attaining a better approximation relating the x-ray intensity and composition, it is well to review the meaning of equations 1.7 and 1.10. In equation 1.7 for which there is strict proportionality of emission and concentration it was assumed that equal surface densities of all elements result in equal retardation of the incident electrons. In the derivation of equation 1.10 the electron retardation which occurs per unit surface density of element j is weighted by a factor A_j / Z_j. Now, if we replace this factor by an undetermined parameter α_i, we would have for the equation analogous to equation 1.10

$$\frac{I_A}{I(A)} = \frac{c_A \alpha_A}{\sum_i^n c_i \alpha_i} \qquad (2.7)$$

The α_i may be determined experimentally to fit a few standard alloys which are known to be homogeneous and whose composition can

be independently determined. For a target consisting of n elements there are n equations of the form of equation 2.7 but only n-1 unknowns since the concentrations, c_i, must sum to unity. Thus, the α_i for one element may be chosen arbitrarily as equal to unity, and all other α_i will then represent what may be called the "electron retarding power" relative to an equal mass of this element.

If the scattering of the electrons in the target were negligible, one might hope that the α_i would be constants depending only on the elements and not on their concentration or on the physical structure of the alloy. But we have seen that the scattering is important and we shall see in the following section that it is not possible to make exact corrections for absorption and for fluorescence radiation. Therefore, it is usually necessary to determine the parameters, α_i, for a series of alloys and select the average value to use in calculating the unknown concentrations from the ratios of the x-ray intensities.

If the deviation of the α_i from their average values is large, the α_i must be determined over the entire range of composition and this is equivalent to plotting a calibration curve. However, we shall see in a later section that it is possible to reduce the spread of the α_i's by compensating for the effective reduction in bombarding intensity from back-scattering of electrons out of the target (see p. 81). In any case, the treatment of data by means of these parameters has two advantages over the use of calibration curves: (1) in the case of a target containing n constituents an n-dimensional calibration curve is reduced to the value of n-1 parameters α_i, and (2) these parameters

are virtually independent of the geometry of the instrument, whereas a conventional calibration curve based on the uncorrected x-ray intensities is not.

In the case of an alloy containing only two elements we may let $\alpha = \frac{\alpha_A}{\alpha_B}$, and this gives

$$\frac{I_A}{I(A)} = \frac{\alpha c_A}{\alpha c_A + (1-c_A)} \tag{2.8}$$

We see that for α equal to unity (retardation of electrons in both elements) this reduces to equation 1.7. When the appropriate value of α has been determined, the concentration can be determined from the ratio of the intensities corrected for self-absorption, fluorescence excitation, background, etc. If k_A is the ratio of intensity from the sample to the intensity from the target of pure A after these corrections have been made, we obtain from equation 2.8 the concentration of A in a binary alloy

$$c_A = \frac{k_A}{(1 - \alpha)k_A + \alpha} \tag{2.9}$$

If we let $c_A = x$ and $k_A = y$ in this formula, the locus of points satisfying the resulting equation $f(x, y) = 0$, is a rectangular hyperbola with center at $x = \frac{1}{1 - \alpha}$, $y = \frac{-\alpha}{1 - \alpha}$. The transverse axis of this hyperbola lies along the line $y = -x + 1$ and is equal to $2\sqrt{\frac{2\alpha}{(1 - \alpha)^2}}$. We will therefore refer to equation 2.7 and equation 2.9 as the hyperbolic approximation.

Castaing (15) has shown that the application of equation 2.9 is capable of about the same order of accuracy as is present in the determination of the x-ray intensities.

C. Corrections for Accurate Quantitative Analysis and Limitations on the Accuracy of the Method

It is convenient to regard the corrections which must be made to the observed x-ray intensities in accurate quantitative analysis as consisting of two distinct types: (1) corrections for errors which exist intrinsically in the method of analysis and which result in a deviation from the hyperbolic approximation given by equation 2.7, and (2) corrections for errors which are instrumental in nature. Those corrections which belong to the first group are necessary in order to minimize the need for comparisons to reference alloys of known composition, while those corrections which belong to the second group can be reduced to some extent by improvement of the instrumentation. The division into these two groups is not a sharp one due to the fact that some of the intrinsic corrections are susceptible to improvement by instrumental techniques, and some corrections which we arbitrarily classify in the second group actually exist in any physically realizable form of the method. We will consider that the first group consists of corrections for (1) self-absorption of the emerging x-rays, (2) fluorescence radiation excited by the absorption of primary radiation in the target, and (3) the background of continuous radiation. The second group will contain all other corrections necessary, such as

corrections for change of the measured intensity due to surface contamination, dead time of the detector, and unavoidable current drifts in the electron probe.

1. Intrinsic Corrections

a. Self-absorption of the x-rays

In the derivations leading to equation 2.7 we neglected the fact that the x-rays suffer absorption as a result of being produced at some depth below the surface of the specimen. If the x-ray absorption coefficients of the elements present in the target are different, it is necessary to correct for absorption before applying equation 2.7. Fortunately, these corrections are not large because in general the retardation of electrons in matter is such as to limit their depths of penetration to layers so shallow that the emergent x-rays are only slightly absorbed.

There are two methods by which one can arrive at a correction for the self-absorption. The first method makes use of the distribution of excitation, $\phi(\rho z)$, which may be known by the method of tracers. Let us assume for the moment that the sample has its surface normal to the electron beam. If the region of interest in the sample has an average mass absorption coefficient for the x-ray line being measured of μ/ρ , the intensity observed at an angle θ with respect to the surface is

$$I' = I_o \int_0^{\infty} \phi(\rho z) \exp\left(\frac{\mu}{\rho}\, \rho z \operatorname{cosec} \theta\right) d(\rho z) \qquad (3.1)$$

where I_o and $\phi(\rho z)$ are as defined in the preceding section. On the other hand, if there were no absorption, the intensity would be

$$I = I_o \int_0^{\infty} \phi(\rho z)\, d(\rho z) \qquad (3.2)$$

Combining equations 3.1 and 3.2 we obtain the desired correction

$$I = I' \frac{F(0)}{F(\mu/\rho \text{ cosec } \theta)} \qquad (3.3)$$

where I is the true intensity, I' is the observed intensity and F(X) is the Laplace transform of $\phi(\rho z)$

$$F(X) = \int_0^{\infty} \phi(u) \exp(-Xu)\, du \qquad (3.4)$$

with $X = \mu/\rho \text{ cosec } \theta$. Castaing and Descamps (18) give correction curves $\log_{10} f(X) = \log_{10} F(X)/F(0)$ for targets of atomic number 13, 29, and 79, and interpolation may be used for intermediate values. These curves are reproduced in fig. 2.

The second method for obtaining the correction for self-absorption involves a direct determination of the function F(X) by measuring the intensity from a pure element in the microprobe as the angle of observation is varied. The observed intensity, I' , is plotted as a function of μ/ρ cosec θ and extrapolated to $\mu/\rho \text{ cosec } \theta = 0$ to obtain I. A plot of I'(X)/I where $X = \mu/\rho \text{ cosec } \theta$ is the desired correction curve. Such a correction curve, plotted by using an arbitrary

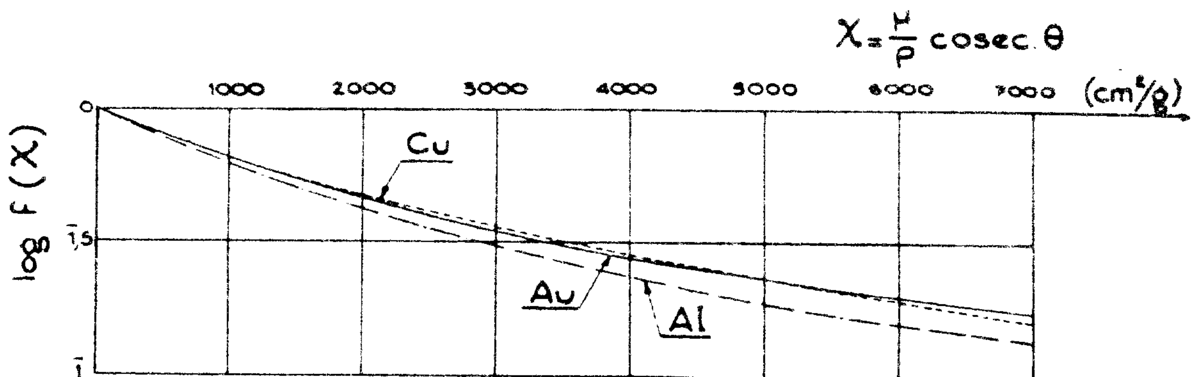

FIG. 2 Absorption correction curves obtained by Castaing and Descamps (18) by integrating $\phi(\rho z)$ from $\rho z = 0$ to $\rho z = 1.6$ mg/cm^2.

element as a target, can be generalized so as to be useful for various targets provided it covers a sufficient range in the variable X.

This can be done by the use of the weighting factors, α_i , defined by equation 2.7. In equations 3.1 and 3.2 one takes in the argument of ϕ the effective density of the alloy,

$$\rho = \sum_i \alpha_i m_i \qquad (3.5)$$

where m_i is the mass/cm^3 of the element i in the region analyzed, and the summation is extended over all elements present in this region. Similarly, the linear x-ray absorption coefficient of the alloy is

$$\mu_{alloy} = \sum m_i \left(\frac{\mu}{\rho}\right)_i \qquad (3.6)$$

where $(\mu/\rho)_i$ is the mass absorption coefficient of the element i . One then obtains

$$I = I' \frac{\int_0^\infty \phi(\sum \alpha_i m_i) \sum \alpha_i m_i \, dz}{\int_0^\infty \phi(\sum \alpha_i m_i) \exp(-\sum m_i (\frac{\mu}{\rho})_i z \operatorname{cosec} \theta) \sum \alpha_i m_i \, dz} \qquad (3.7)$$

which, on change of variable, becomes

$$I = I' \frac{F(0)}{F\left(\dfrac{\sum m_i (\frac{\mu}{\rho})_i \operatorname{cosec} \theta}{\sum m_i \alpha_i}\right)} \qquad (3.8)$$

Thus, in order to use a single curve as a universal absorption curve, one must take for μ/ρ the quantity

$$\frac{\mu}{\rho} = \frac{\sum c_i(\mu/\rho)_i}{\sum c_i \alpha_i} \qquad (3.9)$$

since $m_i = c_i\rho$.

The absorption correction based on a universal absorption curve requires a knowledge of the coefficients α_i . If these quantities are not known (by a prior analysis of an alloy of known composition for which absorption correction may be neglected), one can use a method of successive approximations to avoid solving a large number of simultaneous equations. As a first approximation one assumes that the α_i are all unity. A first approximation to the c_i is obtained from equation 2.7 using the uncorrected x-ray intensities. These values are then used in the formula for the self-absorption correction to obtain the first approximation to the corrected intensities. The corrected intensities may then be used in equation 2.7 with the preliminary values of the c_i to obtain a second approximation to the α_i . One can then find the second approximation to the corrected intensities and use this to obtain a second approximation to the c_i , etc. Castaing (15) has proposed a similar iteration wherein the absorption correction is performed on both I_A and $I(A)$ in the same formula, but this introduces unnecessary complication for understanding the method of the correction.

One cannot be assured that the method of successive approximations is convergent if the elements are widely separated in atomic number

where the α_i might deviate considerably from unity. In this case, it is advisable to use independent measurements for determining the α_i if the "universal" correction curve is being used for the self-absorption correction.

It should be remarked that the experimental arrangement may require some modifications in the correction formulae for self-absorption. The electron beam, for example, may make an angle with the surface of the specimen, or the emitted x-rays which are accepted by the spectrometer may have varying emergence angles with different spectrometer settings. This latter factor is not mentioned by Castaing in his thesis or in his paper with Descamps on the determination of the excitation function because it has negligible effect for all cases discussed. In general, because of the effect of geometry on the self-absorption correction curves, it is hazardous to use correction curves obtained with one instrument to correct data taken on another instrument unless all of the geometrical factors of both instruments are known.*

Let us consider the case where the electron beam is not perpendicular to the surface of the target and where the crystal of the spectrometer is not fixed in space but moves on the arc of a circle. Such an arrangement is illustrated in fig. 3. The angle between the axis of the electron beam and the normal to the surface of the target

---

* Although Castaing states that the curves of fig. 2 were determined with the electron beam normal to the surface, they were actually measured in his original instrument (26) in which $\theta_1 = 10^o$, $\theta_2 = 16^o$ (see fig. 3).

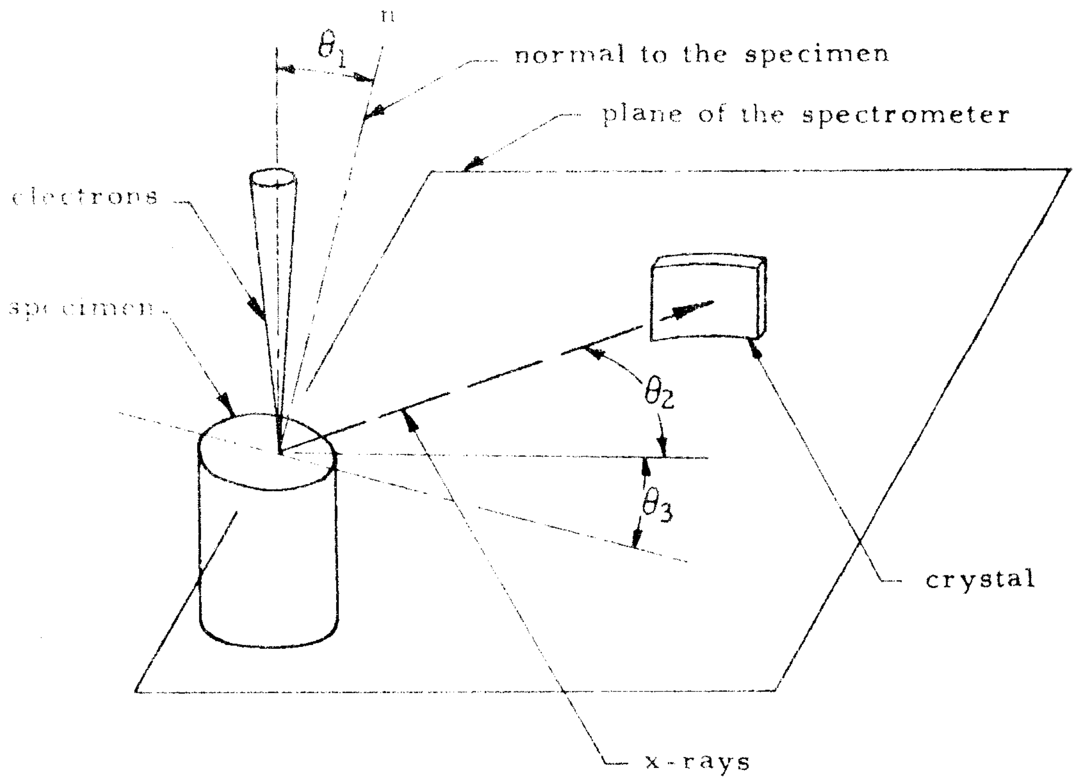

FIG. 3. Geometry of the self-absorption correction.

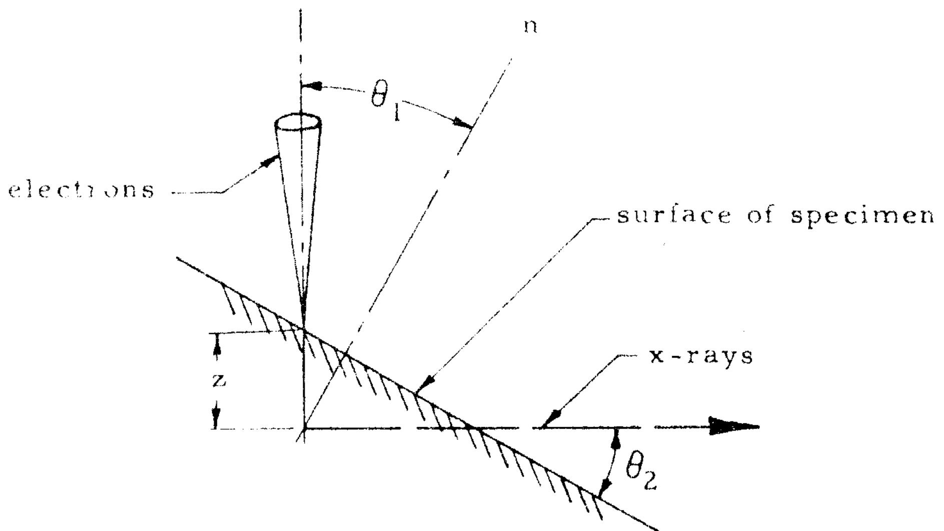

FIG. 3a.

is θ_1 . Only one other angle need be specified, the angle of emergence of the x-rays from the surface of the specimen. However, since the crystal of the spectrometer ordinarily moves in a plane, it is more convenient to specify the angle, θ_2 , between this plane and the surface of the target, and the angle, θ_3 , between the path of the x-rays accepted by the crystal and the plane of the angle θ_1 . Thus, in any given instrument, θ_1 and θ_2 will be fixed by the design of the instrument, and θ_3 will vary with the position of the crystal as it moves about the focal circle of the spectrometer.

This choice of coordinates has a number of advantages. If we imagine θ_3 to be zero for the moment, it is easily seen from fig. 3a that we preserve the definition of $\phi(\rho z)$ if the coordinate z is measured along the axis of the beam and that the self-absorption path for the x-rays is then ($z \cos \theta_1 / \sin \theta_2$). The effect of a non-zero value of θ_3 will be to multiply this path by $1/\cos \theta_3$, a value which is easily calculable for each position of the spectrometer from the Bragg angle. Now, it is convenient for reasons of design and construction to have $\theta_1 = \theta_2$, and therefore, for this case, we can generalize equations 3.3 and 3.8 by replacing cosec θ by cot θ ($\theta = \theta_1 = \theta_2$) and multiplying by $1/\cos \theta_3$. Thus, although the absorption path is different for each setting of the spectrometer, the generality of the absorption correction curves is not affected provided one properly takes account of this additional factor in computing X.

b. Fluorescence excitation

We have seen that the intensity of a characteristic x-ray line is proportional to the concentration chiefly because the behavior of matter with respect to the exciting agent (electrons) is almost independent of the chemical constitution of the matter. However, this is clearly not the case for the secondary radiation which results from the absorption of the primary radiation. This secondary radiation can be excited either by the portion of the bremstrahlung from λ_q to λ_o where λ_q is the wavelength of the q absorption edge and λ_o is the short wave length limit, or it can be excited by those emission lines from elements present in the target whose wavelengths fall in this range. The corrections for fluorescence radiation excited by the bremstrahlung and that excited by the characteristic lines will be discussed separately after a few remarks on the factors which limit their exact calculation and consequently limit the accuracy of the analysis.

The determination of the intensity due to fluorescence radiation will require a comparison of x-ray intensities at different wave lengths since the exciting radiation is necessarily of higher energy than the fluorescent radiation. We have seen that such a comparison is limited in accuracy regardless of whether it is done experimentally or theoretically.

The determination of the fluorescent intensities will also involve a knowledge of the percentage of the atoms excited in their q shells which return to their ground state each second by the emission of a

q photon. This quantity, the fluorescence yield, is less than unity because of the Auger effect and is not involved in the determination of the intensity of the primary radiation because of the proportionality of emission and concentration. In many cases, it is desirable to use the L lines in the analysis and this constitutes a limitation in calculating the fluorescence radiation involving L excitation,for the fluorescence yields may not be known. It is, however, possible to obtain values of the fluorescence yield in some cases of interest by taking the difference of measured and expected values of intensity from a fluorescence excited element in an alloy of known concentration.

Finally, it is important to realize that the fluorescence radiation may be produced in a different region of the sample than the region which is subject to electronic excitation because of the greater transparency of matter for x-rays than for electrons. Thus, in the study of precipitates or inclusions which are of the order of the dimensions of the electron focal spot, the composition of the matrix or of nearby precipitates (some of which may be below the surface) will affect the accuracy of determining the composition.

We will turn now to the evaluation of the fluorescence intensity due to excitation by the continuous radiation. Analytical methods of evaluating this contribution cannot give a useful general expression, because the exciting radiation has an intensity which depends strongly on composition and is not isotropic, having a maximum at right angles to the electron beam. Moreover, the absorption of both the primary continuous radiation and the emerging secondary radiation are functions of composition and energy.

However, it is possible to obtain approximate values for the amount of fluorescence radiation which results from absorption of the continuous radiation by a method which was used by Castaing and Descamps (18). This method is very simple in principle and is analogous to the method first used by Stoddard (27), except for the fact that Castaing and Descamps used the technique of vacuum evaporation. The alloy of interest (which may be a pure metal) is coated by vacuum evaporation with a thin layer of an element whose characteristic lines do not excite the fluorescence line in the alloy. The thickness of this layer is chosen so that all of the electrons of the incident beam are stopped in it, and, consequently, the primary characteristic radiation from the alloy is suppressed. The observed intensity of a characteristic line from the alloy is related to fluorescence which has been excited by the continuum. Three corrections are necessary to compensate for the slight difference in experimental conditions from those existing when the uncoated sample is under the probe: (1) correction for the absorption of the secondary radiation from the alloy in passing through the overlying layer, (2) correction of the resulting intensity by the ratio of the mean atomic number of the alloy to the atomic number of the superficial layer to make up for a slightly different energy of the exciting continuum, and (3) correction for the amount of secondary radiation which would have originated in a layer of the sample equivalent to the applied layer (this correction is difficult to make, but is small and can be neglected or crudely estimated).

It should be remarked at this point that the technique of evaporating a thin layer of metal on the surface of the sample can have other uses beyond an evaluation of the part of the fluorescence radiation which is due to the continuum. A thin conducting film which is partially transparent to the electron beam can reduce excessive temperature and charging effects in specimens which are not good electrical or thermal conductors. By metalizing with layers of 300 to 400 Å thickness, Philibert and Crussard were able to study insulators in an electron probe microanalyzer (28).

While the fluorescence intensity due to excitation by the continuous radiation is small and of about the same order of magnitude for elements which are not widely separated in atomic number, this is not the case for the fluorescence radiation which is excited by the characteristic lines. The contribution of this fluorescence radiation to the total intensity can be an appreciable fraction of the primary line intensity if one element selectively absorbs line radiation emitted by another element present in the target. This effect is most serious for small concentrations of the fluorescer where the primary intensity is weak and the radiation giving rise to fluorescence is strong. For example, Castaing (15) found that for an iron-chromium alloy containing 49.5% chromium the fluorescence intensity of the chromium $K\alpha_1$ line was about 6.5% of the primary intensity while for an alloy containing 10.77% chromium, the fluorescence intensity was 24% of the primary intensity. In this case, there is selective absorption of the $K\alpha$ doublet of iron in the chromium.

It is always possible to analyze at least one constituent of the target (that with the highest atomic number) without correction for the fluorescence excited by the line spectra since the exciting line radiation must always have a shorter wavelength than the fluorescence radiation. However, it is usually desirable to be able to determine the concentration of all elements present and within the range of the spectrometer so that a check is afforded by summing the concentrations. In cases where the study of one constituent is inaccessible to the spectrometer one would like to be able to estimate its concentration by the method of differences. Therefore, it is important to be able to correct for the fluorescence excited by the characteristic radiation.

While it is not possible to make this calculation exact, approximations can be derived which are sufficiently accurate for most purposes. Three approximations will be discussed. The first approximation will be very crude in that it will neglect the effect of a finite depth of penetration of the electrons into the target, serving chiefly to illustrate the physical features of the calculation. The second approximation will be identical with the approximation developed by Castaing in his thesis, except for an allowance which will be made for a change in the angle of incidence of the electron probe on the surface of the target. The third approximation, developed by the writer, will make use of the excitation distribution functions as determined by Castaing and Descamps.

Let us assume that the sample contains elements $Z_1, Z_2, \ldots Z_j$ and let Z_f be that element which has an emission line of frequency ν_f which is fluorescence excited by the emission lines ν_1, $\nu_2, \ldots \nu_i$.

In the derivations to follow, we shall use the following additional notations:

$I_i(Z_j)$	:	Intensity of the primary radiation of frequency ν_i emitted by the element Z_j .
$I_i^o(Z_j)$	:	Intensity of the primary line radiation which would be emitted by a thin target.
$I_f(Z_f)$	:	Intensity of the fluorescence line radiation of frequency ν_f emitted by the element Z_f .
$\nu_i(Z_f)$	:	Frequency of the line in the series of fluorescence lines which corresponds to the same type of transition as the exciting line of frequency ν_i .
$\omega_q(Z_j)$	:	Fluorescence yield of the element Z_j when excited in its q shell.
$\omega_q(Z_f)$	:	Fluorescence yield of the element Z_f when excited in its q shell.
m_j	:	Mass of the element Z_j per cubic centimeter present under the electron probe.
r_f	:	Ratio of the coefficients of absorption of element Z_f on either side of its q absorption edge.
A_j	:	Atomic mass of element Z_j .
$\frac{\mu_i(Z_j)}{\rho_i}$	:	Mass absorption coefficient of element Z_j for radiation of frequency ν_i .
τ_i	:	Linear absorption coefficient of the alloy for radiation of frequency ν_i .
τ_f	:	Linear absorption coefficient of the alloy for radiation of frequency ν_f .

This notation is slightly more cumbersome than the use of double subscripts, but it has the advantage that the meaning of a symbol is easier to remember if one recalls that the subscript f refers to the fluorescence line, the subscript i to the emission lines, and the subscript j, the element in the alloy.

Let us first assume that the primary x-rays are all produced at the surface of the sample, neglecting the effect of a finite depth of penetration of the bombarding electrons. We will assume further for the purpose of the calculation that all the primary radiation originates at a single point on the surface which is at the center of the electron focal spot. Referring to fig. 4, let ξ be the depth in the target measured along a perpendicular to the surface intersecting the center of the electron focal spot. The total primary intensity which exists at the origin of the ξ axis and is capable of exciting fluorescence is then

$$\sum_{i\xi} \frac{4\pi}{\Omega} I_i(Z_j) \tag{4.1}$$

where the summation is extended over all frequencies $\nu_i(Z_j)$ which results in fluorescence excitation of Z_f. The intensity received by a volume element bounded by cones of revolution about the ξ axis of half angle β and $\beta + d\beta$ and the planes at depth ξ and $\xi + d\xi$ is therefore

$$dI_f = \sum_{ij} \frac{1}{2} I_i(Z_j) \sin\beta \exp\left(-\frac{\xi}{\cos\beta}\tau_i\right) d\xi\, d\beta \tag{4.2}$$

where the factor of 1/2 comes from the fact that we are concerned only with the cones lying below the surface of the sample and where the linear absorption coefficient of the alloy for radiation of frequency ν_i is

$$\tau_i = \sum_{ij} m_j \frac{\mu_i(Z_j)}{\rho_i} \tag{4.3}$$

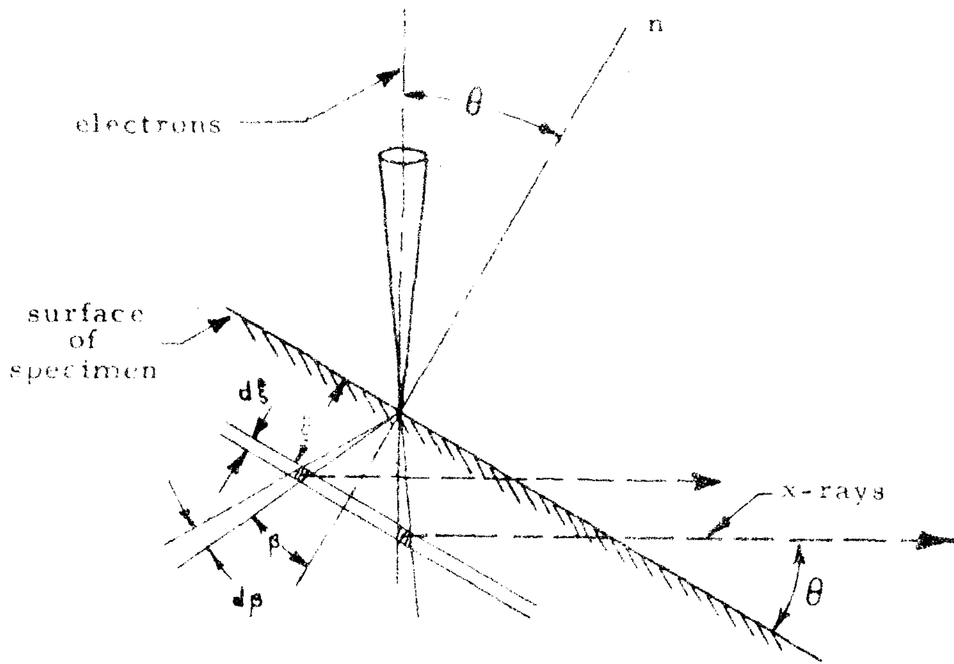

FIG. 4. Geometry of the fluorescence correction I.

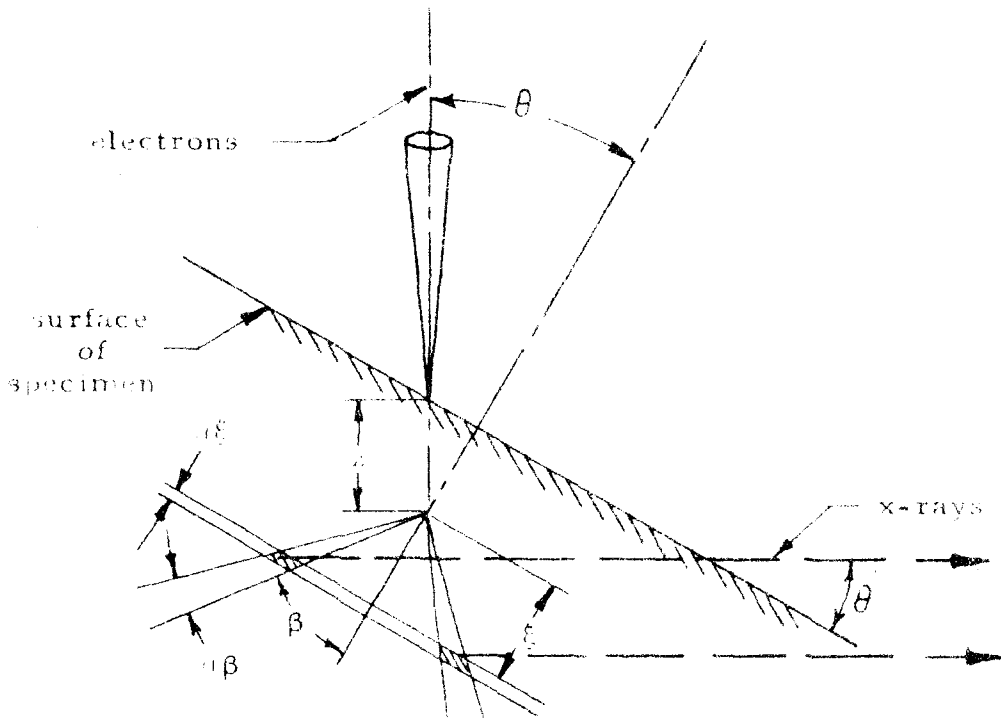

FIG. 5. Geometry of the fluorescence correction II.

The atoms of element Z_f which are contained in this volume element absorb an intensity

$$dI_f' = \frac{m_f \frac{\mu_i(Z_f)}{\rho_i}}{\cos\beta} \sum_{ij} \frac{1}{2} \sin\beta \exp\left(- \frac{\xi}{\cos\beta} \tau_i\right) I_i(Z_j)\, d\xi\, d\beta \qquad (4.4)$$

The fraction of this absorbed intensity which is utilized to produce q ionization is given by the ratio $(r_f - 1)/r_f$ where r_f is the ratio of the coefficient of absorption of element Z_f on either side of its q absorption edge. Therefore, the number of q_f ionizations which is produced per second in the volume is

$$dn = \frac{1}{2} \sum_{ij} \frac{1}{h\nu_i(Z_j)} \frac{r_f - 1}{r_f} m_f \frac{\mu_i(Z_f)}{\rho_i} \tan\beta \exp\left(- \frac{\xi}{\cos\beta} \tau_i\right) I_i(Z_j)\, d\xi\, d\beta \quad (4.5)$$

Now, the number of photons emitted by these excited atoms per second is given by the product of the above number of ionizations per second and the fluorescence yield, $w_q(Z_f)$ which is defined as follows:

$$w_q(Z_f) = \sum_i n_i \Big/ n_q \qquad (4.6)$$

where $n_1, n_2, \ldots\ldots n_i$ is the number of $q_1, q_2, \ldots\ldots q_i$ photons emitted per second and n_q is the total number of atoms excited in their q shells each second.

Not all the photons emitted by the atoms excited in their q shells, however, are detected but only those belonging to the line whose

frequency is ν_f . Therefore we must include another factor which is the ratio of the number of photons/second of frequency ν_f to the total number of photons/second which result from the q ionization, that is

$$x_f(Z_f) = \frac{I_f(Z_f)}{\nu_f(Z_f)} \frac{1}{\sum_i I_i(Z_f)/\nu_i} \tag{4.7}$$

Finally, we must include a factor $h\nu_f$ to convert from the number of photons emitted per second to the intensity in the fluorescence line. The product of this factor and equations 4.5, 4.6, and 4.7 give the intensity in the fluorescence line from the volume element dβ dξ, and this is

$$dI_f = \frac{1}{2}\sum_{ij} x_f(Z_f)\omega_q(Z_f) \frac{\nu_f(Z_f)}{\nu_i(Z_j)} m_f \frac{\mu_i(Z_f)}{\rho_i} \tan\beta \exp(-\frac{\xi\tau_i}{\cos\beta}) I_i(Z_j)\, d\xi\, d\beta \tag{4.8}$$

which we will write

$$dI_f = \sum_{ij} A_{ij} \tan\beta \exp(-\frac{\xi\tau_i}{\cos\beta}) I_i(Z_j) \tag{4.9}$$

where

$$A_{ij} = \frac{1}{2}\sum_{ij} x_f(Z_f)\omega_q(Z_f) \frac{\nu_f(Z_f)}{\nu_i(Z_f)} m_f \frac{\mu_i(Z_f)}{\rho_i} \tag{4.10}$$

The radiation from this volume element will be absorbed on emerging from the sample. Consequently, the intensity observed at an angle of emergence of θ from the target will be

$$I_f = \sum_{ij} A_{ij}(Z_f) I_i(Z_j) \int_0^{\infty}\int_0^{\pi/2} \tan\beta \exp\left(-\frac{\xi\tau_i}{\cos\beta} - \frac{\xi\tau_f}{\sin\theta}\right) d\beta\, d\xi \quad (4.11)$$

where τ_f is the linear absorption coefficient of the fluorescence line in the alloy which is given by

$$\tau_f = \sum_j m_j \frac{\mu_f(Z_j)}{\rho_f} \quad (4.12)$$

Evaluation of the integral in equation 4.11 can be performed directly, integrating first over ξ and then over β, giving the result

$$I_f = \sum_{ij} A_{ij}(Z_f) I_i(Z_j) \frac{1}{\tau_i} \frac{\ln|1+u|}{u} \quad (4.13)$$

where

$$u = \frac{\tau_f}{\tau_i \sin\theta}$$

This expression gives the fluorescence intensity in terms of the primary intensity of the exciting characteristic lines. It is necessary either (1) to relate this theoretically to the intensity of the primary radiation in the fluorescence line, or (2) to compare experimentally the intensities of the different x-ray lines, corresponding to the wavelengths of the exciting lines and the fluorescence line. More will be said of this after the derivation of two more accurate approximations for I_f'.

While it would be expected from the greater transparency of matter for x-rays than for electrons that the approximation of equation 4.13

would be sufficiently accurate, it is impossible to be sure that this is the case without examining solutions of the problem which take into account the finite depth of penetration of the electrons in the target. We shall see that the more accurate correction formulae involve the ratio of the certain coefficients which express the reduction in intensity with depth in the target of the two exciting agents, namely, the electrons and the primary x-radiation. This is to be expected from the fact that the fluorescence radiation comes mostly from the deeper layers in the alloy only if the penetration of the x-rays is much greater than the penetration of the electrons.

We will consider the case where the electron beam is incident on the target at an angle with respect to its surface, since this is almost always the case in instruments which have been devised. Furthermore, we will assume that the angle of emergence of the x-rays is equal to the angle which the axis of the electron beam makes with the normal to the surface of the specimen, since this is true for the instrument which the author has constructed and which will be described in chapter III. The geometry of this correction is illustrated in fig. 5. In order to make use of the function $\phi(\rho z)$ as defined in the preceding section, the coordinate z is measured along the extended axis of the electron beam. We will assume that all the primary radiation produced by the electrons in a layer of thickness ($dz \cos \theta$) and at a depth ($z \cos \theta$) originates at a point on the z axis and that it subsequently produces fluorescence radiation from a volume element lying between planes which are parallel to the surface of the

target at a depth ($z \cos \theta + \xi$) and ($z \cos \theta + \xi + d\xi$). We will further restrict the volume element under consideration by bounding it with two cones of half angle β and $\beta + d\beta$ whose common axis of revolution is the ξ axis.

The fluorescence intensity observed from this volume element will be

$$dI_f' = \sum_{ij} A_{ij}(Z_f) I_i^o (Z_j) \tan \beta \, \phi(\rho z) \exp\left[- \frac{\tau_i \xi}{\cos \beta} - \frac{\tau_f (z \cos + \xi)}{\sin \theta}\right] d\rho z \, d\xi \, d\beta \quad (4.14)$$

where $\phi(\rho z)$ is defined in section B of this chapter. On separating the integration into two parts corresponding to positive and negative values of ξ the total intensity would be

$$I_f' = \sum_{ij} A_i(Z_f) I_i^o (Z_j) \left\{ \int_0^{\pi/2} \int_0^{\infty} \int_0^{\infty} \phi(\rho z) \tan \beta \exp\left[- \frac{\tau_i z}{\cos \beta} - \frac{\tau_f (z \cos \beta + \xi)}{\sin \theta}\right] d\xi d\rho z d\beta \right.$$

$$\left. + \int_{\phi=0}^{\pi/2} \int_{z=0}^{\infty} \int_{\xi=0}^{-z \cos \theta} \phi(\rho z) \tan \beta \exp\left[- \frac{\tau_i z}{\cos \beta} - \frac{\tau_f (z \cos \beta + \xi)}{\sin \theta}\right] d\xi d\rho z d\beta \right\} \quad (4.15)$$

Let us call the value of the above integrals A and B, respectively. For A, integrating first over ξ and then over β we would have

$$A = \int_0^{\frac{\pi}{2}} \frac{\tan\beta}{\frac{\tau_f}{\sin\beta} + \frac{\tau_i}{\cos\beta}} \, d\beta \int_0^{\infty} \phi(\rho z) \exp\left(-\frac{\tau_f z \cos\theta}{\sin\theta}\right) d\rho z \tag{4.16}$$

$$= \frac{1}{\tau_i} \frac{\ln\left(1 + \frac{\tau_f}{\tau_i \sin\theta}\right)}{\frac{\tau_f}{\tau_i \sin\theta}} \int_0^{\infty} \phi(\rho z) \exp\left(-\frac{\tau_f z \cos\theta}{\sin\theta}\right) d\rho z$$

The integral over z is proportional to the intensity which would be observed if the alloy's linear absorption coefficient for the $\nu_i(z_j)$ radiation were τ_f and hence, it can be deduced from the absorption curve. The value of the integral over z is

$$\int_0^{\infty} \phi(\rho z) \exp(-\tau_f z \cot\theta) \, d\rho z = \frac{I_i(z_j)}{I_i^o(z_j)} \, \frac{F\left(\frac{\tau_f}{\rho} \cot\theta\right)}{F(0)} \tag{4.17}$$

The integral B, on integrating over ξ, is

$$B = \int_0^{\frac{\pi}{2}} \int_0^{\infty} \frac{\phi(\rho z) \tan\beta}{\frac{\tau_i}{\cos\beta} - \frac{\tau_f}{\sin\theta}} \left[-\exp\left(-\frac{\tau_i z \cos\theta}{\cos\beta}\right) + \exp\left(-\frac{\tau_f z \cos\theta}{\sin\theta}\right) \right] d\rho z \, d\beta \tag{4.18}$$

Now, only layers relatively deep in the alloy will make a large contribution to this integral, so the approximation which Castaing has used is to replace the function $\phi(\rho z)$ by $\exp(-\sigma\rho z)$ where ρ is the density of the alloy and σ is a coefficient in the neighborhood of the mass absorption coefficient according to Lenard (29). However, since the Lenard law is not strictly correct because of back-scattering, the actual value which Castaing uses for the constant σ is determined from the asymptotic behavior of the absorption curves ($1/\sigma$ is the slope of $F(0)/F(X)$ as X approaches 0).

With this substitution, the integral B becomes

$$B = \int_0^{\frac{\pi}{2}} \int_0^{\infty} \frac{\tan\beta}{\frac{\tau_i}{\cos\beta} - \frac{\tau_i}{\sin}} \left\{ \exp\left[(-\sigma\rho - \tau_f \cot\theta) z \right] - \exp\left[\left(-\sigma\rho - \frac{\tau_i \cos\theta}{\cos\beta} \right) z \right] \right\} d\rho z \, d\beta \qquad (4.19)$$

The integration over z can now be performed and the result is

$$B = \int_0^{\frac{\pi}{2}} \frac{1}{\tau_i} \frac{\rho}{(\sigma\rho + \tau_f \cot\theta)} \frac{\sin\beta}{\left(1 + \frac{\sigma\rho}{\tau_i} \frac{\cos\beta}{\cos\theta}\right)} \, d\beta \qquad (4.19a)$$

Now, since

$$\frac{\rho I_i^o(z_j)}{(\sigma\rho + \tau_f \cot\theta)} = \int_0^{\infty} I_i^o(z_j) \exp\left[-(\sigma\rho + \tau_f \cot\theta) z \right] d\rho z$$

$$= I_i'(z_j) \frac{F\left(\frac{\tau_f}{\rho}\cot\theta\right)}{F(0)}$$

we have

$$B = \frac{1}{\tau_i} \frac{I_i'(z_j)}{I_i^o(z_j)} \int_0^{\frac{\pi}{2}} \frac{\sin \beta}{\left(1 - \frac{\sigma\rho \cos \beta}{\tau_i \cos \theta}\right)} d\beta$$

$$= \frac{1}{\tau_i} \frac{I_i'(z_j)}{I_i^o(z_j)} \frac{\ln \left| 1 + \frac{\sigma\rho}{\tau_i \cos \theta} \right|}{\frac{\sigma\rho}{\tau_i \cos \theta}} \qquad (4.20)$$

Substituting the values of the integrals A and B as given by equations 4.16 and 4.20, we obtain the total fluorescence intensity due to excitation by the characteristic lines

$$I_f = \sum_{ij} A_{ij}(Z_f) I_i(Z_j) \frac{F\left(\frac{\tau_f}{\rho} \cot \theta\right)}{F(0)} \frac{1}{\tau_i} \left[\frac{\ln(1+u)}{u} + \frac{\ln(1+v)}{v}\right] \qquad (4.21)$$

where

$$u = \frac{\tau_f}{\tau_i \sin \theta} \qquad ; \qquad v = \frac{\sigma\rho}{\tau_i \cos \theta}$$

This will be referred to as Castaing's approximation, since it is similar to that developed in his thesis for the case of an electron beam incident normally on the surface of the target. The derivation given here includes the effect of varying the angle of incidence of the electron beam.

It is difficult to visualize the accuracy of Castaing's approximation considering the shape of the experimentally determined curves for $\phi(\rho z)$ (see fig. 1, p. 23). Replacing $\phi(\rho z)$ by $\exp(-\sigma\rho z)$ where σ is

determined by the slope of the tangent to the absorption curve at its origin is equivalent to replacing log $\phi(\rho z)$ by a straight line passing through the point $\rho z = 0$, $\log \phi(\rho z) = 1$. Reference to the experimentally determined curves show that there are in fact two errors: (1) the distribution of primary exciting radiation as a function of is incorrect, and (2) the total amount of primary exciting radiation is too low. The second error is partially corrected after integration over z by putting back the true intensity determined from the absorption curves in place of the rational terms involving σ . It is clear, however, that the maximum which occurs in the curve $\phi(\rho z)$ will in general make the integral B in the above derivation of more importance.

We will now attempt to make a more accurate approximation to integral B. We have seen in section B that it is very difficult to deduce the curves $\phi(\rho z)$ theoretically, and for the purpose of this correction it will be sufficient to use the experimental curves as determined by Castaing and Descamps. In addition to a reasonable fit to the experimental curves, we require only that their mathematical representation be in such a form that the integral B can be calculated. These requirements are satisfied if the function $\phi(\rho z)$ is expanded in a series of the form

$$\phi(\rho z) = \sum_{n=0}^{\infty} a_n \left\{ \exp\left[-b(\rho z - \rho z_o)\right] - 1 \right\}^{2n} \qquad (4.22)$$

where ρz_o is the value of ρz at which the maximum in ϕ occurs. The series is rapidly convergent to $\phi(\rho z)$ for the proper choice of the

constant b, and we can therefore neglect all terms except the first two. The requirement that $\phi(\infty) = 0$ further simplifies equation 4.22 to an equation of the following form:

$$\phi(\rho z) = C \left\{ 1 - \left[\exp(-b(\rho z - \rho z_o) - 1 \right]^2 \right\} \tag{4.23}$$

It is now a simple matter to evaluate the constants C and b to fit the experimental curves at two arbitrary points. Taking these points to be the maximum point and the point at which $\phi(\rho z) = 1$, we obtain the following values of the constants ρz_o, C, and b for aluminum, copper, and gold from Castaing's curves:

	Aluminum	Copper	Gold
ρz_o	$.31 \times 10^{-3}$	$.20 \times 10^{-3}$	$.16 \times 10^{-3}$
b	2.27×10^{3}	2.48×10^{3}	2.73×10^{3}
C	1.91	2.01	2.28

TABLE 1

The fit is very good except for aluminum where equation 4.23 predicts a negative value of $\phi(\rho z)$ for $\rho z = 0$, which is physically impossible.* The error even in this extreme case should be less than that involved in Castaing's approximation, however. Substituting from equation 4.23 in equation 4.19 we obtain for B the following equation:

---

* The fit for aluminum would undoubtedly be better if it were possible to determine $\phi(\rho z)$ using a more favorable tracer than copper.

$$B = \int_0^{\frac{\pi}{2}} \int_0^{\infty} \frac{C \tan \beta}{\left(\frac{\tau_i}{\cos \beta} - \frac{\tau_f}{\sin \theta} \right)} \left\{ 2 \exp \left[-b(\rho z - \rho z_o) \right] - \exp \left[-2b(\rho z - \rho z_o) \right] \right\}$$

$$\times \left\{ -\exp \left[- \frac{\tau_i z \cos \theta}{\cos \beta} \right] + \exp \left[- \frac{\tau_f z \cos \theta}{\sin \theta} \right] d\rho z \, d\beta \right\} \quad (4.24)$$

On integration over z , this becomes

$$B = \int_0^{\frac{\pi}{2}} \frac{C \sin \beta}{\tau_i} \left\{ \frac{\rho\, 2 \exp (b\rho z_o)}{\left(b\rho + \frac{\tau_f \cos \theta}{\sin \theta} \right) \left(1 + \frac{b\rho \cos \beta}{\tau_i \cos \theta} \right)} \right.$$

$$\left. - \frac{\rho \exp (2b\rho z_o)}{\left(2b\rho + \frac{\tau_i \cos \theta}{\cos \beta} \right) \left(1 + \frac{2b\rho \cos \beta}{\cos \theta} \right)} \right\} d\beta \quad (4.25)$$

The integration over β can then be performed

$$B = \frac{C}{\tau_i} \left\{ \frac{\rho 2 \exp (b\rho z_o)}{\left(b\rho + \frac{\tau_f \cos \theta}{\sin \theta} \right)} \frac{\ln \left(1 + \frac{b\rho}{\tau_i \cos \theta} \right)}{\frac{b\rho}{\tau_i \cos \theta}} \right.$$

$$\left. - \frac{\rho \exp (2b\rho z_o)}{\left(2b\rho + \frac{\tau_f \cos \theta}{\sin \theta} \right)} \frac{\ln \left(1 + \frac{2b\rho}{\tau_i \cos \theta} \right)}{\frac{2b\rho}{\tau_i \cos \theta}} \right\} \quad (4.26)$$

Now, it is desirable to eliminate the term $I_i^o (Z_j)$ which appears in equation 4.15 as a factor multiplying B. To do this, we note that the second term in equation 4.26 is in general less than the first term. We can express the second term in terms of the first and also make use of

the relation (4.17) which was used to eliminate the $I_i^o(Z_j)$ multiplying the integral A. Equation 4.17, on substituting for $\phi(\rho z)$ and integrating over z from 4.23 is

$$\frac{I_i(Z_j)F(\frac{\tau_f}{\rho}\cot\theta)}{I_i^o(Z_j)\,F(0)} = \left[\frac{2\exp(b\rho z_o)}{(b+X)} - \frac{\exp(2b\rho z_o)}{(2b+X)}\right] C \qquad (4.27)$$

where

$$X = \frac{\tau_f}{\rho}\cot\theta$$

Solving equation 4.27 for C and substituting the result into 4.26 we would have

$$B = \frac{1}{\tau_i}\,\frac{I_i(Z_j)}{I_i^o(Z_j)}\,\frac{F(X)}{F(0)}\left\{\frac{\ln\left(1+\frac{b\rho}{\tau_i\cos\theta}\right)}{\frac{b\rho}{\tau_i\cos\theta}}\;\frac{1}{\left[1-\frac{(b+X)}{2(2b+X)}\exp(b\rho z_o)\right]}\right.$$

$$\left. + \frac{1}{2\left[1-\frac{2(2b+X)}{(b+X)}\exp(-b\rho z_o)\right]}\;\frac{\ln\left(1+\frac{2b\rho}{\tau_i\cos\theta}\right)}{\frac{b\rho}{\tau_i\cos\theta}}\right\} \qquad (4.28)$$

It is usually the case that X may be neglected compared to b and let us assume that this is the case.

Finally, substituting this value of B and the value of A which we had from 4.16 and 4.17, we would have for the fluorescence correction

$$I_f' = \sum_{ij} A_{ij}(Z_f)\, I_i(Z_f)\, \frac{F(X)}{F(0)} \left\{ \frac{\ln(1+u)}{u} + \frac{\ln(1+y)}{\left[1 - \frac{1}{4}\exp(b\rho z_o)\right] y} \right.$$

$$\left. + \frac{\ln(1+2y)}{2\left[1 - 4\exp(-b\rho z_o)\right] y} \right\} \qquad (4.29)$$

where $A_{ij}(Z_f)$ is given by equation 4.10,

$$X = \frac{\tau_f}{\rho} \cot \theta$$

$$u = \frac{\tau_f}{\tau_i \sin \theta}$$

$$y = \frac{b\rho}{\tau_i \cos \theta}$$

and the values of b and ρz_o are determined from Table 1, with interpolation if necessary.

We have expressed the fluorescence correction in terms of the intensity of the exciting radiation and, therefore, to correct the intensity of radiation which has the wavelength of the fluorescence line we must have some method of comparing the intensities of the two different lines. One possibility of doing this might exist in making use of known intensity ratios of different lines from the same series to calibrate the

spectrometer sensitivity as a function of wavelength. For example, one might use the $K_{\alpha 1}$ and $K_{\beta 1}$ lines for a number of elements. Each element would provide a value for the relative sensitivity of the spectrometer at two different wavelengths. Under the restriction that the sensitivity of the spectrometer is a continuous function of wavelength, it would be then possible to deduce this function. This process, however, in addition to restricting the choice of the detector and crystal to exclude elements which have selective absorption for wavelengths lying within the spectrometer range is also subject to large cumulative errors.

In general, when the correction for fluorescence radiation excited by the line spectra is important, that is, when there is strong selective absorption by one element of the target for the radiation emitted by another element in the target, the fluorescence line of the absorbing element is not widely different in wavelength from the exciting line. Therefore, following Castaing (15) we may assume that the relative excitation of these lines can be obtained from the classical ionization function, for example, Rossland's ionization function (30).

The ratio of the number of q_f and q_i ionizations created per second by the electron beam in the same path length is then

$$\frac{n_{q_f}}{n_{q_i}} = \frac{\phi(E, E_{q_f}, N_{q_f})}{\phi(E, E_{q_i}, N_{q_i})} = \frac{N_{q_f}}{N_{q_i}} \frac{\left(\frac{E - E_{q_f}}{E^2 E_{q_f}}\right)}{\left(\frac{E - E_{q_i}}{E^2 E_{q_i}}\right)} \qquad (4.30)$$

where E_{q_f} and E_{q_i} are the energies necessary for the q_f and q_i

ionizations, E is the energy of the electrons, and N_{q_f} and N_{q_i} are the number of q_i and q_f electrons per unit volume of the alloy. Neglecting E_{q_f} and E_{q_i} compared to E, we have

$$\frac{n_{q_f}}{n_{q_i}} = \frac{N_{q_f}}{N_{q_i}} \frac{\nu_i(Z_j)}{\nu_f(Z_f)} \tag{4.31}$$

Consequently, the ratios of the intensity of the emission line $I_i(Z_j)$ which causes the excitation and the intensity $I_i(Z_f)$ of the corresponding line of Z_f has the following value for each layer of the target:

$$\frac{dI_i(Z_j)}{dI_i(Z_f)} = \frac{\omega_{q_i}(Z_j)}{\omega_{q_f}(Z_f)} \frac{n_{q_i}}{n_{q_f}} \frac{x_i(Z_j)}{x_i(Z_f)} \frac{\nu_i(Z_j)}{\nu_i(Z_f)} \tag{4.32}$$

But we desire a relationship to the intensity of frequency $\nu_f(Z_f)$ and this can be obtained from equation 4.7 and the analogous equation for $x_i(Z_j)$

$$x_i(Z_j) = \frac{I_i(Z_j)}{\nu_i(Z_j)} \frac{1}{\sum_{i'} I_{i'}(Z_j)/\nu_{i'}} \tag{4.33}$$

which gives

$$dI_i(Z_f) = \frac{dI_f(Z_f)\ \nu_i(Z_f)\ x_i\ (Z_f)}{\nu_f(Z_f)\ x_f(Z_f)} \tag{4.34}$$

Substituting equation 4.34 into 4.32 we would have

$$\frac{dI_i(Z_j)}{dI_f(Z_f)} = \frac{\omega_q(Z_j)}{\omega_q(Z_f)} \frac{n_{q_i}}{n_{q_f}} \frac{x_i(Z_j)}{x_f(Z_f)} \frac{\nu_i(Z_j)}{\nu_f(Z_j)} \quad (4.35$$

Let this quantity be M. Now

$$\frac{I_i(Z_j)}{F(0)} F(\frac{\tau_f}{\rho_f} \cot\theta) = \int dI_i^o (Z_j) e^{-\tau_f \cot\theta z} dz$$

$$= \int M dI_f(Z_f) e^{-\tau_f \cot\theta z} = M I_f'(Z_f) \quad (4.36)$$

where $I_f'(Z_f)$ is the observed primary intensity of frequency ν_f .
We can now compute the multiplying factor which appears in all the correction formulae. Let us call this B_{ij} . Combining equations 4.10, 4.31, 4.35, and 4.36 we would have for B_{ij}

$$B_{ij} = A_{ij}(Z_f) I_i(Z_j) \frac{F(\frac{\tau_f}{\rho} \cot\theta)}{F(0)}$$

$$= \frac{1}{2} I_f'(Z_f) (\frac{r_f - 1}{r_f}) \omega_q(Z_i) \frac{\nu_f(Z_f)}{\nu_i(Z_j)} x_i(Z_j) m_f \frac{\mu_i(Z_f)}{\rho_i} \frac{N_{q_i}}{N_{q_f}}$$

(4.37)

A special case exists when both series of lines belong to the same excitation level (K or L) and for atomic numbers greater than 10. In this case

$$\frac{N_{q_i}}{N_{q_f}} = \frac{m_i A_f}{A_i m_f}$$

We may summarize the three approximations as follows:

$$I_f = \sum_{ij} B_{ij} I_f'(Z_f) \frac{F(0)}{F(X)} \frac{1}{\tau_i} \frac{\ln(1+u)}{u} \tag{4.38a}$$

$$I_f = \sum_{ij} B_{ij} I_f'(Z_f) \frac{1}{\tau_i} \left[\frac{\ln(1+u)}{u} + \frac{\ln(1+v)}{v} \right] \tag{4.38b}$$

$$I_f = \sum_{ij} B_{ij}(Z_f)\, I_i(Z_f) \frac{1}{\tau_i} \left\{ \frac{\ln(1+u)}{u} + \frac{\ln(1+y)}{\left[1 - \frac{1}{4}\exp(b\,\rho z_o)\right] y} + \frac{\ln(1+2y)}{2\left[1 - 4\exp(-b\,\rho z_o)\right] y} \right\} \tag{4.38c}$$

where $u = \dfrac{\tau_f}{\tau_i \sin\theta}$

$$X = \frac{\tau_f}{\rho} \cot\theta$$

$$v = \frac{\sigma\rho}{\tau_i \cos\theta}$$

$$y = \frac{b\rho}{\tau_i \cos\theta}$$

and $I_f'(Z_j)$ is the observed primary intensity of frequency ν_f.

c. Effect of fluorescence excitation on the accuracy in the analysis of small precipitates

Because matter is in general more transparent to x-rays than to electrons, there is the possibility that the fluorescence radiation can originate from a larger volume of the sample than the primary radiation. In the absence of fluorescence excitation, the spatial resolution of the analysis is limited only by the size of the electron probe and by the diffusion and penetration of electrons in the target. The size of the volume element which is directly excited by electrons making up the probe is usually of the order of 10 to 30 cubic microns (see p. 67). However, if one attempts to determine the mass concentration of an element in a precipitate which is of this size, an error will result if the matrix also contains the element, since the volume of the region which can be fluorescence excited is larger than the region directly excited. The error due to this fluorescence radiation will depend on the concentration of the element in question in the matrix and in the precipitate. (As a result of the comparison of x-ray intensities from a heterogeneous target with the intensity from a pure element, an error can occur even if the concentration of the element is 0 in the precipitate.)

As a first approximation, if the precipitates or inclusions are at the limit of the spatial resolution of the analysis, we may assume that the primary radiation originates only in the precipitate, while the fluorescence radiation originates mainly in the matrix in which the precipitate is imbedded. In this situation, if estimates can be obtained on the composition of the matrix and precipitate, it is still possible to correct for the relatively large fluorescence excitation which may result

from the selective absorption of the characteristic radiation produced in the target. However, the fluorescence radiation excited by the continuum, although smaller in magnitude, can also result in an error in the determination of the composition of the precipitate; and it is this error which we would like to estimate.

Castaing and Descamps (18) have investigated the magnitude of the fluorescence radiation which is excited in a pure zinc target by the continuum and have considered its effect on the determination of the composition of precipitates in two extreme cases:

(1) The matrix contains none of the element, A, whose concentration is being determined in the precipitate. In this case, the fluorescence radiation present when pure A is being analyzed would be added to the primary radiation. Thus, the apparent concentration c'_A of A in the precipitate which would result from using approximation 2.7 would be given by

$$c'_A = \frac{I_A}{I(A) + I_f(A)} \tag{5.1}$$

where $I_f(A)$ denotes the fluorescence radiation of the $K_{\alpha 1}(A)$ line due to excitation by the continuum when a target of pure A is under the probe. The true concentration, c_A, would be related to the apparent concentration as follows:

$$c_A = c'_A \left(1 + \frac{I_f(A)}{I(A)} \right) \tag{5.2}$$

(2) The matrix consists entirely of the element whose concentration is being determined in the precipitate. In this case, the use of approximation 2.7 would give an apparent concentration c_A' which is

$$c_A' = \frac{c_A I(A) + k\, I_f(A)}{I(A) + I_f(A)} \tag{5.3}$$

where k is the ratio of the mean atomic number of the precipitate and the mean atomic number of the element A. We would then have the following relation between the apparent concentration and the true concentration:

$$c_A' - c_A = \left(1 - \frac{c_A'}{k}\right) \frac{k\, I_f(A)}{I(A) + I_f(A)}$$

$$\doteq \left(1 - \frac{c_A'}{k}\right) \frac{k\, I_f(A)}{I(A)} \tag{5.4}$$

This result differs from that obtained by Castaing and Descamps, and we may attribute the discrepancy to the fact that they have incorrectly taken the denominator of equation 5.3 to be $I(A) + k\, I_f(A)$.

The measured concentration is thus too low in case (1) where the matrix is free of the element being analyzed, and may be either too high or too low for case (2) where the matrix consists entirely of the element being analyzed. In this latter case, the error is an absolute error rather than a relative error and is small only if c_A/k is not too small. If c_A/k is small compared to unity, we have the possibility of the correction factor exceeding c_A' and therefore a large uncertainty.

As an example of the magnitude of the fluorescence radiation due to the continuum, we may cite the results obtained by Castaing and Descamps (18) for a pure zinc target. This is important for estimating the correction in the above formulae and for obtaining limits on c_A/k in the second case, below which it is impossible to make an accurate analysis. The ratio of the intensity of the fluorescence radiation produced to the primary intensity of the Zn $K_{\alpha 1}$ line was found to be approximately 0.068, while the ratio of these intensities actually observed on emerging from the target at an angle of 16 degrees was about 0.036.

d. Limitations imposed by continuous background

The presence of the continuous background of x-radiation imposes a limit on the concentration which can be measured with accuracy and on the concentration which is barely detectable. The x-ray continuum, of course, is not isotropic as is the line radiation emitted by the excited atoms of the target, but is a maximum at right angles to the electron beam (non-relativistic electrons). Unfortunately, because of the physical size of the electron lenses used to form the electron probe, it is necessary to observe the x-rays in a direction close to the direction of maximum intensity of the continuum. In a typical case, with the instrument which is described in chapter III the background is about 1% of the line intensity (unresolved Fe K_α doublet from a pure iron target).

A concentration of 1% would therefore give a signal-to-background ratio of 2. If the signal/background ratio falls much below this, the counting interval to obtain accurate statistics becomes prohibitively long, so this represents a typical value for the lower limit of concentration of an element which must be present in the volume analyzed for quantitative analysis.

The limit of detectability may be taken arbitrarily as that concentration for which the signal is about 10% above background. Thus, in general, concentrations of 1 part in 1,000 are at the limit of detectability, although in certain favorable cases where the mean atomic number of the alloy is very low, smaller concentrations could be detected.

The concentration which can be measured with accuracy and the concentration which is at the limit of detectability are independent of the overall concentration if the alloy is not homogeneous. One must then consider the concentration which is present in the volume which is analyzed. For an electron probe of infinitely small size this volume is probably of the order of 10 cubic microns because of the diffusion of the electrons in the target.* For a probe of about 5 microns in diameter, this volume element is about 30 cubic microns. Consequently, an impurity in an alloy could be detected regardless of overall concentration if it occurs in the form of inclusions or precipitates of greater than 0.03 cubic microns in volume.

---

* Although the electron density falls rapidly with distance from the probe, the size of the volume element at a given distance increases rapidly with r, and this results in a larger contribution to the intensity from distant points than would be estimated on the basis of the one-dimensional diffusion of the electrons.

2. Instrumental Corrections

a. Contamination deposits formed by impact of the electron probe on the specimen

Whenever an electron beam impinges on a surface in a dynamic vacuum system, a layer of contamination is produced as a result of polymerization of organic materials present in the system (31). Extensive studies have been made of these contamination deposits because their insulating properties result in spurious effects in many beam devices, causing apertures and surfaces to become charged and resulting in erratic deflections of the electron beam, or causing an apparent change in the object being studied.

In the electron probe microanalyzer the chief difficulties which are encountered as a result of contamination are (a) a change in the current or size of the probe due to contamination of apertures and (b) a change in the x-ray intensity due to retardation of the electrons which must penetrate the contamination deposits progressively built-up on the specimen. The formation of contamination deposits on the apertures of the beam system requires them to be changed periodically, while the contamination of the surface of the specimen can be simultaneously an advantage and a disadvantage; the brownish deposit can serve to locate the point of impact of the probe, but the reduction of the x-ray intensity as a result of such deposits on the specimen's surface can cause a significant error in the determination of small concentrations where the probe remains fixed for longer periods of time. For example, the intensity of the unresolved Ni K_{α} doublet from a pure nickel target is decreased by about 8% in 10 minutes of bombardment.

In order to minimize the contamination deposit and to understand its effect on the analysis it is desirable to review the mechanism of formation of the deposits and their physical and chemical nature. The constitution of the contamination layer and its rate of formation depends on the nature of the surface being bombarded and the beam current (32), as well as on the nature and quantity of organic vapors present in the vacuum system from diffusion pump fluids, gasket materials, greases, and unclean metal surfaces (33). Usually, the deposit is carbonaceous, light brown to almost black in color, although it may be partly siliceous if silicone greases or fluids are used in the system. The carbonaceous deposits are very hard, have an amorphous structure, and appear in the electron microscope as uniform films or as "shell-round individual particles" (31). They are extremely resistant to chemical solvents and are probably initially a hydrocarbon polymer of the type obtained when a gaseous discharge is passed through hydrocarbon vapor which then becomes partially or totally carbonized under further bombardment. Contamination deposits occur even at very low electron accelerating voltages, because the energy required for these chemical reactions is very small (31).

The thickness of the contamination layer increases almost linearly with time, at least for small current densities, and decreases with increasing temperature of surface bombarded (33). The rate of contamination increases linearly with current density at low current densities but tends to fall off at higher current densities (31), probably because of a limitation in the supply of organic vapors. In relatively

large electron beams, such as would be obtained with an electron gun only, Ennos (31) found that direct condensation of the organic vapors on the surface bombarded was the dominant mechanism, while for electron probes of the order of 10 microns diameter and large current densities (1 - 3 amp/cm^2) Castaing and Descamps (32) found that surface migration of the organic materials to the region under bombardment was most important. In this latter case, the thermal conductivity of the target will determine its temperature and hence, will affect the contamination rate because of the change in the rate of surface migration with temperature.

It is commonly thought that the organic diffusion pump fluids are the worst contributor to the organic vapors present in the vacuum system and that the use of cold traps or mercury vapor pumps will eliminate the source of contamination. However, the work of Ennos on the sources of contamination indicates that this is erroneous (33). The exposure of only a small area of rubber can maintain the vapor pressure of hydrocarbons from the rubber at a level which is very close to the saturation vapor pressure and will result in relative contamination of the order of 1/2 that caused by Apiezon B diffusion pump oil. (Silicone pump oil results in about 1/3 the relative contamination of the organic oil.) Vacuum grease is also an important source of contamination, resulting, in the case of Apiezon M, in a contamination rate of the same order as the organic pump oil. Other sources of contamination are certain plastics and unclean metals (e.g. fingerprints), and these can result in relative contamination rates of the order of 1/2 that of the pump oil.

Ennos found that ordinary grease removers, such as ether or aqueous detergent solutions, were ineffective in eliminating metals as a source of contamination, and that electrical cleanup by a discharge at low pressure also failed to remove the source of contamination on the surface of the metals. Only a chemical cleaning, such as acid attack of the surface layer, was effective, but even in this case parts which subsequently heated in the vacuum, such as parts of the electron gun, could act as a source of contamination unless the parts were baked out in the vacuum at 150 degrees C for several hours.

The difficulties in having a dynamic vacuum system which is free from sources of contamination has led to the development of three methods of reducing the contamination rate other than eliminating the sources of contamination. Ennos found that either heating the bombarded surface to 250 degrees C or surrounding it with a cold trap effectively reduced the contamination rate (31). Castaing and Descamps found that it was not only possible to reduce the rate of formation of the deposits but also to remove existing deposits in an electron probe microanalyzer by directing a jet of low pressure air on the region while it is under the electron probe (32). The pressure of the jet is controlled by a manometer so that the gas flow is limited to 0.025 mg/sec, which enables the pressure in the system to be maintained sufficiently low for the operation of the electron beam.

These methods of reducing the contamination rate have certain practical disadvantages. Heating the sample to 250 degrees is

certainly undesirable in the study of alloys which would undergo changes at these temperatures. On the other hand, the use of a cold trap is impractical because of space limitations in the target region due to the necessity of having a means of viewing the surface of the specimen and of having an unhindered path for the x-rays to the spectrometer. The third alternative, the use of a blast of air as suggested by Castaing and Descamps, has two undesirable effects as a result of operating the beam at higher pressures: (a) the filament life is reduced, and (b) the contamination rate of other parts of the beam system is increased due to greater back diffusion of vapors from the pump.

The simplest solution consists in reducing the sources of contamination as much as possible and attempting to correct for the effect of remaining contamination. Fortunately the effect of the contamination in reducing the intensity of the x-rays is linear for periods of the order of 10 minutes. The results of an experimental verification of this obtained by the author are given in fig. 6. In this figure, the intensity of the unresolved K_{α} doublet from a target consisting of pure nickel is plotted as a function of time of bombardment. The electron probe had a diameter of about 5 microns with a current of 9×10^{-8} amps. One should note that the intensity is plotted on an expanded scale and that the total reduction in intensity in 1080 seconds is about 8%. In the measurements on small concentrations where times of this order may be involved, it is desirable to divide the counting interval into several parts and average the resulting number of counts/unit time.

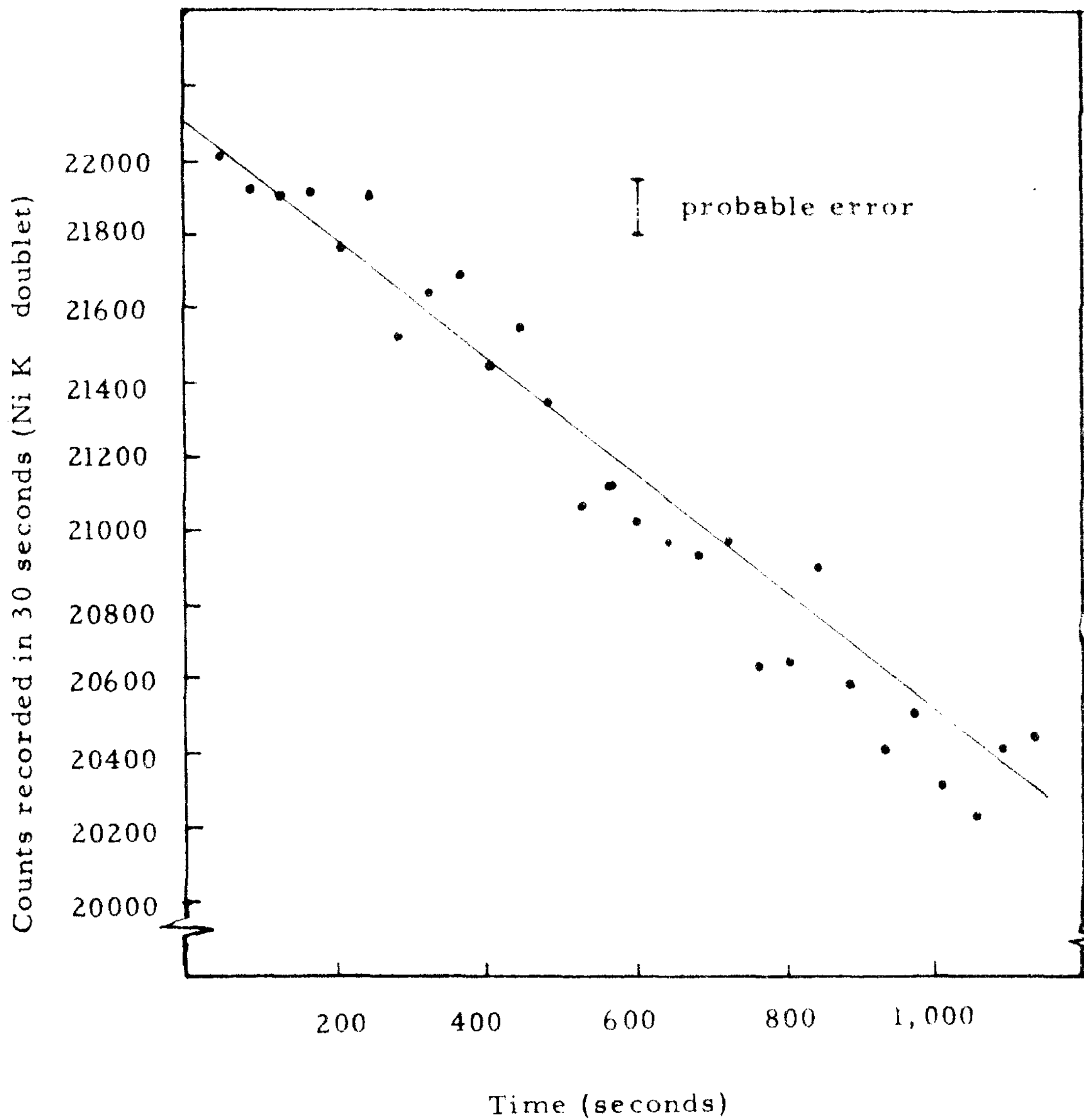

FIG. 6 Reduction in x-ray intensity due to formation of contamination deposit on a nickel target.

The effect of the contamination will also lead to a different value of the x-ray intensities if more than one element is analyzed at each point depending on the order in which the measurements are made. However, the linearity of the reduction in intensity as a function of time makes it possible to correct for this effect by simply repeating the set of intensity measurements at each point in the opposite order and averaging the two values obtained for each element. This procedure does not increase the time necessary for the measurements significantly since the statistical error depends only on the total number of counts recorded.

b. Dead time of the detector

In addition to the corrections which have been discussed, one must correct for the loss of intensity which will occur at high counting rates due to the finite resolving time of the detector. This is important in the method of analysis because of the comparison which is made of the intensities from heterogeneous targets to the intensity obtained with pure metals as targets. On a target consisting of a pure metal counting rates of the order of 1000 counts/second are attained in the microanalyzer if a detector of high efficiency is used. If this detector consists of an ordinary geiger tube, the error in the counting rate can be 10% or more depending on the length of time that the detector is insensitive after each pulse. This insensitive time will be the sum of the dead time which depends on the geometry of the counter, weight and pressure of the fill gas, and operating voltage, and the resolving

time which depends on the operating voltage and the setting of the discriminator. Unfortunately, geiger tubes which are efficient for x-radiation down to wavelengths of 1.1 Å have dead times which are inherently long (≈ 200-300 microseconds) because of the need to use fill gases of high atomic number and relatively high pressure.

The usual procedure for correcting for the insensitive time of the geiger counter is to apply the following formula:

$$N = \frac{N_c}{1 - N_c \tau} \qquad (6.1)$$

where N is the number of ionizing events per second, N_c is the number of counts per second and τ is the insensitive time. A value of may be estimated from the geometry, fill, and operating voltage of the counter, but if the counting rate exceeds 100 counts/second τ must be measured by varying the counting rate in a known way and applying equation 6.1. *

Two difficulties are present in this method of correction: (a) the value of τ is a function of counting rate and (b) the calibration (or value of τ) is subject to hysteresis. The first difficulty

* This can be accomplished in the instrument by using as a source of radiation the characteristic x-radiation from a pure target. The current in the electron probe can be varied independently of the accelerating voltage by varying the temperature of the filament or the bias potential on the grid of the electron gun. It is necessary that the target be insulated so that the beam current can be measured. The true counting rate will be directly proportional to the target current, and the deviation of the observed counting rate from proportionality to the target current is therefore an indication of the dead time.

could be overcome by the use of calibration curves. The second difficulty, however, constitutes a fundamental restriction on the accuracy which is attainable with ordinary geiger tubes.* For example, if the counting rate is suddenly reduced from an initially high value, the ratio of the number of spurious counts to real counts will also decrease but will remain at an abnormally high value for some time.

It is well to consider at this point other detectors which might be used in this application. Beaded-wire geiger counters have been devised which have lower dead times than conventional types due to the fact that the discharge is restricted to the length of wire between beads (34). However, in order to obtain sufficient gas absorption path for sensitivity at the shorter wavelengths either an end-window type must be used or the diameter of the counter must be large, leading to excessive operating voltages. The end-window beaded-wire counter is not suitable for use over a wide range of wavelengths, because the dead time then becomes a function of the wavelength of the x-rays since the number of effective segments is reduced as the radiation becomes less penetrating.

The scintillation counter has the advantages of a high sensitivity and a small resolving time. However, for most scintillation crystals which are efficient in the x-ray region (e.g. NaI) the pulse height from

---

* This restriction can be more important in microanalysis by means of x-rays than the limitation in accuracy due to statistical fluctuations.

the softer x-radiation is of the order of the pulse height due to thermal noise in the photomultiplier tube.* It is therefore unsuitable for measuring intensities of wavelengths longer than 2.75 Å (Ti K_{α}) if these measurements are to be made in a routine fashion (35).

The proportional counter has good sensitivity and small dead times, but the pulse height is about 1/100 to 1/1000 of the pulse height obtained from a geiger counter. This is a serious disadvantage in using a proportional counter in a vacuum spectrometer, since one must either use an amplifier of several stages within the vacuum system or drive an external amplifier through a cable having shunt capacitance to ground.

One can reduce somewhat the long dead times associated with the geiger tube by making use of electronic quench circuits. However, these do not work well if there is a large distributed capacitance in the cable to the geiger tube. Furthermore, there is no assurance that an externally quenched counter will be any more stable with regard to its calibration than a counter which is internally quenched.

One possibility of insuring constancy of the calibration of a geiger counter, however, is simply to use it in such a way that it is never subjected to high counting rates. This could be done by using a

---

* Sternglass (Westinghouse Scientific Paper 8-1043-p3) has recently developed a high-speed electron multiplier which uses secondary electrons emitted from the opposite side of thin insulating films. This electron multiplier might overcome the disadvantage of conventional multiplier tubes in this application because of its low thermal noise. It might also prove feasible to use the photoelectrons emitted by impact of x-rays on the first dynode of this multiplier and hence to eliminate the need for a scintillating crystal.

multicellular geiger tube in which the counting rate received by each cell is only 1/n of the total counting rate where n is the number of cells. Such a counter is particularly adapted to use in a focusing x-ray spectrometer, because the window area necessary for the detection of the x-rays is long and narrow and hence, the cells can be arranged in a linear array. A relatively small number of cells suffices to reduce the dead time correction a large factor.

The number of counts lost as a result of dead time is approximately equal to $N_c^2 \tau$ but each cell receives only 1/n of the total intensity. The counts lost in each cell is therefore $(N_c/n)^2 \tau$, and the total counts lost is $n(N_c/n)^2 \tau$. But there is also a substantial reduction in the value of τ because the diameter of each cell is d/n where d is the diameter of a single cell counter which would suffice to collect the same intensity from the crystal of the spectrometer. Since the dead time of a geiger tube depends roughly on the square of the diameter (36), the overall reduction in the effective dead time of the multicellular geiger counter would be $\approx 1/n^3$. Moreover, the number of spurious counts should not be increased since the cathode area of n cells of diameter d/n is the same as the cathode area of a single counter of diameter d.

An additional advantage of the multicellular geiger counter is a much lower operating voltage for the same pressure of fill gas. This is particularly important in the case of a vacuum spectrometer where some difficulty is caused by the variation of surface resistivity of

insulators which become coated with vapors from the diffusion pump. The author observed a tremendous number of spurious counts due to surface leakage when a vacuum spectrometer was opened to air after evacuation, and this was undoubtedly due to the tendency of such oil films to adsorb water vapor.

c. Drift of the beam current

It is relatively easy to regulate the voltage of the electron beam electronically to a few parts in 10,000. The beam current, however, is much more difficult to stabilize, for even with the use of a self-biased triode electron gun as an electron source in the probe, the beam current is subject to a gradual drift due to the progressive contamination of apertures. One can overcome this difficulty by collecting the current which is incident on the target and either (1) electronically controlling the gun bias so as to maintain this current constant, or (2) integrating the current and using the total charge collected by the target to control the gate in the scaler (the intensity of the characteristic x-ray lines is directly proportional to the beam current). Both of these possibilities are subject to a possible error from the fact that the current collected by the target is always different from the true beam current and will vary with the composition and surface condition of the target. It is necessary to investigate the effect of this on the approximations derived in the preceding sections.

The approximations in the preceding sections were derived assuming that the true beam current remained fixed and that the x-ray

intensities were measured. We will refer to this case as the fixed-time measurement. If the target current is integrated to control the gate of the detector*, on the other hand, the detector records the number of x-ray quanta received by the crystal of the spectrometer for a given charge collected by the target. We will refer to this case as the fixed-charge measurement.

McMullen (4) has found that there exists an angle of incidence for the primary electrons for which the number of secondary electrons received by a collector subtending an angle of 30 degrees is virtually independent of the composition of the target. For primary electrons having an energy of 30 kev this is a grazing angle of about 29 degrees. There is, therefore, a possibility of automatically compensating for the effect of a varying number of secondary electrons in the fixed-charge measurement by choosing the angle of the surface of the target with respect to the axis of the electron beam so that the proportionality of target current and beam current is independent of the composition of the target. One then has the conditions appropriate to the fixed-time measurement, and we have seen that this results in proportionality of the x-ray line intensity to concentration in the first approximation.

We have seen also that the approximation of proportionality of emission and concentration is not the most useful for accurate

---

* This is the simpler of the two means for compensating for current drifts, since the electron gun is about 30 kv negative with respect to the target and electronic control of the bias potential would be difficult.

quantitative work when the atomic numbers of the elements comprising the target are widely different and that it is necessary to introduce empirically determined parameters α_i. Therefore, if the more accurate approximation of equation 2.7 is used in the fixed-charge measurement, it is not necessary to make any correction for variation in the ratio of target current to beam current with variation in target composition since this will merely change the value of the empirically determined parameters, α_i. In this case, there is a possibility that the accuracy of an analysis based on the use of equation 2.7 can be improved by the fixed-charge measurement of the x-rays.

To see how such an improvement can result let us recall that a large number of the high energy secondary electrons (sometimes called rediffused electrons) have energies in the neighborhood of the energy of the incident beam (see p.24). For the most part, they will therefore have not caused ionization of the target atoms in their inner shells. Consequently, if these electrons are not included in the measurement of the current on the target, the measured current is more nearly equal to the "effective" current. In this case, the coefficients, α_i, will be less dependent on the scattering properties of the target and hence one would expect them to be less dependent on the composition of the alloy.

In addition to the high energy secondary electrons, there are also low energy secondary electrons emitted from the surface of the target. The emission of low energy secondary electrons, however, is chiefly a surface effect and will be only of minor importance for primary

electrons, which are incident at large angles to the target's surface and which have energies of 30 kev, because of the large depth of penetration of the primaries. The author has verified this experimentally, using targets of titanium and nickel which were biased at a positive potential ranging from 0 to 300 volts. Since the target is normally in a field-free space, the change in target current with bias voltage will be a measure of the quantity of low energy secondaries which, according to Schonland (25), have energies which seldom exceed 30 ev for velocities of the primary electrons ranging from .2 to .4 of the velocity of light. The total change in target current which the author observed was less than 1 or 2% for target bias up to +300 volts, and most of this change occurred when the bias was only +10 volts. On the other hand, the ratio of the target current to the current collected in a Faraday cage was of the order of 70 to 75%, and therefore the percentage of secondary electrons which had very low energies was a small fraction of the total number of secondary electrons.

Because the emission of low energy electrons is primarily a surface effect, it is necessary to investigate the effect of the progressive building up of a contamination deposit under the electron probe on the current received by the target. The author has experimentally verified that the contamination deposits have a negligible effect on the current collected by the target. The decrease in x-ray intensity with time as a result of the contamination layer must therefore be due to a decrease in the energy of the primary electrons

without change in the number of electrons. (The x-ray self-absorption in the deposits is negligible compared to the energy loss of the electrons.) In the first approximation, therefore, the reduction of x-ray intensity due to the contamination deposit is also linear with the time in the case of fixed-charge measurement. One has second order effects from the fact that the time to collect a given charge may vary slightly with composition of the target.

Let us define r_i as the ratio of the number of high energy secondary electrons to the number of primary electrons incident on a target consisting of element i. Then, to a good approximation, r_i is given by

$$r_i = 1 - \frac{\text{Target current collected on element i}}{\text{Faraday cage current}} \qquad (6.1)$$

Now in the fixed-time measurement the analysis is accomplished by applying equation 2.7 where in the first approximation $\alpha_i = 1$ for all i. This approximation was true to the extent that the integral of $\phi_i(\rho z)$ was a constant independent of the target material. In the case of the fixed-charge measurement we would have a different first approximation. To see what this first approximation will be, let us assume that we make a redetermination of the function under the conditions of the fixed-charge measurement, and let us call the function determined in this way $\phi_i'(\rho z)$. This new excitation distribution function will be related to the old function by an equation involving r_i which is

$$\int_0^{\infty} \phi_i' (\rho z) \, d\rho z \left[1 - r_i\right] = \int_0^{\infty} \phi_i(\rho z) \, d\rho z \tag{6.2}$$

The desired first approximation is therefore

$$\int_0^{\infty} \phi_i' (\rho z) \, d\rho z \left[1 - r_i\right] = K \tag{6.3}$$

where K is a constant.

Let us now consider a binary alloy consisting of A and B. In the limit of small concentration of A, we would have from equations 2.4 and 2.7,

$$\frac{\alpha_A}{\alpha_B} = \frac{\int_0^{\infty} \phi_B (\rho z) \, d\rho z}{\int_0^{\infty} \phi_A (\rho z) \, d\rho z} \tag{6.4}$$

Hence, a suitable first approximation to the α_i in the fixed-charge measurement would be, for the binary alloy,

$$\frac{\alpha_A'}{\alpha_B'} = \frac{1 - r_A}{1 - r_B} \tag{6.5}$$

Up to this point, the argument that the analysis can be improved by compensating for the rediffused electrons through integration of the target current has been founded chiefly on the assumption that the α_i are not independent of the target constitution because of electron scattering. The author has not yet undertaken experiments to verify this, but some confirmation has been obtained by making use of Castaing's

work on aluminum-copper alloys (15). This has been done by modifying the values of $I_{cu}/I(cu)$ which Castaing obtained (fixed time measurement) to correspond to the values which would have been obtained if the gate in the detecting system had been controlled by the charge collected by the specimen. For the target current collected by pure copper, one would have $1 - r_{cu}$ and for that collected by pure aluminum, $1 - r_{al}$. The values of r_{cu} and r_{al} were taken to be .13 and .29 respectively following the work of Schonland (25) on the reflection coefficient for primary electron velocities of .55 the velocity of light. These values are in good agreement with the values obtained by Palluel (24) for primary electron velocities of 0.25 the velocity of light.

Table 2 shows the results of this comparison. Column 1 gives the true mass concentration of copper in the alloy. Column 2 gives the value of $I_{cu}/I(cu)$ which Castaing observed, column 3 gives the value of $\alpha = \alpha_{cu}/\alpha_{al}$ which Castaing obtained from the application of equation 2.7, and column 4 gives the percentage error which results from the approximation that $\alpha = 1$. Column 5 gives the value of $I_{cu} / I(cu)$ which would have been obtained if the measurement had been made over fixed charge collected by the target, column 6 gives the corresponding value of α', and column 7 gives the mass concentration which is obtained from the first approximation for this case, namely $\alpha' = (1 - r_{cu}) / (1 - r_{al})$. The percentage error for this approximation is given in column 8.

1	2	3	4	5	6	7	8
C_{Cu}	$\frac{I_{Cu}}{I(Cu)}$ fixed-time	$\alpha = \frac{\alpha_{Cu}}{\alpha_{Al}}$	% error $\alpha = 1$	$\frac{I_{Cu}}{I(Cu)}$ fixed-charge	α'	C_{Cu} from $\alpha' = .815$	% error $\alpha' = .815$
0.01	0.0099	0.99	1 %	0.0081	0.808	.00994	0.6%
0.04	0.0373	0.93	6.75%	0.0317	0.786	.03855	3.6%
0.53	0.504	0.902	5.1%	0.460	0.755	0.512	3.4%
0.88	0.867	0.89	1.47%	0.848	0.762	0.872	0.91%

TABLE 2

Inspection of this table shows that the spread of the α' is, as we had hoped that it would be, less than the spread of the α. Furthermore, the approximation that $\alpha' = (1 - r_{Cu})(1 - r_{Al})$ apparently is more accurate than the approximation that $\alpha = 1$. The maximum percentage error occurs at the concentration of 0.04 and not at the concentration of 0.53 as would be expected, and this is undoubtedly related to the fluorescence excited by the continuous radiation.

It is interesting to attempt to correct for the fluorescence excitation by making use of the value of $I_f/I(Zn)$ which Castaing and Descamps obtained (see p. 66). Since the atomic number of copper is only one less than that of zinc, only a small error will be made if we

take $I_f/I(Cu) = I_f/I(Zn) = 0.036$. The formula which we will use for correcting for the flourescence is

$$\frac{I_{Cu}'}{I(Cu)'} = \frac{k}{1 - \frac{I_f}{I(Cu)}} - \frac{C_{Cu}\left[(C_{Cu} \cdot 16) + 13\right]}{29} \frac{I_f}{I_{Cu}} \qquad (6.6)$$

where k is the intensity ratio observed and $I'_{Cu}/I'(Cu)$ is the intensity ratio after correction for fluorescence. Using the values of $I_{Cu}/I(Cu)$ from column 5, Table 2, we would obtain the values shown in Table 3.

1'	5'	6'	7'	8'
C_{Cu}	$I'_{Cu}/I'(Cu)$	α'	C_{Cu} from $\alpha' = .815$	% error $\alpha' = .815$
0.01	0.00824	0.823	0.01001	0.1 %
0.04	0.0322	0.790	0.0392	2.0 %
0.53	0.462	0.760	0.513	3.2 %
0.88	0.851	0.794	0.873	0.8 %

TABLE 3

We see that the first approximation is somewhat better after correcting for flourescence radiation. The maximum percentage error now occurs for an alloy whose concentration is $\approx .50$.

III. Design and Construction of an Electron Probe for Local X-Ray Analysis

A. Thermionic vs. Field Emission Sources

Until recently, electron probes have exclusively employed thermionic sources. The suggestion was made by Marton (37) and others that the use of field emission in an electron source for micro-probe devices might result in larger current densities in the electron focal spot. This suggestion was adopted by Pattee (8) at Stanford for application in a scanning x-ray microscope and was also investigated further at the Bureau of Standards (10).

The use of field emission in an electron probe for microanalysis by means of x-rays would have an additional advantage which was first pointed out by Dr. Jesse W. M. DuMond, namely, that because of the small size of the electron source an electron lens system of near unity magnification could be used and would therefore give a greater working distance from the lens to target. This is desirable in order to facilitate the introduction of an optical viewing system which is necessary to locate the point of impact of the probe during the analysis.

As an example of a field emission electron source we may recall the field emission microscope which was mentioned briefly in the first chapter (see p. 4). In this case, the emitter consists of a wire of a refractory metal which has been sharpened by electrolytic etching. Tungsten is most commonly used because of availability and the ease with which it can be etched to form smooth points having a radius of

curvature at the tip of a fraction of a micron. Such an emitter when mounted in a vacuum system and maintained at a negative potential of a few kilovolts relative to an anode at a small distance emits electrons by a mechanism which was first successfully explained by the Fowler-Nordheim theory (38). According to this theory the very high electric field (10^8 to 10^9 v/cm) at the surface of the emitter results in a reduction in the width of the potential barrier which otherwise prevents the escape of the conduction electrons. As a result, the conduction electrons can penetrate or "tunnel" through the potential barrier with a finite probability. The current densities which can be obtained in this way are very high, being of the order of 10^9 amp/cm^2 , but the emission is somewhat unstable unless the pressure of the residual gas in the system is very low (pressures of $< 10^{-12}$ mm of Hg are frequently used). The instability results from changes in work function due to surface contamination and also from bombardment of the emitter by positive ions which are accelerated by the same field as the electrons but in the reverse direction.

The difficulties of applying the field emission source to the electron probe microanalyzer are greater than those involved in its application to the x-ray microscope, for in this latter case the electron beam system can be isolated by the thin foil which serves as a target for the microfocus x-ray tube. The microanalyzer, on the other hand, must not only have a demountable target, but must have a provision for translating the target from outside the vacuum system. Consequently, it is more difficult to achieve sufficiently low pressures in the vacuum system for the field emission source to operate with stability.

In order to investigate the practicability of the field emission source in the electron probe microanalyzer, the author constructed two field emission sources. In the first source an attempt was made to use differential pumping to maintain the cathode assembly at sufficiently low pressures while the target region could be operated at pressures more consistent with reasonable designs for a demountable target which could be moved from outside the vacuum system. This cathode assembly proved completely unsatisfactory, however, and with the development of pulsed thermionic-field emission techniques at Linfield College (39) it became apparent that a field emission cathode based on the application of these techniques had greater promise of success.

In thermionic-field (T-F) emission, the emitter is maintained at an "intermediate" temperature* of about 1800 to 2000 degrees K by means of a tungsten hairpin filament to which the emitter is attached. Under these conditions the application of a dc electric field causes surface migration of the emitter atoms in a manner which leads to instability and eventual breakdown by vacuum arc. However, if the electric field is applied in pulses of about a microsecond duration, stable emission can be obtained at reasonably high residual pressures.

The second field emission cathode which was constructed by the author was devised for pulsed T-F emission and included certain desirable features of the first design, such as provision for orienting

---

* Intermediate between the temperature needed for ordinary thermionic emission and the temperatures at which ordinary field emission is usually studied.

the emitter while the system was evacuated, provision for changing emitters, and provision for viewing the field emission pattern. In addition, this cathode assembly provided for the continuous heating of the emitter and included an intermediate electrode between the emitter and anode to which pulses could be applied. This electrode was intended to serve three purposes: (1) to reduce the height of the pulses which would be needed, (2) to reduce ion bombardment of the emitter by positive ions having the full accelerating voltage, and (3) to give constant accelerating voltage to the electrons making up the electron probe regardless of the height or shape of the pulses. This cathode assembly, along with the pulse generator and other details of the design and application, are described and illustrated in the appendix.

While a modest degree of success was attained with this field emission cathode, experimental tests involving some 17 emitters revealed limitations not only in design but also in the inherent characteristics of this type of source which make it inferior to the thermionic source for an electron probe to be used in x-ray microanalysis. These limitations will be briefly reviewed for the benefit of those who are interested in the practical applications of field emission sources.

1. Temperature effects in the target

The need for using pulsed emission in order to attain stability of field emission in dynamic vacuum systems requires a reconsideration of the effects of heat produced in the target of an electron probe.

The current densities obtained with dc electron probes are many times the current densities which are attained in high power, rotating anode x-ray tubes, but, because of the extremely small dimensions of the electron focal spots, as Castaing (15) has shown, the temperature rise is negligible for targets which are good thermal conductors because of the rapid conduction of heat away from the focus. The calculation of the maximum temperature attained in the target when subjected to bombardment by a pulsed electron probe is given in the appendix.

This calculation shows that the maximum temperature is attained in a period of time which is short compared to pulse lengths of 1 microsecond because of the limited volume in which the heat is produced. We may assume that the sample cools to the ambient temperature in a correspondingly short period of time. Thus, if the current in each pulse is increased so that the average temperature is the same as in the dc case, the maximum temperature will be proportional to the duty ratio of the pulses.

The average temperature, of course, remains about the same, but one is not concerned with the temperature only, but with the resulting changes which will occur in the target as a result of increasing its temperature. Assuming that the target does not undergo a change in state, the chief deleterious effect is that of diffusion. As this effect is not linear with temperature, the amount of diffusion which takes place cannot be described by the average temperature.

The mean square distance which is traveled by diffusion in solids in time t is given by the following formula(40):

$$\overline{\Delta x^2} = \int_0^{\infty} x\omega(x)\, dx = \frac{4Dt}{\sqrt{\pi}} \int_{\infty}^{\infty} e^{-\xi^2} \xi^2\, d\xi = 2Dt \qquad (7.1)$$

where

$$\omega(x) = \frac{C(x,t)}{\int_{-\infty}^{\infty} C(x,t)\, dx} = \frac{1}{2\sqrt{\pi Dt}}\, e^{-\frac{x^2}{4Dt}}$$

in which $c(x,t)$ is the concentration as a function of space and time, and D, the diffusion constant, is defined by the differential equation for diffusion,

$$\frac{\partial C}{\partial t} = \text{div } D \text{ grad } C \qquad (7.2)$$

It is experimentally observed (41) that for fixed concentration D is given by

$$D = Ae^{-\epsilon/kT} \qquad (7.3)$$

where A and ϵ are practically constant, K is Boltzmann's constant, and T, the absolute temperature. The activation energy for the process is ϵ which ranges from about 0.5 to 3.0 ev for common solids. Therefore, substituting equation 7.3 in 7.1 we obtain for the case where D does not depend on concentration

$$\overline{\Delta x^2} = 2Ate^{-\epsilon/kT} \qquad (7.4)$$

The mean square distance traveled by diffusion in the pulsed case is then

$$\overline{\Delta x^2} = 2A\left[e^{-\epsilon/[k(T_o + T_{dc}/w)]} wt + e^{-\epsilon/kT_o} (1-w)t \right] \qquad (7.5)$$

where $T_{dc} = 3p/4\pi J r_o k$ is the temperature attained for a dc probe of the same average current (see appendix), T_o is the ambient temperature, and w is the duty ratio of the pulses. We can now define an effective temperature, T_{eff}, as that steady temperature which would produce the same mean square migration by diffusion in a given time as that produced by the pulsed temperature. Thus, T_{eff} is defined by the following equation:

$$te^{-\epsilon/[k(T_o+T_{eff})]} = wte^{-\epsilon/[k(T_o+T_{dc}/w)]} + (1-w)\,te^{-\epsilon/[kT_o]} \tag{7.6}$$

Taking the worst case, ϵ = 0.5 ev and an ambient temperature of about 300 degrees K, we obtain the values exhibited in Table 4.

Steady State Temperature Rise: $T_{dc} = \frac{3}{4\pi}\frac{p}{J r_o k}$	Duty Ratio w: 0.1	0.01	0.001
1°	1.31^o	14.1^o	220°
2°	3.38^o	62°	338°
3°	7.7^o	111°	398°

TABLE 4 T_{eff} for diffusion in the target for an activation energy of 0.5 ev and an ambient temperature for which $kT_o = 1/40$ ev ($\doteq 300^o$ K).

We see that the diffusion which results from temperature effects using a pulsed electron probe can be considerably greater than for a dc probe having the same average current. It is necessary to restrict the duty ratio to be greater than 0.01 if the diffusion is not to be excessive.

The tests which were made with the field emission cathode assembly described in the appendix covered a range in pulse lengths of about 7 to 12 microseconds and a range of repetition rates from 2.5 to 10 kc/sec. The pulse shape, however, was not rectangular because of the use of a pulse transformer. This makes exact determination of the effective duty ratio difficult. An estimate of the effective duty ratios investigated would give a range from about 0.005 to 0.05. With the cathode assembly described it is doubtful that stable emission could have been attained at higher duty ratios than were investigated.

2. Effect of using a pulsed electron source on the detection of the x-rays

Assuming that it is possible to shield the high voltage pulses so that no spurious effects are caused in any of the other electronic equipment, there is a restriction on the choice of an x-ray detector imposed by the use of a pulsed electron probe. This restriction is associated with the dead time of the detector; if this is the order of or greater than the duration of the pulses, at most one count can be registered for each pulse of x-radiation regardless of the intensity of the x-rays. The corrections for dead time of the detector which were derived in a previous section do not apply to this case, and the only

solution to the difficulty consists in using lower average beam currents or in using detectors which do not record individual pulses but which measure the average x-ray intensity.

3. Stability of field emission sources

Two instabilities were observed in the field-emitted current by visual observation of the field emission pattern on a fluorescent screen located on the aperature stop of the cathode assembly. This pattern was characteristic of oxygen-contaminated tungsten in all cases where the emission was stable enough for this pattern to be observed.

One instability which was present in the pattern was a fluctuation of rapid frequency which could be observed in the form of bright specks which rapidly appeared and disappeared. This speckling of the pattern is presumably due to positive ion bombardment which is important at the pressures used (about 10^{-5} mm of Hg), and might be considerably reduced if the vacuum were improved by an order of magnitude. The fluctuation in beam current as a result of this, however, is of such a frequency that the time average over the period of time required for an x-ray intensity measurement would tend to zero if the pressure in the system remained approximately the same.

A more serious instability was present in the form of a gradual reduction in the field currents which were obtained with pulses of a given size. This is due to a gradual change in the radius of the emitter such that the current could only be restored to its former value by increase of the pulse voltage. After periods of operation of

about 1-2 hours, however, the pulse voltages required were beyond the capacity of the pulse generator (about 6 kv).

The mechanism which produced this emitter dulling was observed directly in the form of bright rings in the emission pattern, which originate at the boundaries of the strongly emitting regions and move inward and disappear at the point corresponding to the apex of the emitter. These rings have been observed by Trolan et al and have been correlated with the emission from atomic lattice steps on the surface of the emitter which move as a result of evaporation or surface transport of the tungsten atoms (42).

The suggestion was made by W. P. Dyke that the dulling of the emitters might be counteracted by maintaining a bias field at the emitter between pulses (43). Following this suggestion, the author tried bias fields ranging from 15 to 30% of the pulsed fields. For low bias, no decrease in the rate of dulling could be observed. At 20% bias, the emission was noticeably less stable with brighter speckling at the edges of the areas of greatest emission. With 30% bias, the emitter arced over after 40 minutes of operation. This breakdown was preceded by a bright spot in the pattern which resembled the surface of a boiling incandescent liquid. This coruscation increased in size to about 1/3 of the normal emission area just before breakdown. Such a breakdown may have been initiated by an impurity center in the tungsten lattice and is not uncommon.

In all cases, the field-emitted current which was observed was somewhat less stable than thermionic currents.

4. Emitter life

Of the seventeen emitters which were tried in the field emission cathode, only 2 had a life of over 25 minutes. These rather poor results were certainly due to inexperience in technique, because in most cases in which the emitter failed after a few minutes of operation the failure could be attributed to inadequate degassing of the emitter tip either from insufficient heating of the filament or from excessive radiative losses occasioned by too great a distance from filament to the emitter tip.

The longest lifetime observed was about 2 hours, and this could undoubtedly be increased by improvement in technique and improvement in the vacuum. However, attaining reliable lifetimes of the order of 10 hours or more, which is common in the case of tungsten hairpin filaments used in electron microscopes, would have required considerable effort.

5. Alignment requirements

In the field emission cathode assembly it was necessary to align the position of the emitter tip very accurately with respect to the electrode on which the pulses were applied, and to orient the axis of the emitter in such a way that one of its strongly emitting directions was along the axis of the electron lens. The latter adjustment can be made while the cathode assembly is evacuated and will be independent of the former adjustment only if the position of the emitter tip has also been properly aligned with respect to the constraints which permit variation of the angular position of the emitter axis. While most of

the time necessary to change the emitters was spent in their alignment, it was felt that satisfactory alignment was never actually achieved.

The need for accurate alignment is inherent in the nature of the field emission source. This is not the case, however, for thermionic emission, particularly in the case of the self-biased triode electron gun where the current is partly space charge limited and small misalignments are compensated by the distribution of the space charge.

6. Currents possible in the electron focal spot

While at first sight it would seem that the greater current densities which can be obtained from field emission cathodes than from thermionic cathodes would result in greater currents in the refocused image of the source, this is actually the case only under certain restricting conditions. In any comparison of current densities which might be obtained with the two sources it is necessary to consider situations which can be realized in practice, and this means that one must consider that the electron lenses for focusing both sources will have considerable spherical aberration.

The field emission case is notably different from the thermionic case. In an electron probe with thermionic emission, one must select a ratio of the size of the gaussian image to the size of the circle of confusion due to spherical aberration which maximizes the current on a real focal spot of given size. In this case, the specific emission of the cathode is determined by the temperature and nature of the cathode

surface. With field emission, on the other hand, the size of the gaussian image is negligible in comparison to the size of the circle of confusion. The specific emission is then fixed by the voltage and the radius of curvature of the emitter. While the specific emission can be extremely high, of the order of 10^7 amps/cm^2, the emission takes place over very large angles and as a result, the current density per unit solid angle can be lower for the field emission source than for the thermionic source.

Because the size of the focal spot which can be attained with field emission as a source is limited chiefly by spherical aberration, the fact that emission takes place over very large angles can be a serious disadvantage in its practical use as a source in electron probes. In order to collect all of the field-emitted currents, the spacing of the emitter and anode would have to be impractically small. Even if this could be achieved in practice, the spherical aberration would be large because the radius of the circle of confusion due to spherical aberration increases with the cube of the aperture angle according to the formula:

$$r_s = C_s u^3 \tag{8.1}$$

where C_s is a constant characteristic of the electron lens and the power at which it is operated, and u is the half-angular aperture of the imaging pencil.

As a result of the large value of C_s which is characteristic of all electron lenses currently in practical use, it is probably advantageous to use only a portion of the current emitted from the field emitter.

This current should be obtained from a preferred direction in the field emission pattern, namely that direction corresponding to the 310 direction in the tungsten crystal. For this direction, the current density may be 3.7 to 4.2 times the average current density and 1600 times the current density from the 110 direction* (44).

Let us now attempt to deduce the value of currents which can be obtained from a field emission source under these assumptions and compare it to the current densities possible using thermionic emission. The total current drawn from the field emitter will be constant for a given emitter and voltage. A reasonable value for the case of pulsed emission is 10^{-3} amps, and about 30% of this comes from 6% of the area (46). Assuming that the total emission occurs over angles up to 60 degrees, we would have for the half-angular aperture u_o', which corresponds to 6% of the total area of the pattern, the following equation:

$$\frac{1 - \cos u_o'}{1 - \cos 60^o} = 0.06 \qquad (8.2)$$

so $(u_o')^2 \doteq 0.06$ (u_o is in radians).

The current collected by a lens which accepts a pencil of electrons with half-angular aperture of u_o is then

$$I_{f.e.} \doteq 0.3 \cdot 10^{-3} \frac{u_o^2}{u_o'^2}$$

$$\doteq 0.3 \cdot 10^{-3} \frac{u_o^2}{0.06} \qquad (8.3)$$

---

* The 110 direction is commonly oriented along the axis of the wire from which the emitter is fabricated, and therefore it is essential that the cathode assembly provide for orienting the emitter in the most favorable direction if only a portion of the total amount is used.

The imaging pencil will have a half-angular aperture of u_o/M where M is the magnification. The diameter of the circle of least confusion* is then

$$d \doteq \frac{C_s}{2} \left(\frac{u_o}{M}\right)^3 \qquad (8.4)$$

And hence, the current on a focal spot of diameter d is

$$I_{f.e.} \doteq 5 \cdot 10^{-3} \left(\frac{2M\,dz}{C_s}\right)^{2/3} \qquad (8.5)$$

Let us now turn to the case of the thermionic electron source in the form of an electron gun. The beam from an electron gun is limited, in the absence of material diaphragms, by an exit pupil known as the "cross-over". In the formation of an electron probe, the virtual source which is imaged by the electron lenses consists of this exit pupil. The current density in the cross-over is a maximum at its center , and according to Langmuir (45) this is given by

$$I_c = I_o \left(\frac{eV}{kT} + 1\right) \sin 2\alpha \qquad (8.6)$$

where I_c is the current density at the center of the cross-over, I_o is the specific emission of the cathode, V is the accelerating voltage, k is Boltzmann's constant, T, the absolute temperature of the cathode,

---

* The diameter of the circle of least confusion which exists in a plane slightly closer to the lens than the gaussian image plane is, according to Zworykin (46), only 1/4 the size of the circle of confusion in the gaussian image plane.

and α is the divergence angle of the electrons. Let us define the brightness as the current/ unit area/ unit solid angle. Then, the brightness is given by

$$B = \frac{I_o}{\pi}\left(\frac{eV}{kT}\right) \tag{8.7}$$

neglecting 1 compared to eV/kT. This must be constant for all images formed in field free space. The current on a focal spot of gaussian diameter d_1 is then

$$I_d = \frac{\pi^2}{4}(d_1)^2 \, Bu^2$$

$$= \frac{\pi}{4}(d_1)^2 \, I_o \frac{eV}{kT} \, u^2 \tag{8.8}$$

where u is the half-angular aperture of the imaging pencil. The current distribution in the real focal spot is the result of a two-dimensional folding of the current distribution in the gaussian image and the current distribution in the spherical aberration figure. The diameter of the real focal spot over which there is appreciable current will therefore be given by

$$d_2 \doteq d_1 + \frac{C_s u^3}{2} \tag{8.9}$$

With this substitution, equation 8.8 becomes

$$I_{f.e.} = \frac{\pi}{4}\left(d_2 - \frac{C_s u^3}{2}\right)^2 I_o \frac{eV}{kT} \, u^2 \tag{8.10}$$

This has a maximum for a value of u such that

$$\frac{C_s u^3}{2} = \frac{d_2}{4} \tag{8.11}$$

which means that we must restrict the aperture to such a value that the diameter of the circle of confusion is 1/4 the real diameter of the focus. Substituting 8.11 in 8.10 we find the maximum current on a focal spot whose real diameter is d_2. This is

$$I_{t.e.} = \frac{9}{64} \frac{(d_2)^{8/3}}{(2C_s)^{2/3}} I_o \frac{eV}{kT} \qquad (8.12)$$

This value is subject to an error because it assumed that the current density over all parts of the cross-over was equal to its maximum value and also because electron guns do not always have an efficiency of 100%. Consequently, equation 8.12 should be multiplied by factor ϵ, which represents the efficiency of the electron gun.

We can now compare the current from the two types of sources as given by equations 8.12 and 8.5. The ratio of the currents which can be attained with thermionic emission and with field emission on a given size focal spot would be

$$\frac{I_{t.e.}}{I_{f.e.}} \approx 564 \, I_o \frac{eV}{kT} \frac{\epsilon}{(M)^{2/3}} d^2 \qquad (8.13)$$

Assuming I_o = 10 amps/cm^2, ϵ = .10, V = 30,000 volts, M = 1, T = 3000° K, the two sources would give equal currents for a diameter of the probe given by

$$d \doteq 0.12 \text{ microns} \quad .$$

On the other hand, assuming $I_o \epsilon = .14$ amps/cm^2, which is the value obtained by Castaing, we would have

$$d \approx 0.32 \text{ microns} .$$

Another comparison of the currents possible in electron probes using field emission and thermionic emission has been given by Cosslett and Haine, assuming that the field emission is focused by an electron lens of given aperture (47). For this case, there exists an optimum position for the cathode and consequently an optimum magnification. This optimum magnification is equal to 3 for an ideal thin lens and about 2 for a magnetic lens with bell-shaped field. If the distance from emitter to lens is taken to be the optimum value, this becomes impractically small for a lens operated at maximum strength and for the emitter voltages of 10 kv which Cosslett considered. Consequently, the electron lens for the focusing of the field emission must be operated at reduced power which results in a larger value of the spherical aberration constant, C_s , than can be used in the focusing of thermionic emission.

Cosslett and Haine find that for these conditions equal currents will be attained on a focal spot of diameter equal to 0.18 microns and that the dependence of current on diameter of the focal spot for the two cases is the same as given by equations 8.5 and 8.12.

The value of the critical diameter as given by equation 8.13 is in qualitative accord with the estimate of Cosslett and Haine. For focal spot sizes sizes larger than this the thermionic source will give larger currents than the field emission source. It appears, therefore,

that in the electron probe microanalyzer, where focal spots smaller than one micron are of little importance because of the diffusion of electrons in the target, there is little or no advantage in using a field emission electron source.

B. Realization of an Electron Probe Microanalyzer Using Thermionic Emission

Since July 1, 1953, work has been in progress at Caltech under contract DA-04-495-Ord-463 to develop an electron probe microanalyzer. At first, it was planned to employ in the electron probe a field emission source and a single electrostatic electron lens. However, by February, 1956, it had become apparent from the results obtained with the field emission source that more time would be needed to perfect the field emission source than would be required to reconstruct the beam system for a thermionic source. Moreover, as we have seen in the preceding section, the use of field emission in the electron probe would have little advantage other than novelty over the use of thermionic emission.

The conversion to a thermionic electron source rendered obsolete the electrostatic electron lens which had been constructed, and in the new beam system it was decided to use magnetic lenses because of their inherently lower spherical aberration.

A general view of the completed instrument is shown in fig. 7. A schematic view of the instrument and its associated electronics is shown in fig. 8. In the schematic view the electronic components are shown in approximately the same relative spatial position as in

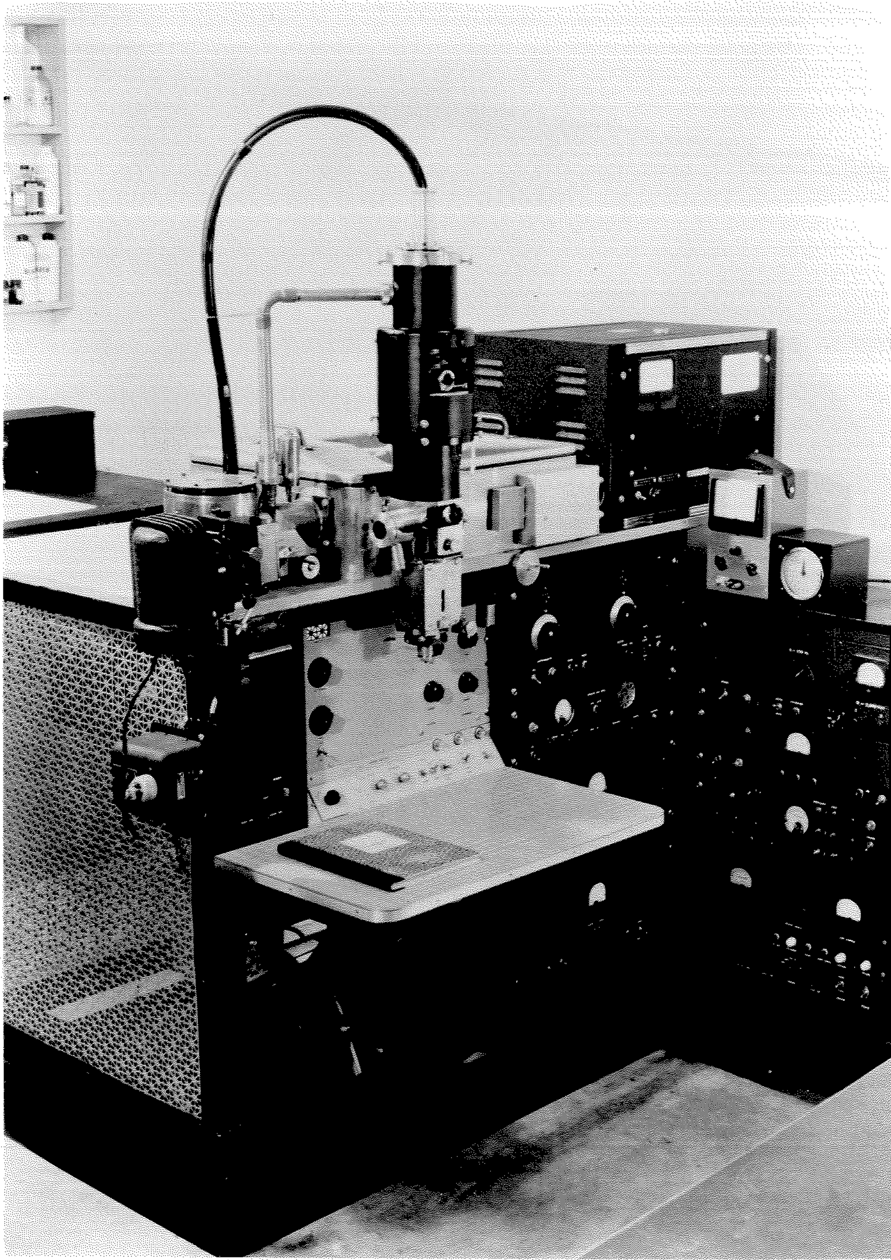

FIG. 7 General view of the electron probe microanalyzer.

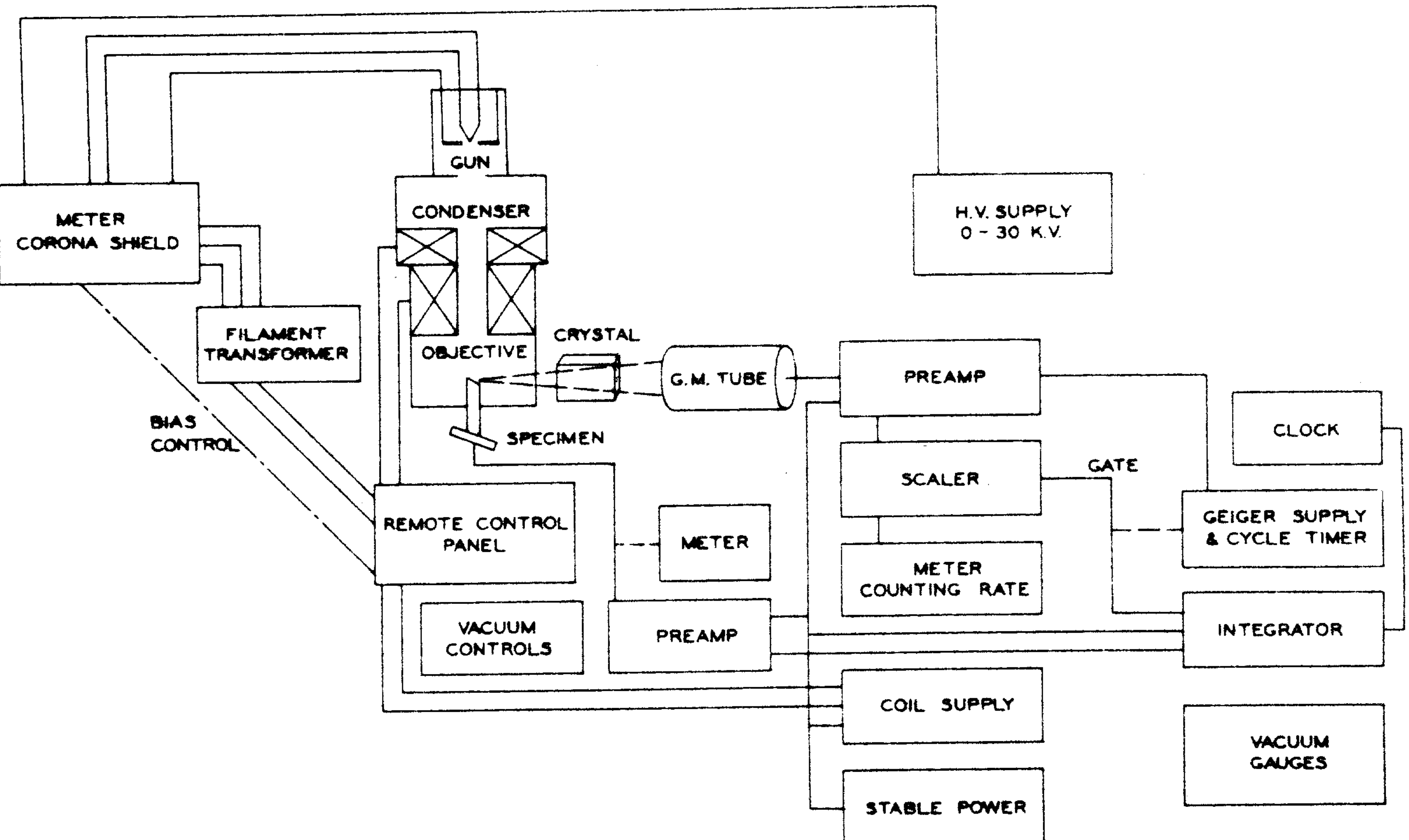

FIG. 8. Schematic of the electron probe microanalyzer.

fig. 7. The purpose of the various electronic components will be described in the detailed discussion which follows. For the purpose of this discussion it is convenient to regard the instrument as subdivided into the following systems: (1) the electron probe, (2) the vacuum system, (3) the sample support and viewing system, and (4) the vacuum x-ray spectrometer and associated equipment.

1. The electron probe

The electron probe is similar in construction to the electron probe which is employed by Cosslett and Pearson in an x-ray shadow microscope (9). It consists of a self-biased triode electron gun and two magnetic electron lenses which will be referred to as the condenser and the objective for convenience.

The electron probe system is shown in fig. 9. The entire column is supported from the side of the spectrometer housing on brass ways so that the location of the electron focal spot may be adjusted relative to the focal circle of the x-ray spectrometer. An "O" ring maintains the vacuum seal between the specimen housing and the spectrometer housing which is also evacuated in the normal operation of the instrument. An additional pumping connection is made to the electron gun housing at the top of the column with an "O" ring coupling to facilitate assembly and disassembly of the beam system. A brass tube connects this coupling to a brass bellows which is attached to the main vacuum manifold.

The controls for the beam system, which include filament power, grid bias resistance, and coarse and fine adjustments for the

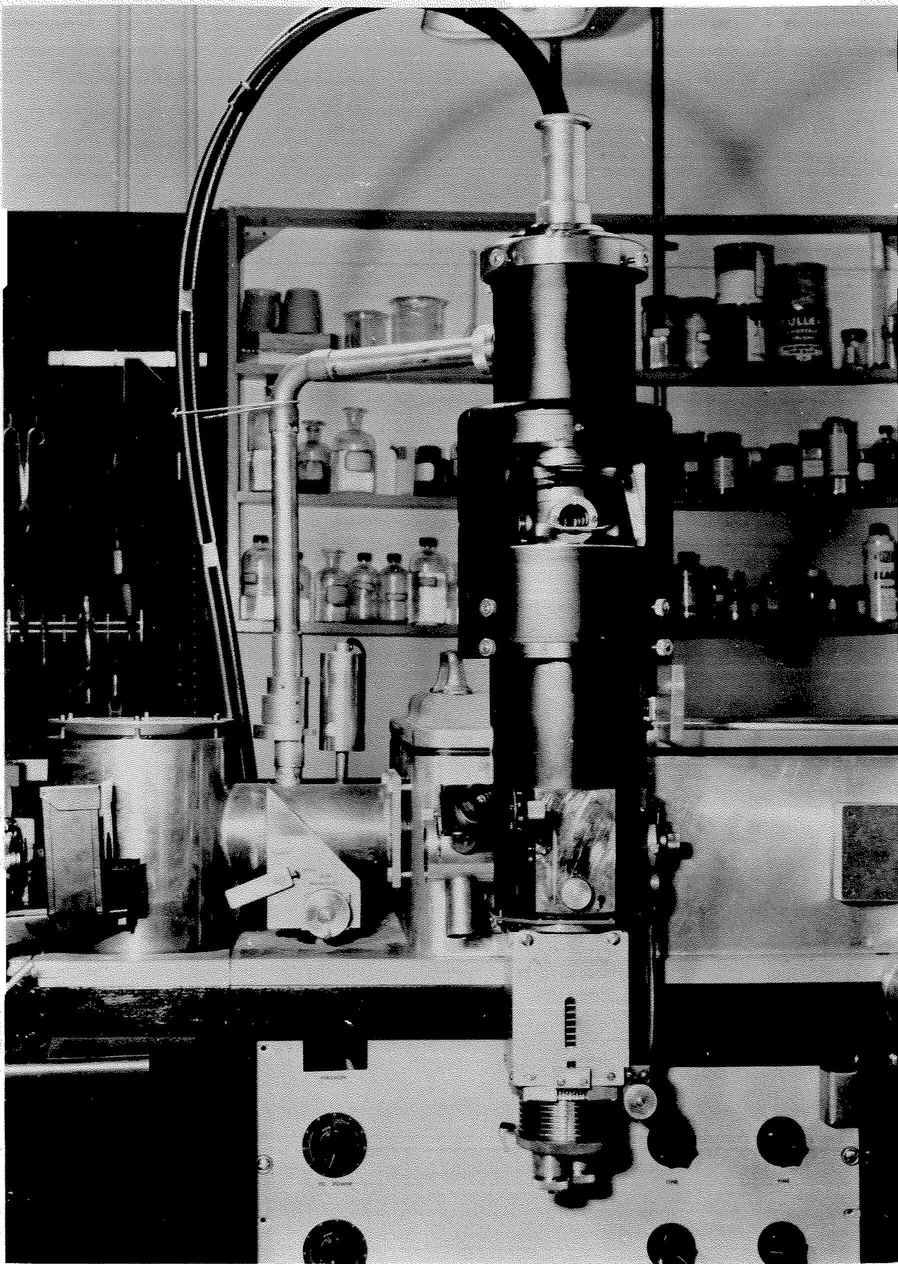

FIG. 9 General view of the probe system.

current of the two magnetic lenses, are located on a remote control panel immediately below the beam system. It is necessary that these controls be within reach of an operator looking through the eyepiece of the viewing system. An opening in the remote control panel which can be seen in fig. 9 to the left of the beam column enables the operator to view the emission current which is measured by a meter in series with the high voltage supply. This meter is housed in a corona shield which also contains the variable bias resistor and parts of the filament supply for the electron gun. The corona shield is suspended from the underside of the instrument table with insulators and may be seen in fig. 10, which shows the side of the instrument with the protective grill removed.

A simplified frontal cross section of the electron beam system is shown in fig. 11. The grid and filament assembly of the electron gun were obtained from the North American Phillips Company and are identical to those used in their electron microscopes. The use of this commercial component saved much time in construction, since it has the necessary provision for adjustment of the filament relative to the grid and uses standard filaments. The filaments which are manufactured for this gun, however, are fabricated from 8 mil tungsten wire, and it was found advantageous to fabricate special filaments for the electron probe. The special filaments were made from 4 mil tungsten wire using a technique developed by the author to obtain V-shaped filaments for which the apex was nearly hemispherical and the apex angle very small (48). This technique involves altering the cross section of the wire to the shape of a half-moon in the region

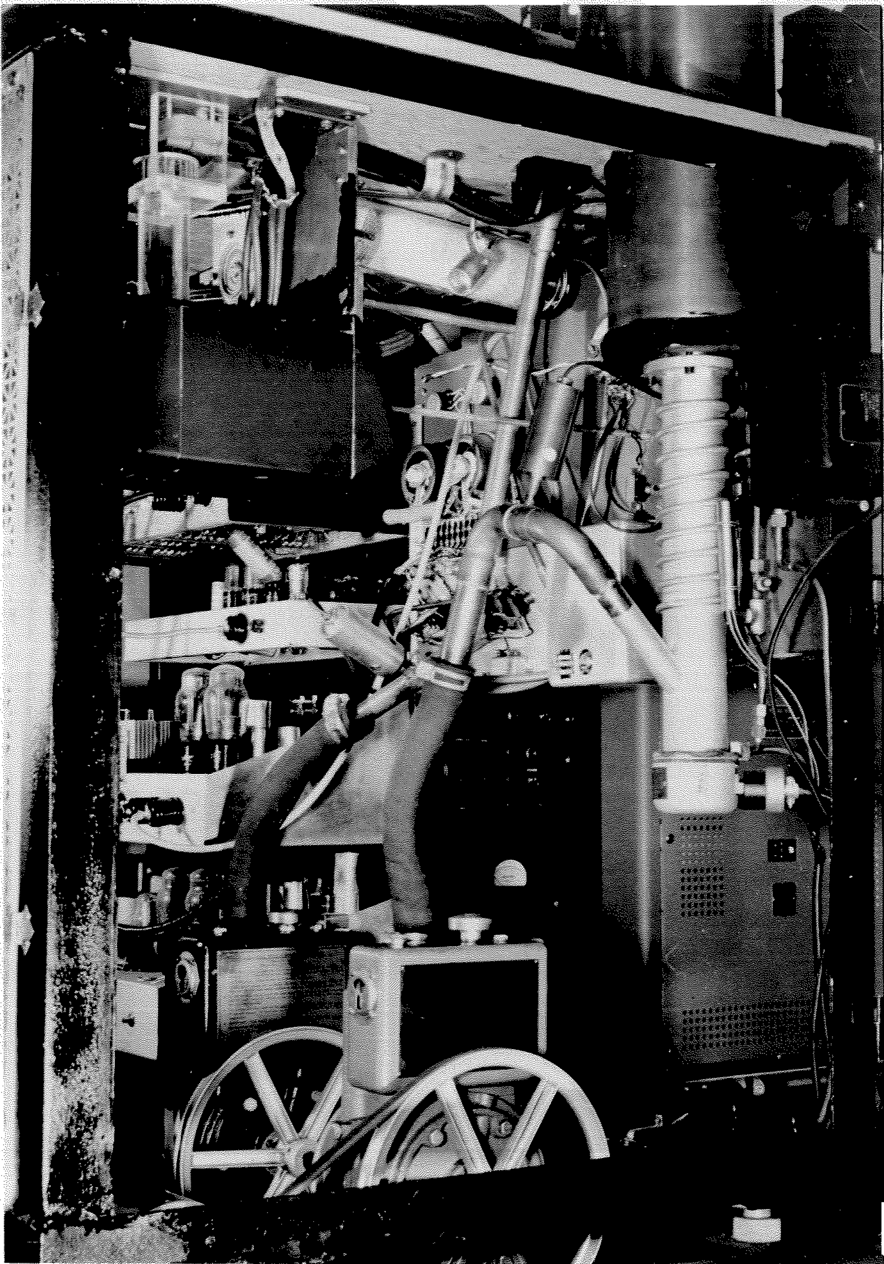

FIG. 10 View of the left side of the instrument with the protective grill removed.

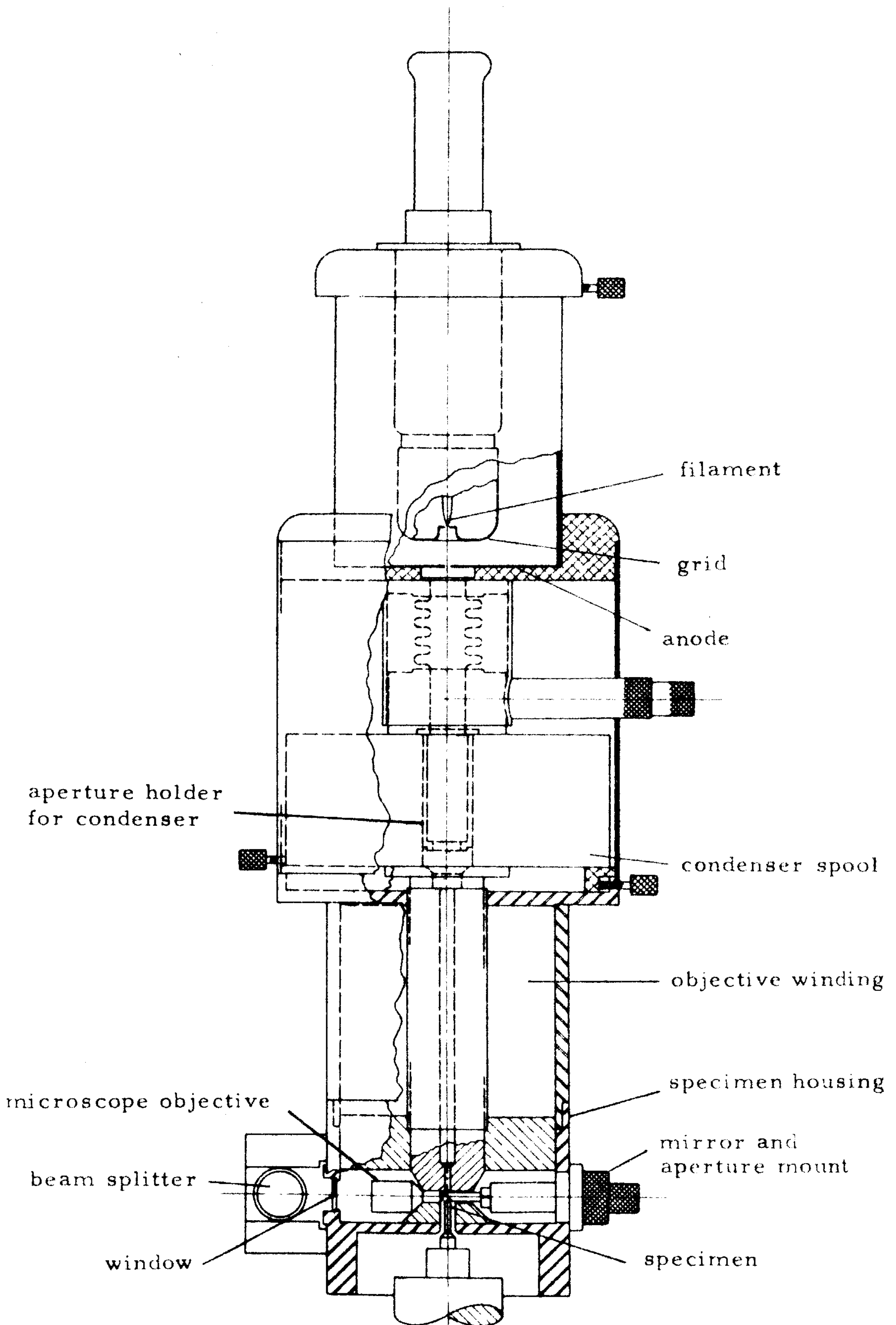

FIG. 11 Simplified cross section of the probe system.

where the bend is to be made. The necessary alteration can be accomplished by electrolytically etching or mechanically polishing the wire. The special filaments are spot-welded to the terminals on the standard sintered-glass filament holders.

The anode of the electron gun consists of a stainless steel disk with an aperture of 4 mm in diameter. It is located about 1 cm from the grid of the electron gun, which may be translated with respect to it by means of screws on the sides of the flange which supports the grid. The vacuum seal is maintained during this adjustment by an "O" ring which lies in a groove in the gun housing and makes a face-seal with the flange. A tilt adjustment of the grid with respect to the anode was originally provided but was eliminated when it was found that it resulted in an uncertainty in the position of the grid when the system was reduced to air and then re-evacuated. The mechanical tilt adjustment is, in fact, superfluous since a tilt of the electron beam can be produced by a deflection of the beam near the edges of the pinhole electron lens existing at the anode aperture.

Below the electron gun is a fitting consisting of two flanges which are equipped with "O" rings and connected with a spring-loaded bellows. The lower flange makes a vacuum seal with the condenser coil casing. The bellows permits the necessary flexibility for adjustment of the condenser relative to the electron gun and also permits the entire fitting to be removed for the purpose of introducing apertures in the condenser lens without altering the location of the condenser relative to the electron gun. The lower flange of this fitting is also equipped with a means for introducing a fluorescent

screen for viewing the emission from the electron gun, and prisms or mirrors for aligning purposes.

The condenser lens consists of a spool of soft iron in which a brass spacer has been soldered to make a gap of about 1/4 inch. The spool has a bore of about 1 inch in diameter which is threaded for the insertion of pole pieces. It is wound with 10,417 turns of no. 26 heavy formvar insulated wire which has a dc resistance of about 380 ohms. A cylindrical sleeve of soft iron fits over the spool to complete the magnetic circuit. This lens may be used in either of two ways for the formation of the electron probe: (1) it may be used with or without pole pieces as a condenser lens to vary the effective distance from the source to the objective lens, or (2) it may be used with the pole pieces to form an intermediate image of the source.

A dummy condenser lens which is made of aluminum and which has the same dimensions as the real condenser is used in place of the condenser when the electron probe is formed with the use of the objective lens only. In many cases, the use of only a single electron lens for forming the electron probe gives adequate performance. In other cases, where it is necessary to use both lenses, the use of the dummy lens facilitates alignment of the electron probe, since the alignment of the objective lens can be accomplished without the restriction in aperture which results from the condenser with its pole tips. It is possible to remove the dummy condenser and insert the true condenser without causing a misalignment of the gun relative to the final lens by more than a few thousandths of an inch.

As can be seen by inspection of fig. 11 adjustments are provided whereby the electron gun and condenser may be translated with respect to the objective lens. This choice of constraints is the most convenient where the condenser is used to vary the effective source distance, since the condenser in this case may be regarded as part of the illuminating system.

The objective lens has a coil casing which is somewhat smaller in diameter than the condenser in order to permit the crystal of the spectrometer to move as close as possible to the x-ray source. As in the case of the condenser, the objective coil is wound on a spool, but in this case the lower flange of the spool consists of a nonmagnetic material (brass). The magnetic circuit is completed through the specimen housing which is made of iron and which has a partition on which rests the lower pole tip. The specimen housing is octagonal in shape (fig. 9), and this facilitates mounting portions of the viewing system, aperture holders, etc., as well as mounting the beam system to the spectrometer housing.

A vacuum seal is made between the brass flange of the coil spool and the specimen housing so that the coil winding is not under vacuum. The winding consists of 11,200 turns of no. 26 heavy formvar coated wire and has a dc resistance of about 320 ohms. The lower resistance of this coil compared to the condenser is due to its smaller mean diameter and results in greater efficiency of energizing this lens.

The pole pieces of the objective lens are made of armco iron. The upper pole piece makes a snug fit into a bore in the objective coil spool and has an axial hole 1/4 inch in diameter up to about 1/2 inch

of the pole tip. Near the pole tip, the size of the bore is reduced to 3/16 inch, and this results in about 10% less excitation required for a given focal length of the objective lens than would be required if the larger bore extended completely through. The lower pole tip and also the partition on which it is supported have a bore of 1/4 inch for the insertion of the specimen. The focus of the electrons takes place under normal conditions of operation at a point slightly above the lower pole tip so that the x-rays produced can pass out of the specimen housing and into the spectrometer without being obstructed by the pole pieces. This can be visualized by referring to fig. 12 which shows a cross section of the specimen housing, spectrometer, and specimen airlock at right angles to the preceding section.

The surface of the specimen is inclined at an angle of 75 degrees to the axis of the electron beam which is vertical. The plane of the spectrometer is horizontal, and consequently, the angle of emergence of the x-rays is in the vicinity of 15 degrees.

The gap for the objective lens is determined by an aluminum spacer and is about 0.26 inches in width. The diameter of the flat portion of the pole tips is 3/4 inch, and the sides are tapered at 30 degrees to obtain maximum field in the gap without excessive saturation effects. The design of the pole tips of the objective lens was based on the work of Liebman and of Liebman and Grad (49) on the properties of magnetic lenses, and of Liebman (50) and Mulvey (51) on the magnetic circuit and saturation considerations in magnetic electron lenses.

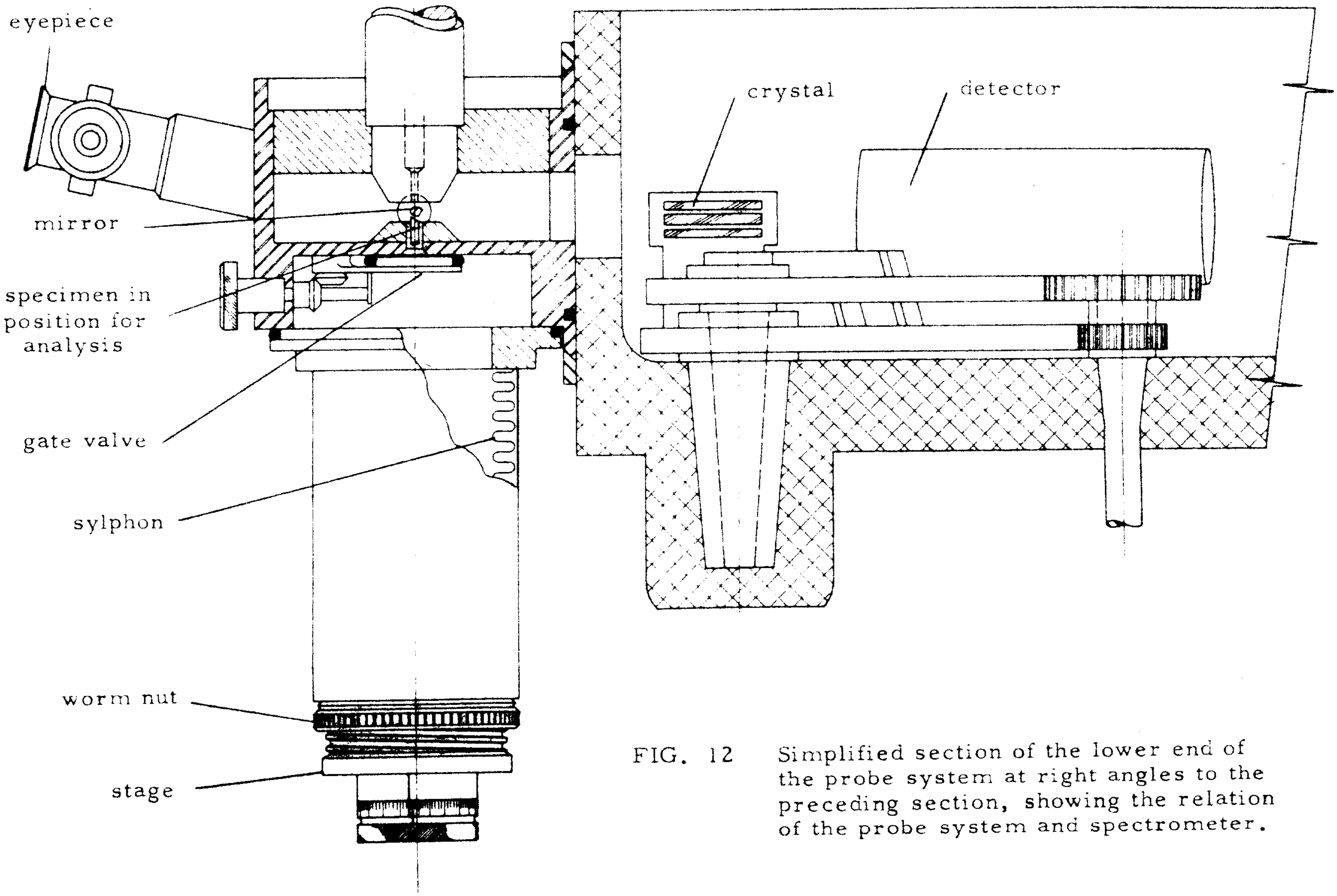

FIG. 12 Simplified section of the lower end of the probe system at right angles to the preceding section, showing the relation of the probe system and spectrometer.

According to Liebman (49), for a lens of this geometry an excitation of about 2000 ampere turns would be required to obtain a focus at the desired point (just above the lower pole tip). At this excitation the effective focal length would be .16 inch or 4.1 mm. These values may be slightly modified by the effects of leakage flux in the specimen housing and the effect of reducing the bore in the upper pole tip, but exact calculation of the focal length is difficult and, in fact, not necessary.

The lens coils are supplied with regulated current from the coil supply whose schematic diagram is given in fig. 13. The amplifiers in this power supply receive regulated B^+ voltage and filament current from a central power supply whose schematic diagram is given in fig. 14. The central power supply also provides power for other units which will be described in the following sections, namely, the preamplifier for the scaler and the target current integrator. The two regulated power supplies are located at the bottom right of the main instrument table (fig. 7).

The accelerating voltage for the electron probe is provided by a regulated rf-type high voltage supply manufactured by the Spellman Television Company. This supply furnishes negative voltage which is continuously variable from 3 to 30 kv at 1 ma. It consists of a separate oscillator and buffer feeding the power oscillator into a doubler-rectifier. Regulation, which maintains the voltage constant to better than .5%, is accomplished through feedback into a dc amplifier plus simultaneous output control of the buffer. This unit is located on the top of the instrument table at the right (see fig. 7).

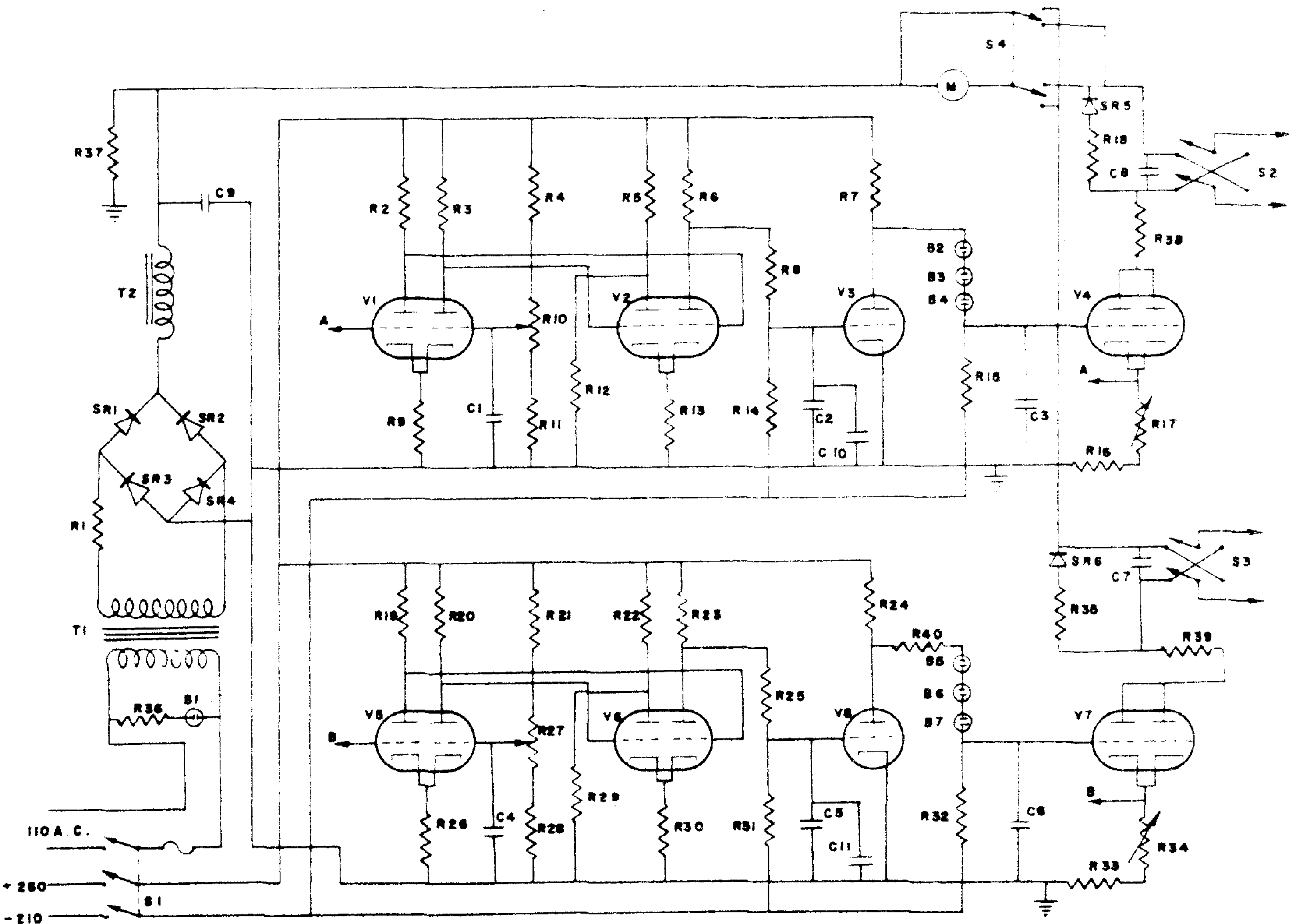

FIG. 13 Circuit diagram of the power supply for the magnetic lenses.

Key to FIG. 13

Components for the coil current supply

V1, 2, 3, 5, 6, 8--12AX7 (fil.in series string, regulated B+)
V4, 7--6AS7

R1--10 Ω, 5 w
R2, 3, 19, 20--360K, 2 w*
R4, 21--220K, 2 w*
R5, 6, 7, 22, 23, 24--100K, 2 w
R8, 25--1.8M, 1 w
R9, 26--25K, 2 w*
R10, 25--2K, 2 w AB pot. "Fine" (on remote panel)
R11, 28--25K, 2 w*
R12, 29--1.8M, 1 w
R13, 30--68K, 1 w
R14 ,31--1M, 2 w
R15, 32--1M, 2 w
R16, 33--100 Ω, 20 w (on remote panel)
R17, 34--1K, 100 w reostat "Coarse"(on remote panel)
R18, 35--47 Ω, 2 w
R36--180K
R37--2K, 20 w
R38--75 Ω, 10 w
R39--100 Ω, 10 w
R40--47K, 1 w

C1, 4--1 μFd, 200 v
C2, 5--0.25 μFd, 400 v
C3, 6--1000 μμFd
C7, 8--40 μFd, 400 v elect.
C9--2 x 150 μFd, 300 v
C10, 11--100 μμFd

B1--Ne-51 neon bulb
B2-7--Ne-2 neon bulbs

M--0 -500 ma. meter

T1--110 v to 220 v transformer 1000 va.
T2--2 chokes in series, 7 Ωdc.

SR1-4--350 ma. 135 v selenium rect. (2 in series)
SR5-6--65 ma. 135 v selenium rect.

---

*precision or temperature stable resistor

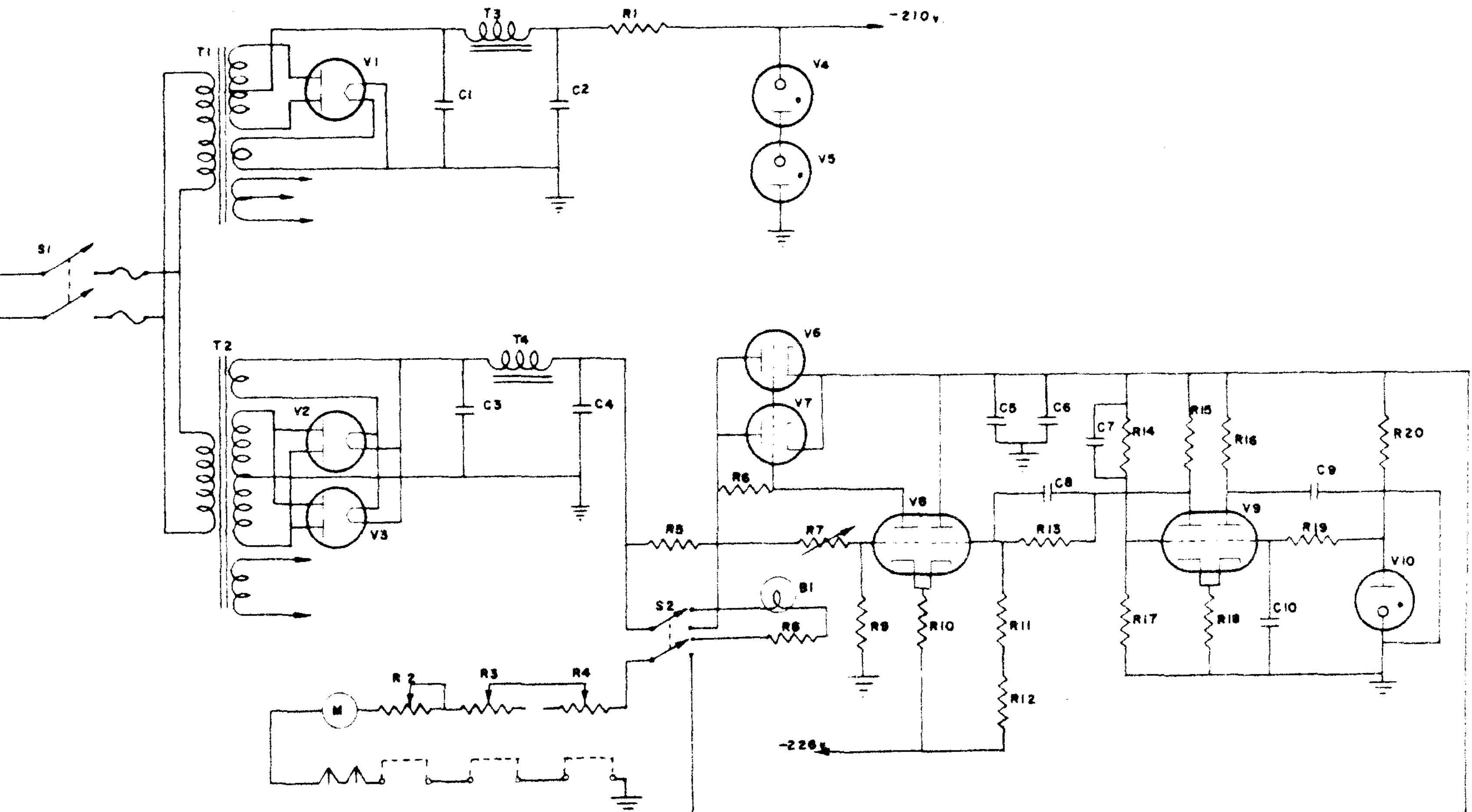

FIG. 14 Circuit diagram of the central power supply.

Key to FIG. 14

Components for the main power supply

V1, 2, 3--5T4
V4, 5--OC3/VR-105
V6, 7--6AS7
V8, 9--12AT7 (fil. in series string, regulated B+)
V10--5651

R1--4K, 20 w
R2--100 Ω, 20 w reostat
R3, 4--950 Ω, 100 w adjustable
R5--3.3M, 1 w
R6--100K
R7--2M, AB pot. "Hum"
R8--1K, 10 w
R9--75K, 1 w
R10--40K, 2 w*
R11, 13--3M, 1w*
R12--400K, 1 w
R14, 15, 16, 18--100K, 2 w*
R17--40K, 2 w*
R19--100K, 1 w*
R20--150K, 2 w*

C1--16 μFd, 450 v
C2--8 μFd, 450 v
C3, 4--25 μFd, 500 v
C5--0.01 μFd
C6--90 μFd, 500 v
C7--0.02 μFd
C8--0.01 μFd
C9--0.03 μFd
C10--1 μFd

S1--DPST toggle switch, "Power"
S2--DPDT toggle switch, pos. 1 "Warmup", 2, "Operate"

T1--300-0-300 at 75 ma., 6.3 v at 3 amp, 5 v at 2 amp
T2--400-0-400 at 300 ma., 6.3 v at 5 amp, 5 v at 4 amp
T3--10 H, 50 ma.
T4--10 H, 300 ma.

B1--No. 47 pilot lamp

M--0-200 ma. meter

---

*precision or temperature stable resistor

It was found by the author that the use of dc for heating the filament of the electron gun resulted in an increase of the beam current by as much as a factor of 4 over the beam current available when ac was used to heat the filament (48). This is apparently due to the deflections of the electrons in the magnetic field of the heater current which can be of the order of magnitude of the aperture angle of the electron pencil accepted by the electron lens (about 0.0005 radian when using the objective lens alone). When ac is used for heating the filament these deflections are not constant, and, as a result, the electron lens aperture is filled with maximum current for only a portion of the time. On the other hand, with dc the deflections are constant and can be compensated for by an adjustment of the position of the electron gun.

The direct current for operating the filament of the electron gun is obtained by rectifying and filtering 60 cycle ac from the filament transformer. The filament transformer has had the secondary rewound with a center tap so that full wave rectification may be achieved with two silicon diodes. These diodes have high current ratings, a small forward voltage drop, and high efficiency, so that it is possible to control the filament current by means of a variable auto-transformer in the primary of the filament transformer. Filtering is accomplished by means of a special filter choke having very low resistance and electrolytic capacitors of large capacitance.

Some mention must be made regarding the procedure of alignment of the electron probe. Alignment of the filament with respect to the grid of the electron gun is made at the time the filament is

mounted in the gun assembly. It is sometimes necessary, however, to remove the assembly and re-center the filament because of distortion due to recrystallization of the tungsten on undergoing transformation to the bcc structure as a result of being heated. The alignment of the filament with respect to the aperture in the grid is not critical, however, because of the presence of the space charge as a result of the grid being maintained negative with respect to the filament.

The other adjustments of the electron probe cover a total of only 4 degrees of freedom for the case where a single electron lens is used, and 6 degrees of freedom for the case where two lenses are used. This, of course, does not include the alignment of the aperture relative to the objective lens and this will be discussed later. It might be supposed that a planned procedure of alignment would be necessary, but this is actually not the case because it is possible with an insulated target to monitor the beam current. In the case where only the objective is used for the formation of the probe, the alignment can be accomplished rather quickly by successive approximations until the current collected by the target is a maximum. Furthermore, as mentioned earlier, it is possible to align the objective without the condenser in place and then to insert the condenser without altering the alignment excessively.

There are present additional variables in the form of the emitter temperature and the value of the bias resistance. These can also be optimized by successive approximations and will be virtually independent

of the mechanical adjustments if the filament is well centered with respect to the grid of the electron gun. In addition to the value of the target current the emission current from the filament can be measured so that there is little danger of its being accidentally overheated. Furthermore, the bias resistor can be adjusted so that the electron pencil from the electron gun is quite narrow, and hence is operating at high efficiency by maximizing the ratio of the beam current to the total emission current.

The distance of the electron gun to the center of the gap of the objective lens is about 300 mm. Using the objective lens alone, with a current of about 210 ma, a focal spot of 5 microns in diameter with a maximum current of about .11 microamp was obtained at an accelerating voltage of 30 kv. The size of the electron focal spot could not be determined with certainty from the use of fluorescent screens in the focal plane due to excitation of fluorescence by the x-rays, and therefore it was necessary to observe the shadow pictures cast on a fluorescent screen by a fine wire in the focal plane of the probe.* For this purpose, a wire was made by electrolytically etching a 1 mil tungsten wire until its diameter was 5 microns as

---

* A special dummy stage assembly was constructed for viewing shadow pictures of wires on a distant fluorescent screen. However, it is also possible to view such shadow pictures of wires without the use of a special stage. This is done by preparing a specimen having a wire mounted over a recess about 1/10 inch deep; the bottom of the recess is normal to the viewing system (see p. 138) and is coated with fluorescent material. When the wire is in the focal plane of the viewing microscope, the shadow picture can be seen on the fluorescent screen by looking through the microscope objective with the eyepiece removed.

measured under a light microscope with a filar micrometer eyepiece. It was possible to obscure the electron beam completely with such a wire provided the aperture stop of the electron probe was free of dust and contamination.

The presence of contamination or foreign particles on the aperture is graphically demonstrated by viewing the shadow pictures of wires as the objective coil current is varied. At lens coil low excitation the distortion of the image is only slight and becomes progressively worse as the excitation approaches values necessary to produce a focus in the plane of the wire. It is impossible to produce small focal spots unless the aperture is clean, and as a result it is necessary to be able to replace the apertures in a routine fashion.

The apertures which are used in the electron probe consist of disks of copper or bronze a few mils in thickness and 1/8 inch in diameter with a hole in their centers 10-20 mils in diameter. They are supported on a holder which extends through the wall of the specimen housing and which can be removed as a unit from the instrument without altering any of the other adjustments of the electron beam system. The holder permits adjustment of the position of the aperture with respect to the axis of the electron lens while the system is under vacuum. This adjustment is readily accomplished by making use of the rotation property of the magnetic lens. To do this, a specimen having a coating of fluorescent material (fluorescent grade zinc silicate with a small quantity of lacquer or collodion as a binder) is mounted in the instrument. The image of the focal spot of the electrons can be observed by means of the optical system which is

built into the instrument (see p. 139), and the aperture is adjusted until the electron spot remains stationary as the objective coil current is varied.

2. The vacuum system

A schematic view of the vacuum system is shown in fig. 15. The system consists of a National Research type H-2-P purifying oil diffusion pump backed by a Welsch Duoseal No. 1405 mechanical pump and isolated from the instrument with an internal cold trap. Five valves are provided as shown in this figure, and all of these valves are located within reach of an operator seated before the instrument. Valve 1 is a simple flapper valve which permits continuous operation of the pumps and cold trap while the spectrometer or beam system may be reduced to atmospheric pressure. Valve 2 connects the main vacuum manifold to an auxiliary manifold. This auxiliary manifold, which may be evacuated by means of a second mechanical pump, communicates with the specimen airlock through valve 3 and with dry atmospheric air through valve 4. The second mechanical pump may therefore be used to "rough down" the main system or to evacuate the airlock after changing specimens.

Valve 5 separates the airlock from the rest of the electron beam system. It consists of a blade, containing an "O" ring, which is pivoted about a vertical axis and which is coupled by means of a bevel gear to a shaft extending through the wall of the specimen housing (see fig. 12). This arrangement occupies little space in the vertical direction, and, as a result, the specimen holder need not travel a large distance in the course of changing specimens. Some difficulty

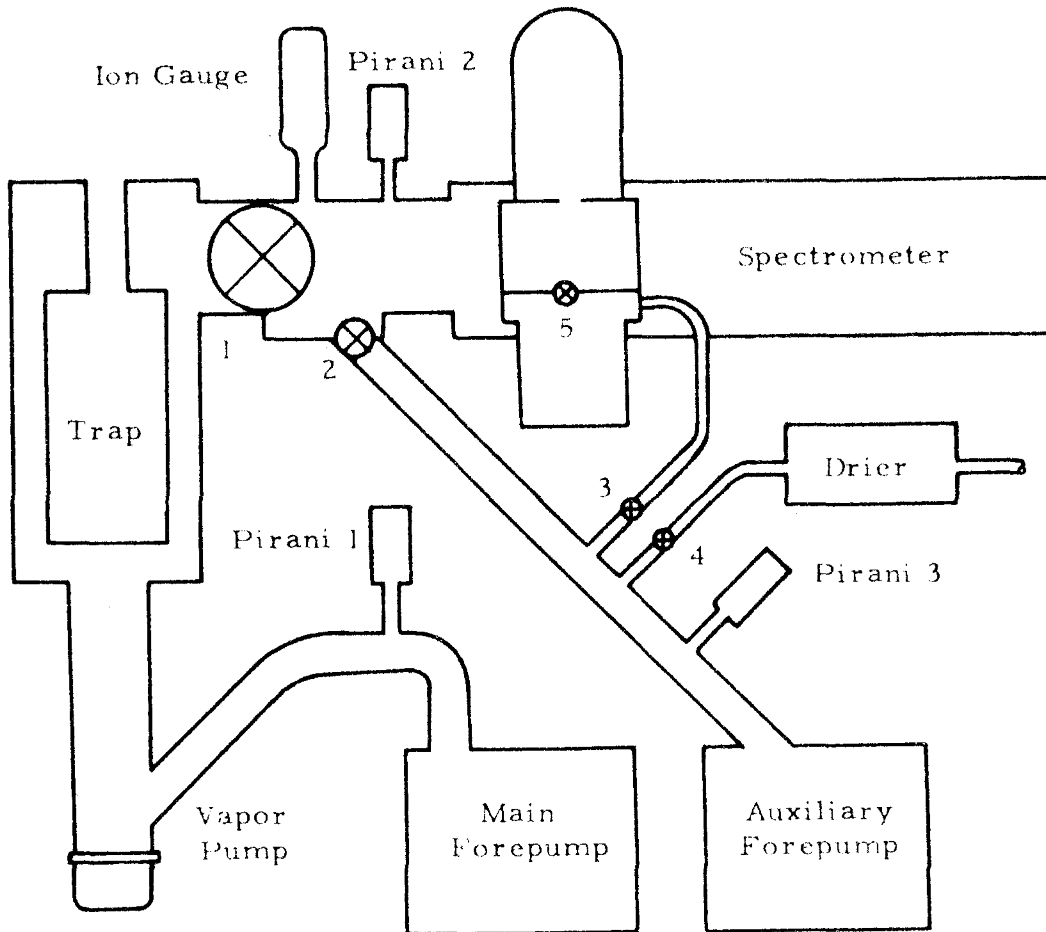

FIG. 15 Schematic of the vacuum system.

was experienced at first with the proper seating of this valve, but this was overcome by allowing the "O" ring plate two rotational degrees of freedom through the use of gimbals. The frame containing the gimbals is forced upward by cams as the valve is closed to provide the initial squeeze on the "O" ring.

The vacuum system is provided with three Pirani gauges and an ionization gauge. The ionization gauge indicates the pressure in the main system and may also be used to locate leaks in the vacuum system. If the suspected parts are sprayed with a jet of illuminating gas, the ionization current will increase when the jet strikes a leak. Pirani no. 1 is located on the high pressure side of the diffusion pump and serves as a check on the function of the diffusion pump. Pirani no. 2 is located on the low pressure side of the diffusion pump and indicates when the pressure in the main system is sufficiently low for the operation of the diffusion pump. Pirani no. 3 is located on the auxiliary manifold and serves to indicate the pressure in the airlock.

The procedure for changing specimens while the system is under vacuum is as follows. In normal operation of the instrument, valves 1, 4, and 5 are open and valves 2 and 3 are closed. The stage assembly on which the specimen is mounted is first lowered by means of a 1/15 horsepower motor which drives a threaded nut through a worm gear (this worm gear can be seen in fig. 12). A flexible brass bellows permits the stage to move downward about an inch while vacuum is still maintained. With the stage assembly in the lowered

position (see fig. 9) valve 5 may be closed and the airlock let down to air by opening valve 3. The stage assembly is removed and a new specimen mounted in it. The auxiliary forepump is started, the stage assembly replaced, and valve 4 is closed. When Pirani no. 3 indicates sufficiently low pressure, valve 3 is closed, the forepump is shut off, and valve 5 is opened. The motor which drives the stage assembly up and down is reversed by means of a switch and started. As the specimen moves upward it gradually comes into view in the viewing microscope, and the motor is stopped when the specimen reaches the focal plane. Small adjustments of the vertical positioning can be made by manually adjusting a knurled knob on the shaft of the worm gear.

For the benefit of those who will be concerned with operating this instrument in the future, it is well to consider a few practical aspects of the operation of the vacuum system. Both organic diffusion pump oil (Narcoil-20) and Silicone diffusion pump fluid (Dow No. 702 Fluid) have been tried in the diffusion pump. While Ennos (33) recommends avoiding Silicone pump fluids because of the reduced electrical conductivity of the contamination deposits, this was not found to be a serious limitation and the use of the Silicone fluid avoids the necessity of cleaning the diffusion pump frequently.

The cold trap has been operated with liquid air, a mixture of dry ice and acetone, and without refrigeration. With liquid air, the trap required filling about every four hours and did not effectively trap the oil vapors, unless it was filled more frequently, because of the variation in the cold zone as the liquid air level varied. With dry

ice and acetone the trap required filling a few times a week and was effective in trapping the oil vapors because the thermal conductivity of the acetone resulted in a more nearly constant cold zone. The temperature of the dry ice - acetone mixture is not sufficiently low to trap water vapor effectively, but this is not a serious limitation because the dryer removes moisture from the air which is periodically admitted to the system. Operation of the cold trap without refrigeration resulted in large quantities of pump oil collecting in the pumping manifold due to "creep" or back diffusion and eventually resulted in very poor operation of the diffusion pump as a result of the loss of this oil. Even without refrigeration, however, it was possible to operate the beam system although the contamination rates were higher.

In the alignment of the spectrometer it is necessary to operate the spectrometer in air, since the alignment is accomplished by successive approximations. The spectrometer case, however, is ordinarily a link in the vacuum line from the main manifold to the electron probe. It is therefore necessary to use a special fitting which connects the opening in spectrometer case leading to the pumping manifold with the opening leading to the specimen housing. This fitting is clamped temporarily in place by brackets and has "O" rings which seat on machined faces on the inner sides of the spectrometer case (see fig. 18, p. 143). The fitting is L-shaped in order to facilitate moving the spectrometer crystal close to the specimen and has a window of Mylar 1 mil thick and 2 inches in diameter opposite the opening leading to the specimen housing. The Mylar window

is sufficiently thick to support atmospheric pressure but results in negligible absorption of the x-rays (about 2% for copper K α).

The pressures normally attained in the operation of the instrument are about 2 x 10^{-5} mm of mercury. The mean free path of electrons in air is about 20 meters at this pressure (52). Although one requires only a pressure sufficiently low that the mean free path of the electrons is long compared to the dimensions of the probe system (e.g. 10^{-3} mm of Hg), lower pressures than this are desirable to reduce the formation of contamination deposits and increase filament life.

3. The sample traverse mechanism and viewing system

The stage assembly which is used to produce a translation of the specimen under the electron probe is illustrated in fig. 16. The cover of this assembly has been removed in order to show the mechanism which is used to accomplish the translation. The vacuum seal between the stage assembly and the instrument is made by means of a greased taper joint which permits a rotation of the entire assembly about the axis parallel to the electron beam. This feature was provided in order to facilitate establishment of the curve for x-ray self-absorption correction, but it is not essential to the operation of the instrument since the absorption curve can be obtained by other means.

Two shafts are introduced in the base of the stage assembly through "O" ring seals. Each shaft has a precision thread of 1/2 mm pitch on which a split bronze nut travels. The nut in each case is

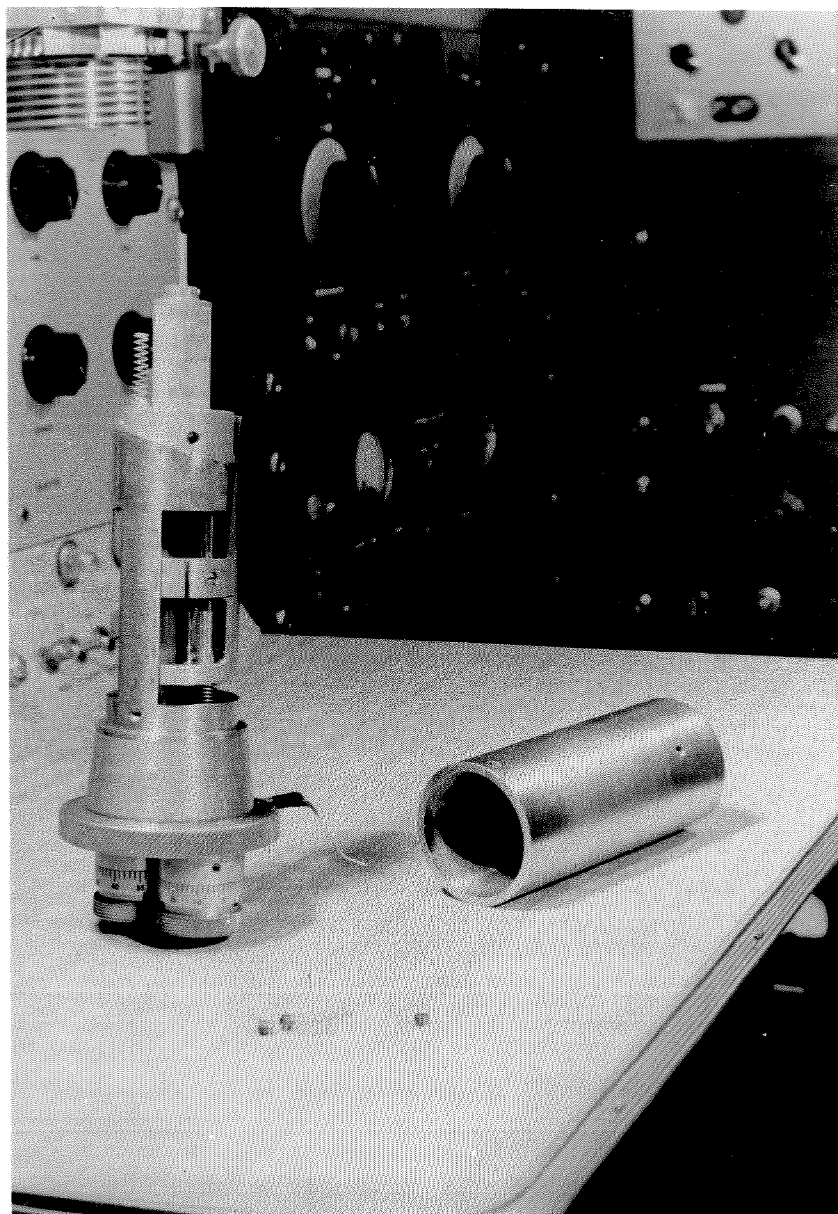

FIG. 16 The stage assembly used to translate the specimen under the electron probe.

constrained by the shape of the body of the assembly in such a way that rotation is prevented, and is spring-loaded with respect to the body by a helical spring coaxial with the shaft. The upper end of each shaft has a recess containing a ball bearing which rides in an insert of Morganite mounted in the body of the assembly. Affixed to each nut is a polished steel wedge which, on rotation of the calibrated knob attached to the shaft, translates the stage in a plane inclined at 15 degrees to the horizontal. The lines of intersection of the polished faces of the wedges with this plane are mutually perpendicular, and consequently the motion which is conveyed to the stage itself takes place independently in two mutually perpendicular directions. The stage makes contact with the face of one of the wedges at two points and with the face of the other wedge at one point. This kinematic feature was found to result in rectilinear motion to a high degree. Helical springs exert a downward force on the base of the stage when the cover is in place, and other helical springs exert lateral forces which are necessary to maintain contact between the stage and the surfaces of the wedges.

The stage contains a polystyrene insulator in which is mounted a brass bushing. The specimen which has the form of a rod 1/8 inch in diameter and 1 1/16 inch long fits into the bushing and is held in place by a set screw. The brass bushing is connected to a flexible wire which passes through a glass tube extending to the outside of the vacuum system and permits the beam current collected by the specimen to be measured. The glass tube is drawn to a capillary

for a distance of several inches from the bushing to provide the flexibility necessary to allow movement of the stage.

The specimen can be translated a distance of 2 mm in each direction in very small increments, since the angle of the wedges was chosen so that each revolution of the shafts corresponds to a movement of the stage of about 50 microns. For linearity of the calibration it is necessary that the eccentricity of the shafts (or more precisely, the axis of the precision thread with respect to the axis of rotation of the shafts) be made very small, and this constitutes a serious disadvantage of the design.

Another limitation as a result of the design is large hysteresis in the movement of the stage due to friction at the sliding contacts. This trouble is augmented by the difficulty of lubricating these sliding contacts, in addition to the thrust bearing and threads, when the stage is under vacuum. The use of Silicone vacuum grease caused severe binding because this grease permits the metal parts in contact to "seize". Organic diffusion pump oil or Lubriseal vacuum grease have been used as lubricants with greater success.

Some mention should be made about the orientation of the specimen in the stage assembly. Surface irregularities will produce errors in the analysis if they result in a change of the self-absorption path of the x-rays which are analyzed. Such surface irregularities are difficult to avoid because there is no known method of producing a perfectly flat smooth surface on a specimen which is not homogeneous. For example, in the case of a linear diffusion couple, the various

diffusion zones corresponding to different composition will be affected differently by mechanical polishing and electrolytic or chemical etching. Whenever possible it is desirable to orient the specimen in such a way that the boundaries of regions of different composition are parallel to the direction of the emerging x-rays which are accepted by the spectrometer.

In the study of the composition of regions on the surface of an alloy it is necessary to know at any given time on what region of the surface the electron probe is impinging. This can be done by a variety of methods. In England attempts are being made to utilize the probe itself to obtain this information by causing the probe to scan the surface and by reconstructing an image of the surface on a cathode ray tube which is modulated with the x-ray signal (6) (7). In such a scanning arrangement it is also possible to employ secondary electron emission as in the secondary emission microscope of Zworykin (3), but this is susceptible to a greater difficulty of interpretation. Castaing has employed a special optical microscope objective and a small perforated mirror in the original version of his instrument, which had electrostatic focusing (15). In a later version, in which magnetic focusing was used, he uses a reflecting microscope objective which is contained in the upper pole piece of the objective lens. In this country Fisher and Swartz have attempted to overcome the difficulties resulting from the small working distance of the objective lens of the electron probe by using a magnetic repeater lens of near unity magnification to refocus the electron spot, and by

inclining the specimen at an angle of 45 degrees to the axis of the electron beam. The objective of the light microscope can then view the surface in the usual fashion. This procedure, however, results in lower currents possible in the electron probe because of the additional spherical aberration of the repeater lens.

The solution which was used in the Caltech instrument was to place the viewing system in the gap of the lower magnetic lens. This would not be possible with ordinary microscope objectives because of the large size of the lens mounting, but a Zeiss objective which is used in the "Ultropak" dark field illumination system has small external size and can be modified to fit between the pole pieces. The objective then views the surface of the specimen by means of a small mirror which is mounted on the aperture holder and which moves with it. It is not necessary for this mirror to be perforated, as the electron beam can pass over its edge if the surface of the specimen is inclined with respect to the electron beam. At the present time the surface of the specimen must be inclined at an angle of 15 degrees to conform to the constraints of the stage assembly, and this results in a small sacrifice in the numerical aperture of the system. An improvement of the viewing system could be made by modifying the stage assembly so that the full numerical aperture of the objective (N.A. = 0.25) could be used,but the angle of inclination of the specimen should not be increased more than necessary since the finite depth of focus of the microscope will result in an error of parallax in the location of the electron probe.

The completed viewing system is shown in fig. 17, which shows the sample housing with the rest of the electron beam system removed. The microscope objective can be seen to the left of the center of the housing. The mirror used to view the surface of the specimen is inclined at 45 degrees to the surface of the specimen, but is not visible in the photograph since it is mounted on the lower side of the aperture holder.

The specimen housing has a glass window for light to pass into and out of the vacuum system, and this is inclined slightly with respect to the axis of the objective to prevent back-reflection. Just outside the vacuum window is a beam splitter which serves the double purpose of admitting the illumination and permitting visual observation of the specimen. The beam splitter is housed in a cylindrical aluminum box attached on the left of the specimen housing (fig. 17). This box has an eyepiece tube of adjustable length at right angles to the axis of the objective. The axis of this tube is parallel to the surface of the specimen so that the orientation of the image can be related most easily to the orientation of the specimen. The eyepiece which is shown in fig. 17 is a filar micrometer eyepiece and may be used for measuring distances on the specimen.

Illumination for the microscope is provided by a ribbon filament illuminator which is located on the corner of the instrument table (see fig. 7).

The alignment of the optical system is accomplished in the following manner. With the instrument in the state of assembly shown in fig. 17 the aperture is adjusted to be approximately centered

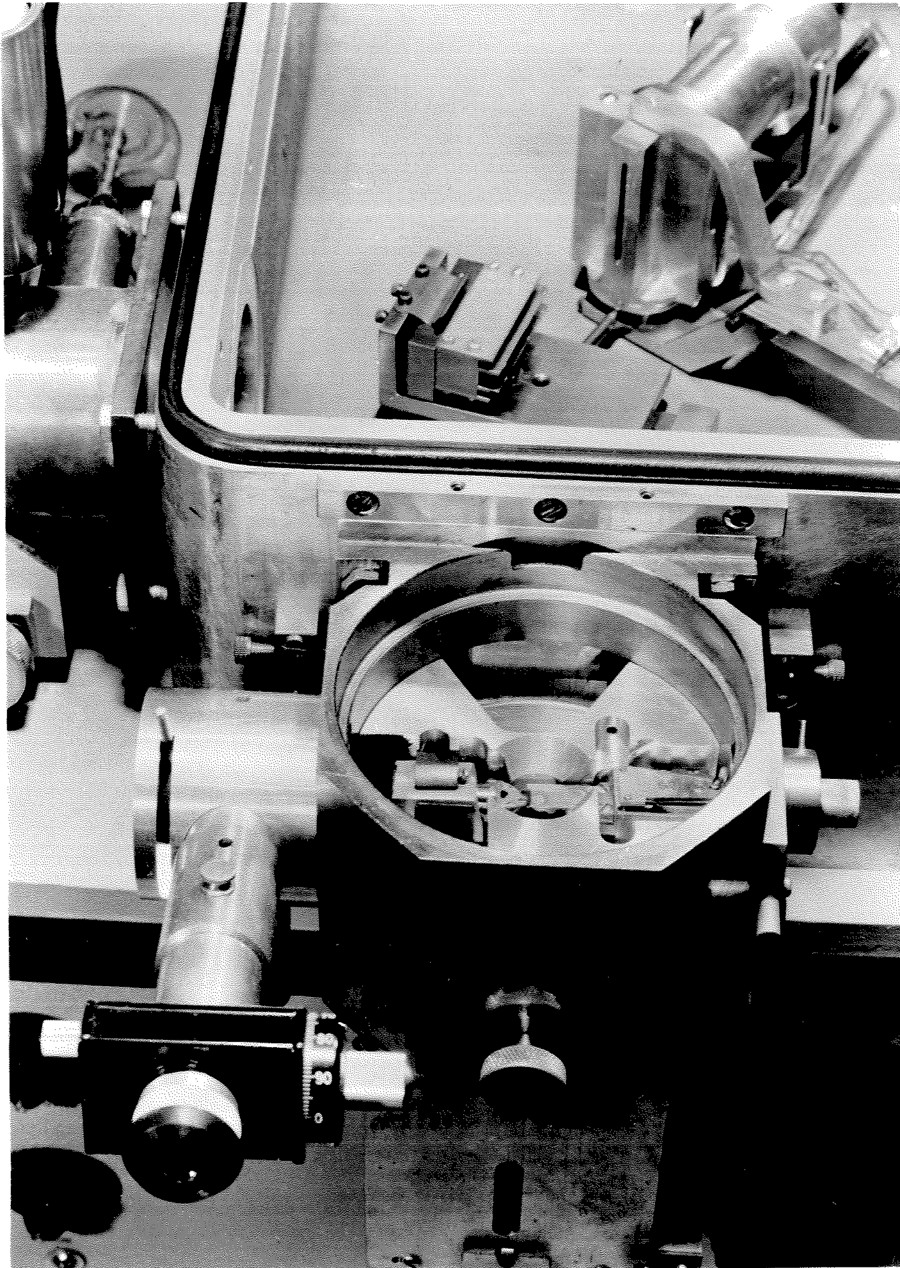

FIG. 17 View of the sample housing which shows the aluminum pole-tip spacer, the viewing microscope, the mirror and aperture mount, and portions of the spectrometer.

with respect to the bore in the lower pole piece. The objective is then adjusted for position along its own axis so that the optical path from objective to the plane of the specimen is approximately equal to the working distance of the objective (5.8 mm). The beam system is then assembled and with the probe in operation, the aperture is centered by the method described in the preceding section (p.127). The beam system is dismantled again to the state shown in fig. 17, a specimen is placed in the proper position, and the axial position of the objective readjusted to focus on the specimen. At this time, the tube length of the microscope is also adjusted to correct for the spherical aberration which results from the presence of the vacuum window in the optical path. When these two adjustments are satisfactory, the corresponding locking screws are tightened and the rest of the electron probe system is assembled.

The alignment of the illuminator is not critical, but should be adjusted properly to minimize glare. The condensing lens of the illuminator may be adjusted by placing a grid (tissue paper or other textured translucent material will also serve this purpose) and moving it along the light path until a sharp shadow picture is seen through the microscope when it is focused on a specularly reflecting sample. Without moving the grid the condenser is then adjusted to focus in the plane of the grid. The optical axis of the illuminator must also be adjusted to coincide with the axis of the objective. This is accomplished by removing the eyepiece of the microscope and viewing the reflections from the various lens surfaces of the objective. Proper alignment

is indicated when these reflections all lie on a line passing down the center of the objective.

As a final adjustment with the probe in operation and with a fluorescent screen as a target, the objective is translated perpendicular to its axis by means of the two screws, which may be seen on the front of the specimen housing, until the image of the electron focus coincides with the intersection of two hairlines in the eyepiece.

4. The spectrometer and associated equipment

The spectrometer, which is used to analyze the characteristic radiation emitted by the part of the specimen under the electron probe, is of the Johann-DuMond type. This type of spectrometer is ideally suited to this application because of the small size of the source of x-rays and because the focusing action of the crystal helps to compensate for the low intensity of radiation at small concentrations.

A general view of the spectrometer is shown in fig. 18. The casting was made by the Aluminum Company of America using 356-T6 aluminum and has two bronze taper bearings set in the bottom which serve as female taper bearings for the shafts on which the gears are mounted. The crystal and detector arms are mounted on 120 degree sectors of Boston gears NA 200 and NA 180, respectively. These gears are driven by Boston gears GA 25 and GA 45 which are mounted on a common shaft brought out of the vacuum system through an "O" ring seal. The use of commercial gears in this spectrometer was possible, because it is not necessary to make precise wavelength measurements in the analysis, but only to be able to set the spectrometer reproducibly on known lines. The gear ratio between the

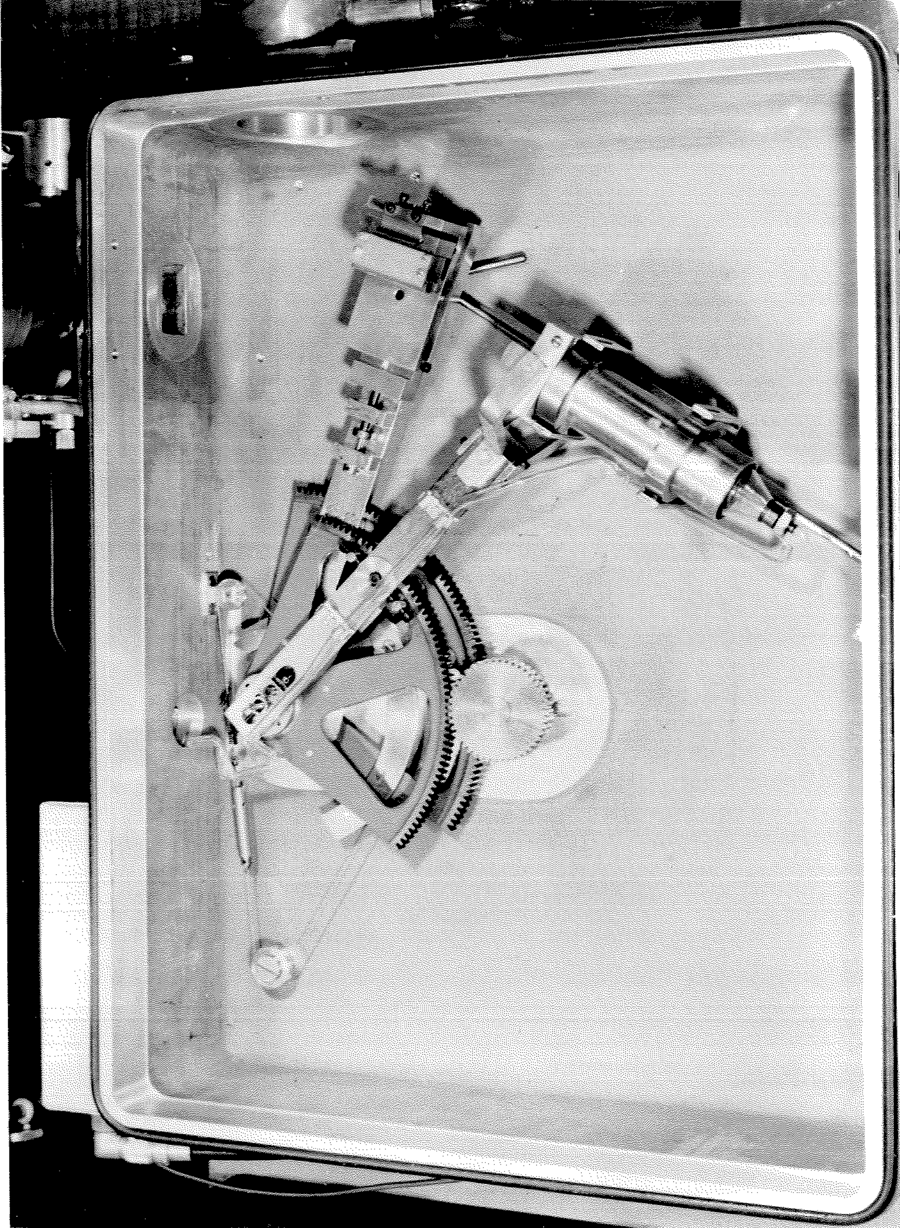

FIG. 18 The vacuum x-ray spectrometer.

detector beam and the crystal beam is 2 to 1, and therefore the crystal and detector are in the correct relation to satisfy the Bragg conditions for all positions of the spectrometer.

Backlash is removed from the spectrometer gear train by means of a braided phosphor-bronze cable which is attached to a pulley sector on the detector gear at one end and to a pulley sector on the crystal gear at the other end. This cable is supported at two other points by fixed pulleys attached to the spectrometer casting. Tension is maintained in the cable by means of a helical spring and a turnbuckle, resulting in a torque between the detector gear and the crystal gear in such a way that the teeth of each gear always have the same side in contact with the teeth of the driving gear. There is no change in the tension in the cable for the different spectrometer settings, since the ratio of the diameter of the crystal pulley and the diameter of the detector pulley is the inverse of the gear ratio.

The shaft to which the driving gears are affixed extends through the bottom of the spectrometer case and through the top of the instrument table. Located below the top of the instrument table on this shaft is a 12-inch-diameter drum and a worm wheel. The drum consists of a pulley having a 1-inch face. The crown of this pulley has been turned off, and the resulting cylindrical surface divided into 225 equal divisions, each division corresponding to an angular displacement of the crystal equivalent to 1/10 degree of the Bragg angle. Other markings can be put on the face to correspond to the location of the various characteristic lines of interest if this should prove desirable.

The calibrations can be viewed through an opening in the remote control panel by means of a prism (see fig. 9). Illumination is provided by a lamp house below the prism. The fiduciary for the scale consists of the hairline from a 6-inch slide rule which has been etched with additional divisions corresponding to 0.02 degree of Bragg angle.

The worm wheel is driven by a shaft which extends to the front of the instrument and which can be rotated by means of a handwheel. This handwheel may be seen in fig. 7 to the right of the viewing prism. The worm wheel has 30 teeth, giving a gear ratio from the hand wheel to the spectrometer driving gears of 30 to 1. This ratio should be increased to give greater sensitivity in setting the spectrometer.

The crystal used in the spectrometer consists of a quartz lamina measuring 3.5 cm by 1.43 cm. It is one of five such lamina obtained by Dr. DuMond from Jobin and Yvon, 26 rue Berthollet, Paris, France. The lamina has been ground to a radius in the unstressed state of about 53.08 cm. The planes which are used are the $10\bar{1}1$ planes with a grating constant of 3336.2 X.U. (53), and these planes make an angle of about 3 degrees with the surface of the crystal at its center. This gives rise to an asymmetry in the spectrometer which can be very useful in this application. The crystal is mounted so that the angle between the crystal and source is $(2\theta + 6)$ degrees where θ is the Bragg angle, and the angle between the crystal and detector is $(2\theta - 6)$ degrees. This overcomes the difficulty of the large size of the electron lenses in the electron probe

system, which would otherwise make it impossible to obtain settings of the spectrometer corresponding to small Bragg angles.

The crystal mounting provides for 5 degrees of freedom and the detector mounting for 2 degrees of freedom. The detector is constrained so that the end-window geiger tube is always directed with its axis toward the center of the crystal. Two slits restrict the x-rays which are accepted by the geiger tube. The first slit, which is nearest the geiger tube window, may be adjusted symmetrically about its center by means of a screw which can be seen in fig. 18. The second slit is of fixed size and serves only to prevent the direct radiation from the source from entering the defining slit (see fig. 17).

The spectrometer covers a range in wavelengths from about 1.1 to 3.5 Å. It is therefore possible to study elements of atomic number 20 (Ca) through 33 (As) by means of their K_α radiation, and atomic numbers 50 (Sn) through 83 (Bi) by means of their L_α radiation. In addition, limited study of elements of atomic numbers 34 to 46, and 83 to 92 is possible by obtaining the K_α and L_α reflections in the second order. However, the intensity of the second order reflections is quite low for the crystal planes which are used, being only 15% of the first order (53).

The procedure for aligning the spectrometer is that suggested by Castaing in his thesis (15). In this method, after a preliminary adjustment of the radius of the source, crystal and detector, the

spectrometer is adjusted by successive approximations using two different x-ray lines corresponding to different parts of the focal circle. The K_α doublets of nickel and titanium were used, since both of these lines can be obtained with the spectrometer operating in air and the vacuum bypass in place. For the purpose of this adjustment, a specimen consisting of a piece of nickel wire and a piece of titanium wire pressed into a brass tube is used as a target. By translating the stage it is therefore possible to convert rapidly from a nickel to a titanium target and vice versa.

An improvement over Castaing's method of alignment can be obtained if one makes use of the calibration of the spectrometer in terms of Bragg angles. The Bragg angle scale, of course, has an arbitrary zero, since the adjustment of the position of the source relative to the spectrometer axis does not take place along a radius vector. However, it is possible to calculate separately the zero position of this scale with reference to each of the two lines since the grating constant of the crystal is known. If these two values do not agree, a misalignment is indicated, and the direction of the adjustments which must be made is partly indicated by noting whether the zero position calculated from the location of the titanium line is higher or lower than the zero calculated from the nickel line. The indication is not unique, however, so there is still need for some "trial and error" methods. It might be possible to make a further improvement in the method of adjustment by using the zero of the

Bragg angle scale calculated with reference to the lines from three elements.

At present, the detector which is used in the spectrometer is a type D-34 A geiger tube manufactured by Nuclear Chicago. This tube has a neon fill and is not efficient for the shorter wavelengths of the spectrometer's range. It is hoped that this tube can be replaced in the near future with a special multicellular geiger tube now under construction. This tube has 4 end-window cells 1/4 inch in diameter and 4 inches long arranged in a linear array. It has a window of mica about 1.3 mg/cm^2 surface density and will be filled with argon and an organic quench at approximately atmospheric pressure. The window is capable of supporting atmospheric pressure in either direction and should have a transmission of about 60% at the longest wavelengths in the spectrometer range.

The cables from the geiger tube consist of bare wires insulated with segments of glass tubing. The connections are brought outside the vacuum system by means of a header plate which is sealed to the spectrometer case with an "O" ring. A preamplifier, consisting of a pentode and cathode follower, is mounted on the side of the spectrometer case (see fig. 7). From the preamplifier the pulses pass through coaxial cables to a double scaler. This scaler is identical to those in use at the Caltech Synchrotron Laboratory and may either be used with two input channels each having electronic scales of 99 and a high speed mechanical register, or with a single input channel having an electronic scale of 9999.

The double scaler is located at the top of the instrument rack on the main table (see fig. 7). Below the scaler and in the same rack is a counting-rate meter which is operated by a signal obtained from the scaler. The counting-rate meter has a meter movement for semi-quantitative work and a loudspeaker for audio indication of the counting rate. The audio indication may be in the form of individual clicks or in the change in frequency of a tone from a frequency modulated audio oscillator. This latter form of audio indication makes it easier to discern changes of counting rate, particularly at high counting rates, and has proved to be very useful for locating lines of unknown elements in the target and also for aligning the spectrometer.

The instrument is equipped with provision for measuring the x-ray intensities for a given interval of time or for a given total charge collected by the target. In the fixed-time measurement the gate in the scaler is controlled by a timer which is adjustable for periods of 3 to 120 seconds. The timer is incorporated in the power supply for the geiger tube which is located in the auxiliary instrument rack (see fig. 7). In the fixed-charge measurement the gate in the scaler is controlled by a current integrator. The current collected by the target charges one of three polystyrene film capacitors (0.01, 0.05, 0.1 μFd), and the gate in the scaler is closed when the voltage across this capacitor reaches a predetermined value set by a decade of precision resistors and a helipot. The integrating capacitors are mounted on a plug-in unit in the preamplifier which may be seen to the left of the vacuum controls and just below the remote control panel in fig. 7.

The circuit diagram for the preamplifier and the current integrator is reproduced in fig. 19. The potential of the grid in the electrometer tube in the preamplifier is maintained constant by feedback from the main amplifier to the opposite side of the integrating capacitor. The grid bias of the electrometer tube is adjusted so that the tube is always operating in a portion of its characteristic where minimum grid current is drawn. Additional advantages of this arrangement are maximum stability and a constant potential of the target during the integrating cycle. A meter and selector switch in the feedback circuit permits monitoring the potential difference across the integrating capacitor (α charge) or the time derivative of this potential (α current) during the period of integration.

In the use of the current integrator it is desirable to know the time which is required to collect a given charge on the target. This can be important to obtain a first approximation to concentration (see p. 79 ff.). A clock is therefore provided which records the time that the gate in the scaler is open.

Both the current integrator and the cycle timer have a provision for automatically resetting the electronic registers of the scaler at the start of the counting cycle if this is desired. On the other hand, if the counting interval (time or charge) is to be doubled or tripled for some of the measurements, the reading on the electronic registers can be retained by disabling the automatic reset by means of a switch.

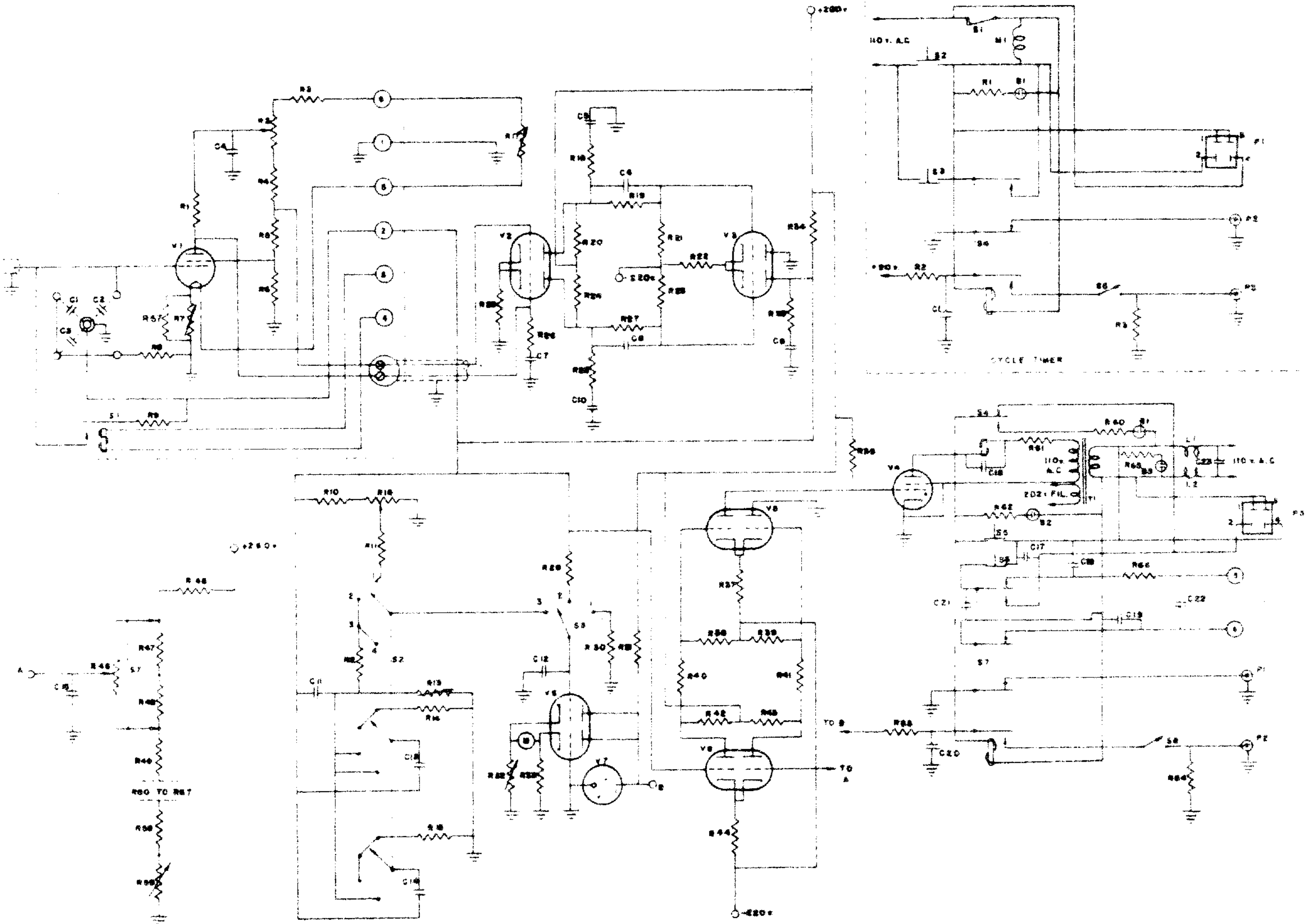

FIG. 19 Circuit diagram of the current integrator used for fixed-charge measurement of the x-rays. The circuit diagram of the cycle timer which may be used for fixed-time measurement is also shown.

Key to FIG. 19

Components for the integrator

V1--CK5886 (Raytheon)
V2, 8--12AX7 (fil. in series string, regulated B+)
V3, 4--12AT7 (fil in series string regulated B+)
V4--2D21
V5--12AT7
V6--12AU7
V7--OB2

R1--1M, 2 w*
R2--10K, 2 w pot. "Amp zero"
R3--225K, 2 w*
R4--14K, 2 w*
R5--7.5K, 2 w*
R6--7K, 2 w*
R7--500 Ω, 2 w* AB pot. "Bias"
R8--1M, 2 w*
R9--200K, 1 w
R10, 11, 12--1M
R13--2.5M, 2 w, AB pot. "Cal. current"
R14, 15--4.7M
R16--25K, 2 w, AB pot. "Cal. charge (volts)"
R17--25K, 2 w pot. "Fil.current"
R18, 28--10K, 1/2 w
R19, 27--3.3M, 1 w
R20, 24--200K, 2 w*
R21, 25--1.5M, 1 w
R22--33K, 2 w*
R23--16K, 2 w*
R26--100K, 1/2 w
R29, 30--1M
R31--6K, 10 w
R32--2.5K, 2 w AB pot. "Zero V.T.V.M."
R33--1.5K
R34--100K, 2 w
R35--820 Ω
R36--470K, 2 w
R37--100K, 2 w
R38, 39--1.5M, 2 w
R40, 41--2.2M, 2 w
R42, 43--100K, 2 w*
R44--330K
R45--150K, 2 w*
R46--20K helipot "Gate set, fine"
R47-58--10K, 1/2 w*
R59--500 2 w, AB pot. "Gate zero"
R60, 62, 65--60K, 1/2 w
R61--2K, 5 w
R63--4.7M
R64--100 Ω, 1 w
R66--100 Ω, 1 w
R67--250 Ω, 2 w*

C1, 2, 3--polystyrene film capacitors, 0.01, 0.05, 0.1 μFd, 400 v, on plug in unit
C4--0.005 μFd, 600 v
C5, 10--0.06 μFd
C6, 8--0.002 μFd
C7--0.02 μFd, 600 v
C9--0.04 μFd
C11, 13--0.25 μFd, 400 v
C12--0.1 μFd
C14--0.5 μFd
C15--1 μFd, 200 v
C16--50 μFd, 50 v
C17, 18, 19, 23--0.01 μFd, 400 v
C20, 21, 22--0.1 μFd, 600 v

P1--SO239 "Gate"
P2--SO239 "Reset"
P3--4 pin Jones plug to clock, 1 and 3 common, 2 brake release, 4 motor

L1, 2--No. 26 wire on 1/2" form 1-1/2" long (not crit.)

M--0-1 ma.

B1--NE51, "Zero indicator"
B2--NE51, "Integrate"
B3--NE51, "Power"

S1--DPST Relay 110 V.A.C. coil, modified for low leakage
S2--3 pole 4 pos. rotary sw., "Monitor", pos. 1 reads voltage, pos. 2, 3, 4 read dV/dt, rel. scale factors of 1, 2, 4
S3--1 pole 3 pos. rotary sw., pos. 1 reads V.T.V.M. zero, pos. 2 reads voltage, max. sensitivity, pos. 3 monitors as selected by S2
S4--SPDT plate circuit relay
S5--NO push button sw, "Start"
S6--NC push button sw, "Stop"
S7--4PDT relay, 110 V. ac. coil
S8--SPST toggle sw; "Reset"; open- "Manual", closed- "Automatic"
S9--2 pole 11 pos. rotary "Gate set, coarse"

---

*precision or temperature stable resistor

IV. A Preliminary Application of the Electron Probe Microanalyzer

In order to demonstrate the use of the instrument described in this thesis and of the correction formulae which must be used to obtain quantitative information from the relative x-ray intensities, it is desirable to consider a specific application. A useful alloy for such a preliminary application would be an alloy containing iron and chromium, since this case involves the use of both the self-absorption correction and the fluorescence radiation correction because of the selective absorption of the characteristic x-radiation of the iron in chromium. Moreover, in this case the specimen is ferromagnetic and it is of practical interest to demonstrate that it is possible to study ferromagnetic materials in an electron probe instrument which employs magnetic electron focusing.

The iron-chromium alloy, however, does not permit a comparison of the fixed-charge measurement of the x-rays with the fixed-time measurement, since the atomic numbers of iron and chromium are quite close together. We will assume that in this case the first approximation to the concentration is given by the proportionality of the intensity of an emission line of an element and the mass concentration of that element. We will attempt to illustrate the magnitude of the corrections in this case, the computation of the mass concentrations, and the check which is afforded by summing the concentrations.

The specimen which was studied consisted of electrolytic iron impregnated with chromium. The process by which this is done is known as chromizing and is carried out by treating the iron with $CrCl_2$

at a temperature of 1300 to 1400 $^{\circ}$C. The $CrCl_2$, which is produced by reaction of hydrogen and hydrogen chloride with chromium, reacts with the iron at the surface of the specimen to form iron chloride and metallic chromium. The iron chloride passes off in the vapor phase, and the chromium diffuses into the specimen at a rate which depends on the temperature at which the process is done.

The chromizing was done by the Chromalloy Corporation, 450 Tarryton Rd., White Plains, N.Y. (courtesy of Richard P. Seelig) and is referred to as their process number Crel 95.15 fal. After chromizing, the specimens were plated with 0.010 inch of hard nickel so that rounding of the edges would not take place in the polishing of sections.

At first, a specimen having a volume of about 20 mm^3 was examined in the microanalyzer, but it was found that as the specimen was translated under the electron probe the focal spot was displaced. This displacement resulted in a shift in the setting of the spectrometer for which the intensity of the x-ray line was a maximum because of the high spatial resolving power of the curved crystal spectrometer (about 40 microns). If the spectrometer setting was held constant, as the specimen was translated the sensitivity of the spectrometer varied with specimen position, which also gave erroneous results.

A specimen having a volume of 3 mm^3 still resulted in this type of error, but the effect was practically negligible for a specimen of 0.2 mm^3 in volume. The preparation of a specimen of this size was accomplished by attaching it to the end of a brass rod with silver paint and then embedding in plastic using a special holder. The holder

served the dual purpose of determining the angle of the specimen's surface during polishing and of permitting the specimen rod to be extracted from the plastic without damage to the polished surface. As the plastic was transparent (lucite) it was a simple matter to polish the specimen to a thickness of a few thousandths of an inch. When the specimen was removed from the plastic, sufficient plastic was left around the specimen to keep it in place on the brass rod, but it was found that the surface of this plastic would become charged and deflect the electron probe unless it was coated with silver paint.

Since the concentration of chromium at the surface of a specimen of chromized iron is less than unity (being limited by the equilibrium of the displacement reaction), it was necessary to make use of a standard sample containing pure iron and pure chromium. The volume and shape of this standard were nearly the same as that of the chromized specimen and made it possible to determine the ratio of the intensity of CrK_{α} and FeK_{α} radiations from pure targets. This ratio was used to calculate the intensity which would have been obtained from pure chromium in the specimen by multiplying by the observed intensity from pure iron in the specimen (after corrections for dead time).

A photomicrograph of the specimen's surface after the analysis is shown in fig. 20. The trace of the contamination deposits where the focal spot remained for an x-ray intensity measurement can be seen as well as the boundary between the nickel plating and the surface of the chromized specimen (arrow A). The mottled portion in the

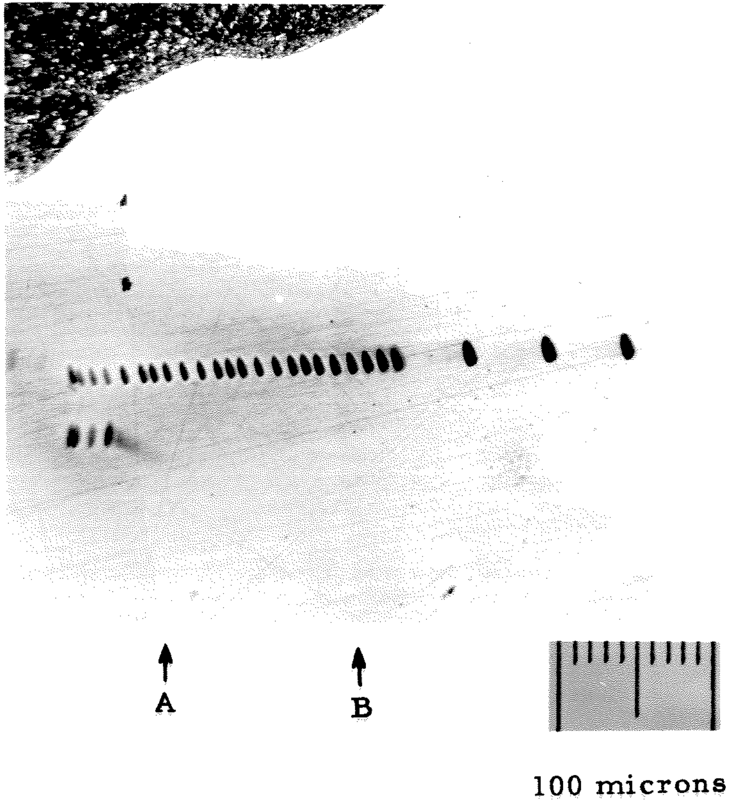

FIG. 20 Photomicrograph of the chromized iron specimen after analysis.

upper left corner is silver paint which was carried over the surface of the specimen to insure good electrical contact. It will be noticed that the contamination deposits are elliptical in shape and this is undoubtedly due to astigmatism in the electron probe. The variation in the size and density of the contamination deposit is probably due to the variation in thermal properties with composition, although there may be some effect of the ferromagnetic material in changing the focal length of the electron lens.

The electron focal spot was about 5 x 10 microns and had a current of about 0.4 microamp. This resulted in an intensity of the unresolved FeK_{α} doublet of about 2050 counts per second from a target of pure iron, and the dead time correction is very important at these high counting rates. A plot showing the calibration of the geiger tube is shown in fig. 21. The experimental points are not well represented by an equation of the form

$$N = \frac{N_c}{1 - N_c \tau} \tag{5.1}$$

as can be seen from the dashed curve plotted for τ = 281 microseconds which was selected to fit the experimental curve at low counting rates. In general, it is best to reduce intentionally the intensity of the beam if the dead time correction is more than about 10% because of greater uncertainty in the dead time correction at high counting rates.

The intensity of the FeK_{α} radiation must be corrected for self-absorption since the absorption coefficient of the alloy for radiation

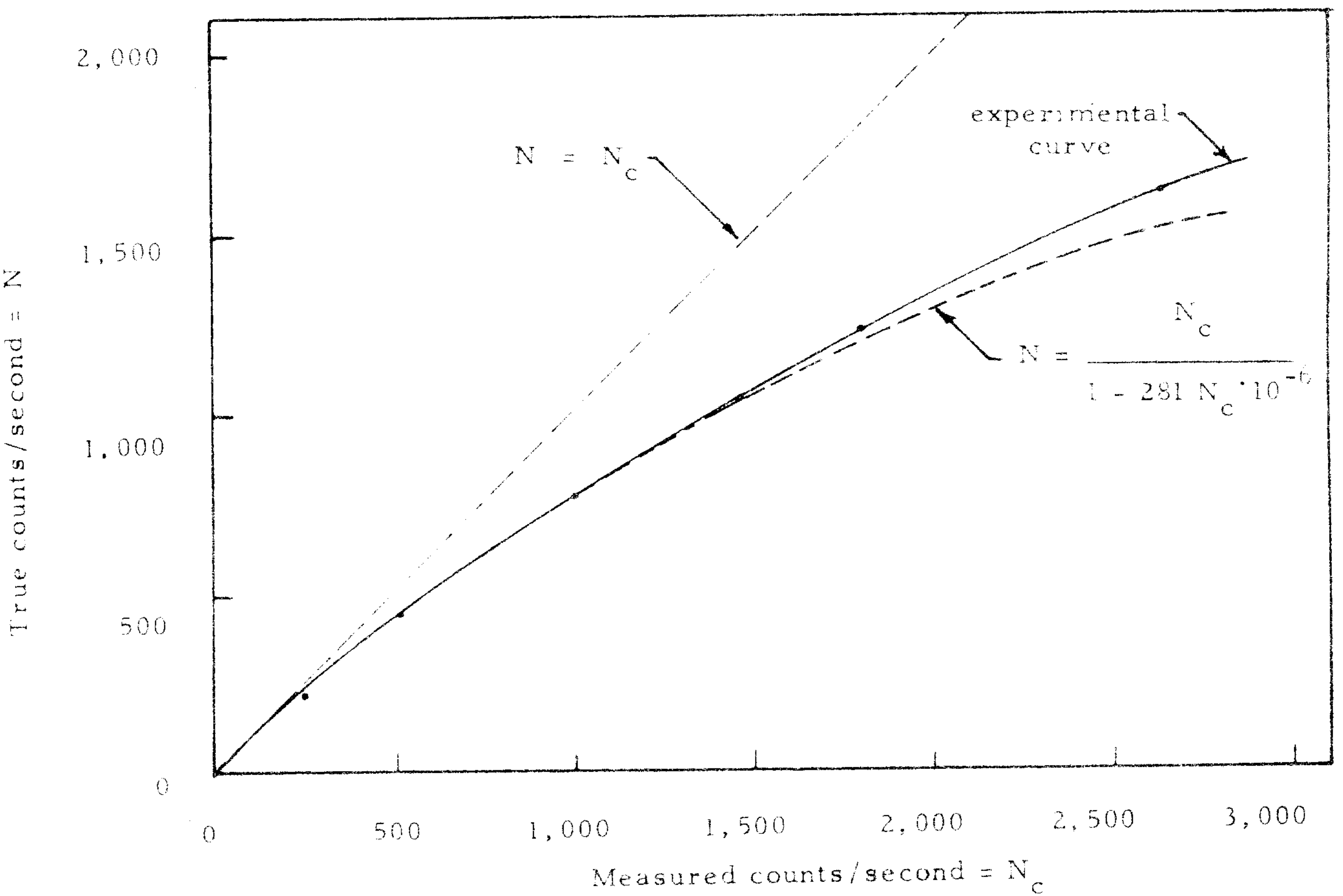

FIG. 21 Calibration curve for the detector (Nuclear Chicago D-34 geiger tube).

of this wavelength varies widely with composition. The intensity of the CrK$_\alpha$ radiation must be corrected for fluorescence excitation, which is particularly important at low concentrations of chromium. The fluorescence correction gives the fraction of the observed intensity which is due to fluorescence; it would be necessary to correct also for self-absorption of the CrK$_\alpha$ radiation were it not for the fact that the mass absorption coefficients of iron and chromium are nearly the same for radiation of this wavelength.

The first step in making the necessary corrections is to obtain values for all of the quantities which appear in the correction formulae. The values which were used in correcting the data from this preliminary experiment may be tabulated as follows:

	Exciting radiation		Fluorescence radiation
	FeK$_\alpha$	FeK$_{\beta 1}$	CrK
λ Å	1.9350	1.7530	2.285
$\mu/\rho(Fe)$ $\frac{cm^2}{gm}$	71.2	54	118
$\mu/\rho(Cr)$ $\frac{cm^2}{gm}$	500	366	93
Relative intensities (Williams) (54)	($\alpha_1 + \alpha_2$) 1.5	0.182	
x_i (Fe)	.9	.1	
Atomic no. A_j	58.8		52

$r_K(Cr) = 9$

$w_K(Fe) = 0.306$ (Castaing) (15)

$\sigma = 2080$ (Castaing)

$b = 2.48 \cdot 1,0^3$ (using value for Cu)

$\rho z_0 = 0.20 \cdot 10^{-3}$ (using value for Cu)

TABLE 5

The self-absorption correction curves which were obtained by Castaing and Descamps (see fig. 2, p. 32) were determined in Castaing's original version of the instrument in which the axis of the electron probe made an angle of 10 degrees with the normal to the specimen's surface, and the emerging x-rays made an angle of 16 degrees with the specimen's surface. Consequently, there is a small correction which must be made in applying these correction curves to data taken on the instrument described in this thesis. This factor can be included in computing the value of X in the following way:

$$X = \frac{\mu}{\rho} \frac{\cos\theta}{\sin\theta} \frac{\sin 10^{\circ}}{\cos\theta_3}$$

where θ is 15 degrees in our instrument and θ_3 depends on the spectrometer setting.

By simple geometrical considerations it may be shown that θ_3 is given by

$$\theta_3 = |\theta_o - \theta_B|$$

where θ_o is a constant depending on the location of the x-ray source relative to the axis of rotation of the spectrometer crystal, and θ_B is the Bragg angle corresponding to the x-ray line which is being measured. Since the value of θ_3 involves the difference of these angles, they may be measured on the angular scale of the spectrometer in spite of the fact that this scale has an arbitrary zero. The value of θ_o depends slightly on the spectrometer alignment and had a value of 13.25 degrees for this experiment. The iron line had a maximum intensity at 6.94,

and the chromium line had a maximum intensity at 10.11. In this case, the refinements to the geometry of the self-absorption correction have only small effects and will affect the accuracy of the correction to a lesser degree than one's ability to read points from the curves of fig. 2.

Both the self-absorption correction and the fluorescence correction involve a knowledge of the concentration of the specimen. Consequently, if the corrections are to be made directly on the intensities observed, it would be necessary to use successive approximations. This can be avoided by using the correction curve to determine the correction for a series of known concentrations. These corrections may be plotted as a function of either the intensity which would be observed,or the ratio of this intensity and the intensity from a target of pure iron. The latter choice of variable gives a better concept of the magnitude of the error which would result if the absorption correction were not made and if one assumed that the observed intensity were proportional to the concentration.

The plot of the corrections to be applied in the case of an alloy of iron and chromium is shown in fig. 22. In this graph, the mass concentration (C) divided by the observed intensity ratio (k') is plotted as a function of the observed intensity ratio. While it is clear that it would suffice to plot the concentration as a function of the observed intensity in the manner of a conventional calibration curve, the representation which was chosen gives a better picture of the magnitude of the correction itself and is capable of slightly greater accuracy in reading the graph.

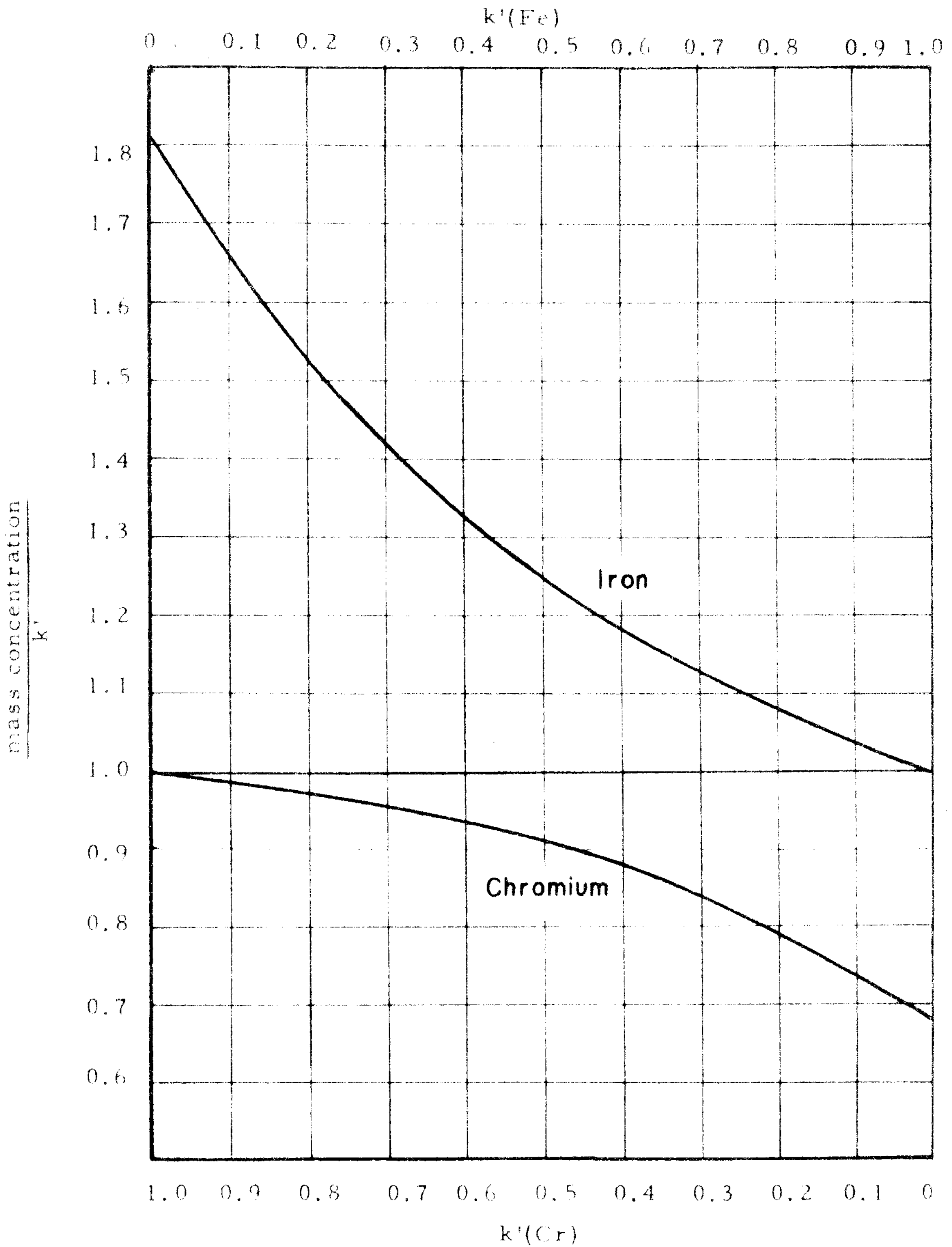

FIG. 22 Corrections for the iron-chromium system. The variable k' is the ratio of the measured intensity to the intensity from a pure target. Fe K_{α} is corrected for self-absorption and Cr K_{α} is corrected for fluorescence excitation.

The fluorescence correction was made by using the correction formula which was derived in this thesis (equation 4.38c, p. 62). It is clear from the magnitude of the quantities shown in Table 5 that the contribution of the Fe $K_{\beta 1}$ line is considerably less than the contribution from the Fe K_{α} doublet ($\approx 6\%$), and consequently the excitation can be assumed to be caused entirely by the K_{α} doublet. Furthermore, because the $K_{\alpha 1}$ and $K_{\alpha 2}$ are very close together, they may be treated as a single line. Castaing's approximation for the fluorescence correction for this case and for the same neglect of the Fe $K_{\beta 1}$ line gives values which are about 5% smaller, and this is to be expected from the representation of the function $\phi(\rho z)$ by an exponential.

The reduced data for this experiment are shown in fig. 23 in which the mass concentration of iron and of chromium are plotted as a function of distance from the edge of the specimen of chromized iron. The abrupt descrease in the concentration of chromium corresponds to the concentration of chromium for which the α solid solution of chromium in bcc iron cannot exist in equilibrium at the temperature at which the process was done. Beyond this point, any chromium which exits must be the γ solid solution in fcc iron. One must conclude that the diffusion rate of chromium in the γ phase is much less than the diffusion rate in the α phase at this temperature.

It is interesting to note that the position of the discontinuity in chromium concentration is visible (at arrow B) at the photomicrograph. The surface of the specimen was subjected to mechanical polishing with 1 micron "diamet" and was not subsequently etched.

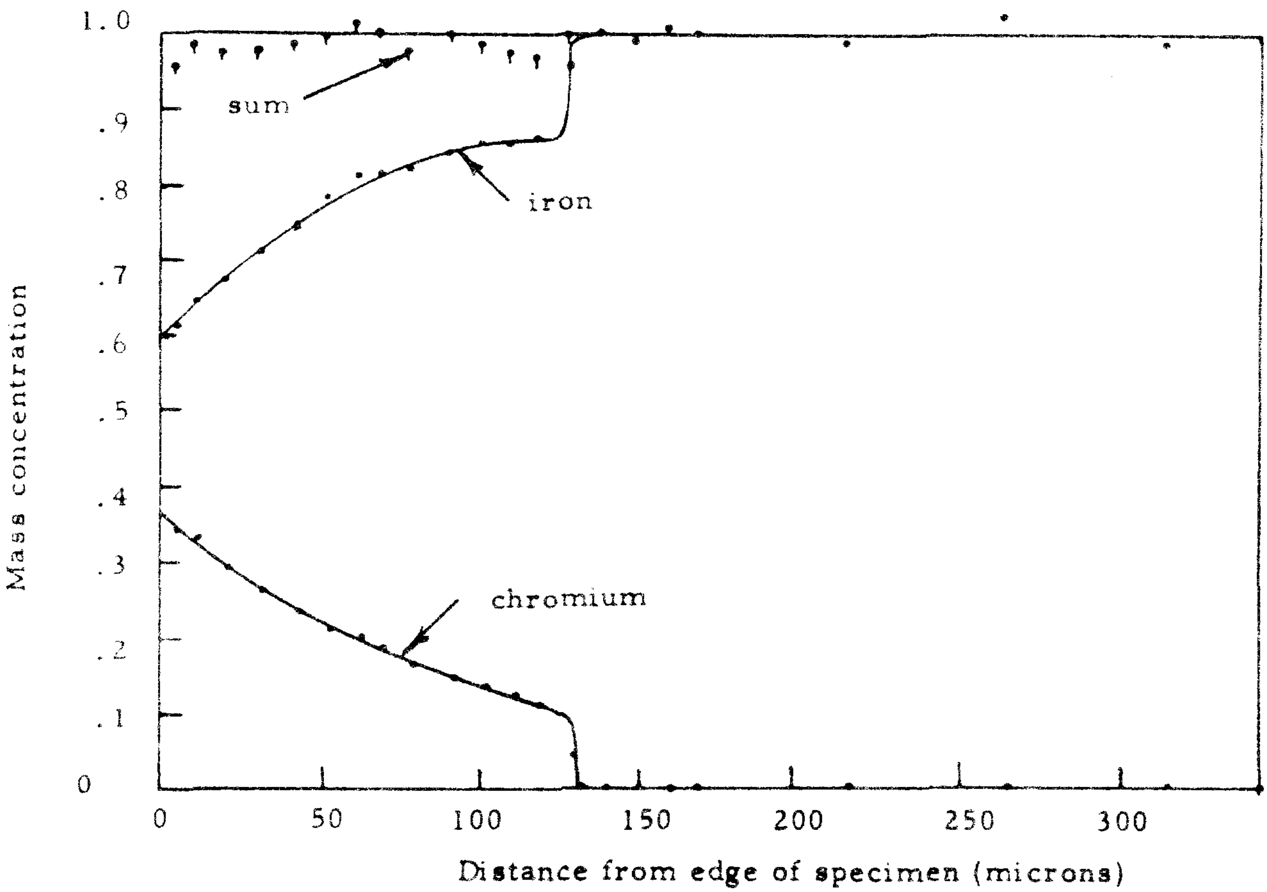

FIG. 23 Local concentration of the chromized iron specimen.

The experiment shows that the concentration of chromium at the edge of the specimen is about 37% ± 2%. The sum of the concentrations of iron and chromium deviates from unity by .04 at most and is, in general, somewhat less than this. This should not be interpreted as being typical of the accuracy possible in the method of analysis, because this case is one for which the corrections are particularly large and the corrections were made without an attempt to obtain maximum accuracy. In addition, there is a large uncertainty in the dead-time correction because of the high intensity of the electron beam. The statistical errors are virtually negligible in comparison to these other errors, being less than 0.7% (probable error) for all concentrations greater than 0.1.

Appendix

A. An Experimental Field Emission Cathode

A useful field emission cathode assembly must satisfy the following design considerations:

(a) Provision must be made for allowing the electron focusing system to collect electrons from one of the directions of strong emission.

(b) A means must be present for indicating the adjustment necessary to obtain emission from the most favorable directions.

(c) It must be possible either (1) to degas the emitter thoroughly before use and to maintain a very high vacuum in the cathode region or (2) to heat the emitter continuously and apply the electric field in pulses.

(d) An aperture stop must be provided to limit the electron beam entering the focusing system.

(e) Adjustments must be provided for aligning the emitter and aperture stop so as to coincide with the axis of the focusing system.

(f) Replacement of the emitters must be possible.

(g) The emission current should be susceptible to adjustment independent of the accelerating voltage.

A cathode assembly which satisfies these requirements is shown in fig. (a) and fig. (b). The emitter itself is mounted on a hairpin tungsten filament which is supported by gimbals so that the tip of the emitter remains approximately fixed in space. Its angular orientation may be adjusted from outside the vacuum system by means of two concentric shafts to which lucite disks are attached. Rotation of the disk attached to the inner shaft causes a variation of the polar angle of the emitter with respect to the vertical, while rotation of the disk

attached to the outer shaft varies the azimuthal direction of the emitter. The field emission pattern is observed on a fluorescent screen on the aperture stop, and therefore the adjustment can be made to cause a direction of maximum emission to coincide with the hole in the aperture stop.

The motion of the shafts for adjusting the emitter axis is coupled to the emitter holder in a manner shown in fig. (a). The outer shaft is rigidly attached to a cover (not shown in this view), which is dome-shaped to prevent corona and which has a pin normally engaging the notch (1) in the ring (2). This ring therefore can rotate with the cover. Fixed to this ring are parallel horizontal bars (3) and (4) spaced from each other by a distance slightly greater than the diameter of the cathode holder (5). The edges of these bars facing each other have grooves which constrain a wire slider (6) having the form of a hexagonal loop, one end of which is attached to a spring (7) which is connected to the ring (2). The cathode holder (5) screws into the inner gimbal which is pivoted about the axis (8-9) (12-13) at right angles to the axis (8-9). The tip of the emitter is approximately fixed in space at the intersection of these two axes; a rotation of the ring (1) therefore gives an azimuthal rotation to the axis of the cathode holder and leaves one remaining degree of freedom which can be determined by fixing the cathode holder at some point along the bars (3) and (4).

This degree of freedom is determined by a slider (14) having a "U" cross section and straddling the bars. A knob (15) projects

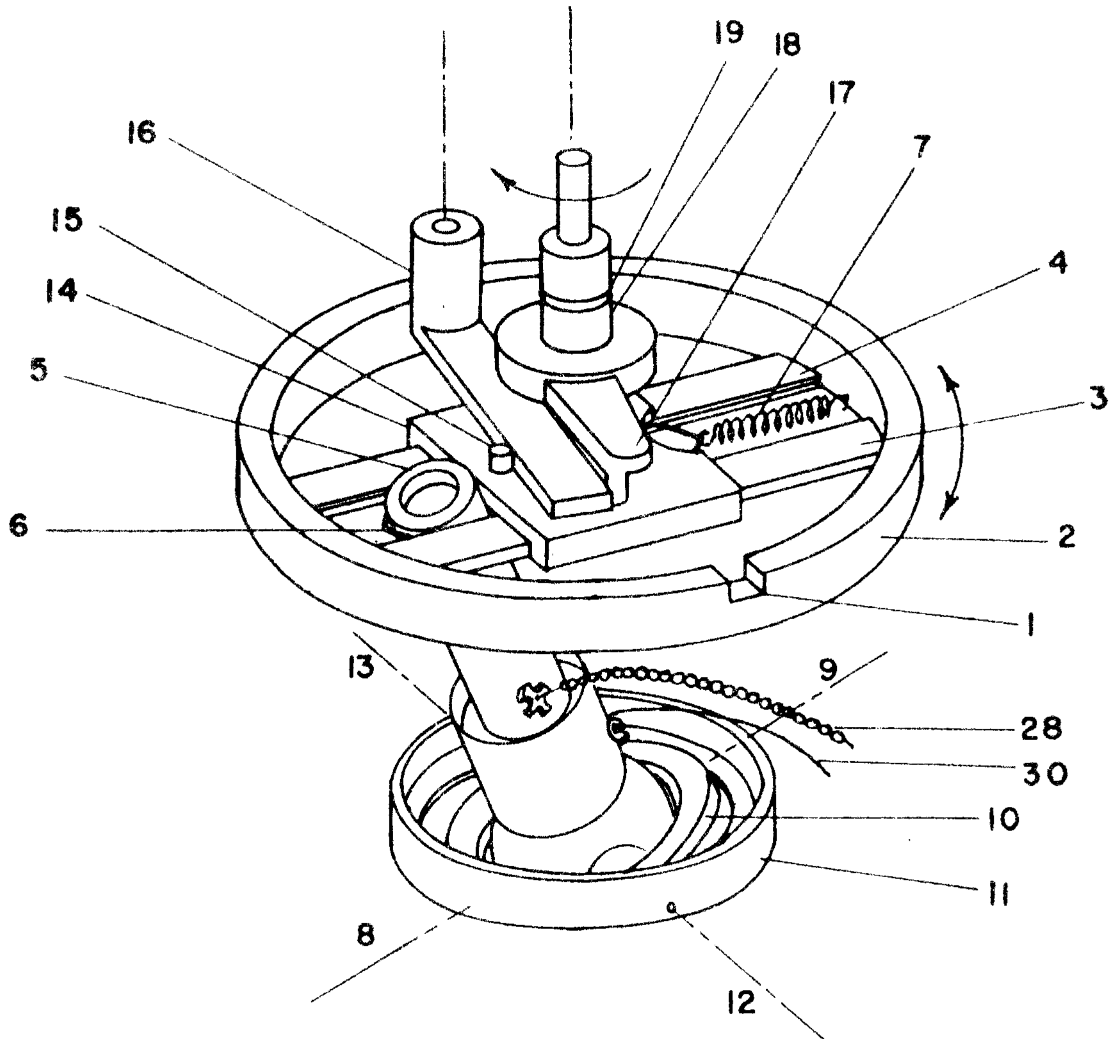

FIG. (a) Isometric view showing the holder for the field emission cathodes and means of adjustment.

above the slider so that it may be engaged by a lever (16) which is pivoted at one end about a vertical axis fixed in the cover. This lever can be rotated by pressure from a crank (17) on the shaft (18). Friction at the "O" ring seal (19) prevents any motion of the crank unless the shaft is rotated by manipulating one of the lucite disks. On the other hand, the spring (7) maintains the contact at all of the linkages. Thus, with the shaft (18) in some position in which the spring (7) is not extended, the cover of the cathode assembly can be removed for the purpose of replacing emitters.

A cross section of the complete cathode assembly is shown in fig. (b). The fixed ring (11) of the gimbal assembly is held by three screws in a stainless-steel tube (20) having holes for vacuum relief and mounted in a brass body (21). The body has a conical cavity to permit movement of the cathode holder, an "O" ring (22) for sealing to the glass insulator (23), and recesses for Stupekoff seals (24) and (25) which support an intermediate electrode (26). The electrode (26) will be called the emission control electrode, since, in the operation of the cathode assembly, it is pulsed with voltages which determine the quantity and duration of the field emission. The recesses containing the seals (24) are filled with Apiezon "W" wax which has excellent resistance and prevents the pulses applied to the emission control electrode from arcing across the short leakage paths of the seals. Another recess in the body at 90 degrees to the plane of the section contains a similar seal for connecting to one side of the tungsten hairpin (27) by means of a beaded flexible wire (28) and connecting

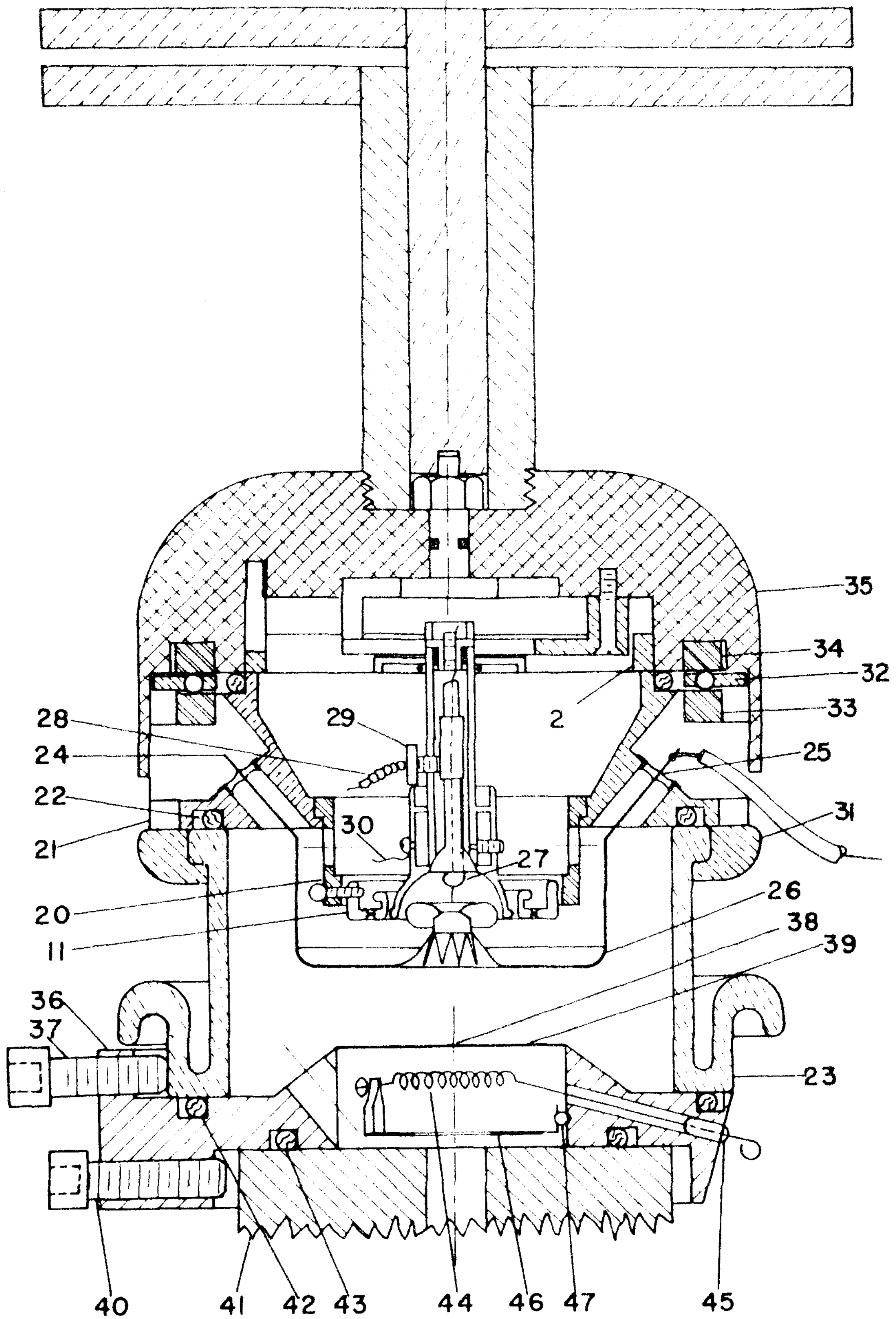

FIG. (b) Sectional view of the complete field emis on cathode assembly.

plug (29). The other side of the tungsten hairpin is grounded to the body by the flexible lead (30).

A split clamping ring (31) hold s the brass body to the glass insulator with four screws which are accessible when the ball bearing retainer (32) and lower ball bearing race (33) are removed. The function of the ball bearings is to reduce friction on rotation of the cover (35) relative to the rest of the assembly, and also to determine the compression of the "O" ring which maintains the vacuum seal during this rotation. The upper ball bearing race (34) is press-fitted into a g roove in the aluminum cover.

The aperture plate (36) has three push screws, of which (37) is one, for translating the glass insulator relative to the aperture hole (38) in the molybdenum aperture plate (39). Three other screws, of which (40) represents one, translate the aperture relative to the electron lens (41). During these adjustments the vacuum seal is maintained by the "O" ring seals (42) and (43). A fluorescent screen is mounted on the aperture plate (38) which requires degassing. Because of the close proximity of "O" rings, degassing by heat must be rapid so that a high temperature can be attained on the aperture plate in a short time without raising the temperature of the "O" rings excessively by thermal conduction.

This is accomplished by electron bombardment from a filament (44) which is supported below the aperture stop by three Stupekoff seals of which (45) is one. A stainless steel shield (46) which is clamped to one of the lead-in wires and supported at two other points

by glass beads, e. g. (47), reduces the emission current on the top of the electron lens. A small power transformer with windings of 5 v and 6.3 v connected in series across the filament and a 600 v winding connected between the filament and the aperture plate (35) furnishes from 20 to 60 watts of emission current for short periods of time, most of which is collected by the aperture plate.

The cathode assembly described satisfies all the design requirements and, in addition, has a compact physical size and smooth exterior which are very desirable for a component which is to be operated at a potential of -30 kv. The use of "O" rings placed a serious restriction on the lowest pressures which could be attained in the cathode assembly (about 5×10^{-6} mm of Hg). The dual requirements of adjustability and replaceability of the emitter were most easily satisfied by the use of "O" rings, however, and therefore the chance was taken that they might not impair the performance of the emitter when operated under pulsed T-F conditions (see page 90).

The emission control electrode can be expected to have a lens effect on the emission current. This was observed in the form of a reduction in area of the field emission pattern as viewed on the fluorescent screen, the reduction being greater the higher the voltage of the pulses applied to the emission control electrode. This effect is not disadvantageous except for the possible spherical aberration which is introduced as a result of this lens effect.

Pulses were applied to the emission control electrode from a pulse generator which is shown schematically in fig. (c). In this circuit a signal from a variable-frequency, free-running multivibrator,

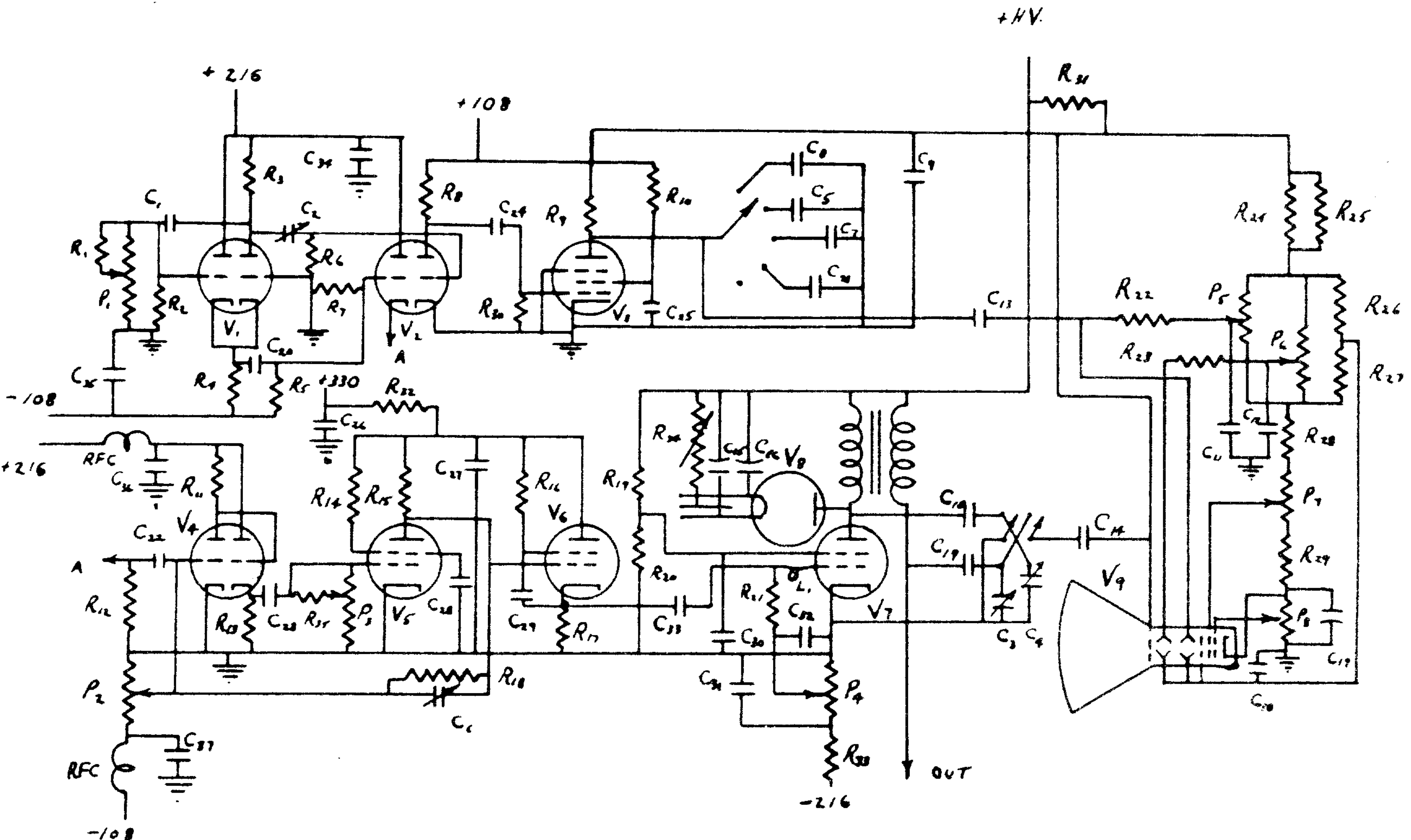

FIG. (c) Circuit diagram of the pulse generator.

Key to FIG. c

Components for pulser

V1, 2, 4--6SN7
V3--6AC7
V5, 6--6L6
V7--3D21
V8--5U4--GB
V9--3JP7

R1--10K
R2--240K
R3, 4--6.8K, 2 w
R5--100K
R6--47K
R7--33K
R8--10K, 2 w
R9--4.4M, 4 w
R10--15K
R11--10K, 2 w
R12--1K
R13--15K, 10 w
R14, 16--10K, 10 w
R15, 17--5K, 25 w
R18--330K
R19--150K, 30 w
R20--80K, 20 w
R21--15K, 2 w
R22, 23--4.7M
R24, 25--3.3M
R26, 27--560K
R28--1M
R29--50K
R30--1.33M
R31--100K
R32--100 ohms
R33--5K
R34--1000 ohms, 25 w
R35--6.8K, 2 w

C1, 5--500 μμFd
C2, 3, 4--4-30 μμFd
C6--5-40 μμFd
C7--150 μμFd
C8--0.001 μFd
C9, 10, 11, 12, 13, 14--0.005 μFd 6 Kv
C15, 16--0.1 μFd, 1 Kv
C17--2-1/8" RG11U coax
C18--6" RG8U coax
C19--0.25 μFd, 200 v
C20, 21, 23--47 μμFd
C22--330 μμFd
C24-37--0.1 μFd, 600 v

P1--2M, "Rep. Rate"
P2--250K (2 w), "Sync."
P3--250K, "Length"
P4--50K, Screwdriver adj.
P5--5M, "Hor. cent."
P6--5M, "Vert. cent."
P7--600K, "Focus"
P8--100K, "Intensity"

L1--0.03 microhenrys with 100 ohms 1 w carbon in parallel

V1, is amplified by one section of V2 and triggers a univibrator, V4, whose unstable state can be adjusted to control the pulse length. The resulting pulse is amplified by V5 and fed to a cathode follower, V6, which drives the grid of the switch tube, V7. A pulse transformer, which has its primary in the plate circuit of the switch tube, inverts the pulse and gives a voltage gain of about 3. A damper diode, V8, shunts the primary of the pulse transformer and controls the back-swing of the pulse which results from the collapsing flux in the transformer.

In addition, the pulse circuit provides a monitoring oscilloscope whose horizontal sweep is furnished by V3 which is triggered by a signal from the free-running multivibrator after it has been amplified by the second section of V2. By triggering the sweep out of phase with the trigger fed to the univibrator, it is possible to have the entire pulse on the scope for a wide range of pulse lengths and repetition rates. The parameters have been chosen to produce pulses at repetition rates varying from 2 1/2 to 40 kc/sec and lengths from 1 to 20 microseconds. Rectangular pulses and pulses of length less than 7 microseconds, however, can only be obtained if a load resistor is used in place of the primary of the pulse transformer, since the pulse transformer was not designed for short pulses. It is not possible to obtain good performance with pulse transformers over wide ranges of pulse lengths. For pulse lengths of about 10 microseconds and about 2 kv on the plate of the switch tube it was possible to secure pulses of roughly triangular shape and a height of 6 kv.

Using the coupling means shown in fig. (d), with C = 500 and R = 400 K ohms, about 90 to 95% of the pulse appears across R. Therefore, the emission control electrode, which is normally at cathode potential (-30 kv), goes positive with respect to the cathode during a pulse. If the pulse has overshoot, there is no adverse effect at the field emitter. However, because of the close spacing of the emission control electrode and aperture stop there is undesirable field emission from surface irregularities of this electrode, and there is also greater tendency of the switch tube of the pulser to spark. These effects require that the overshoot of the pulse be restricted by the damper diode, V8, in the pulser.

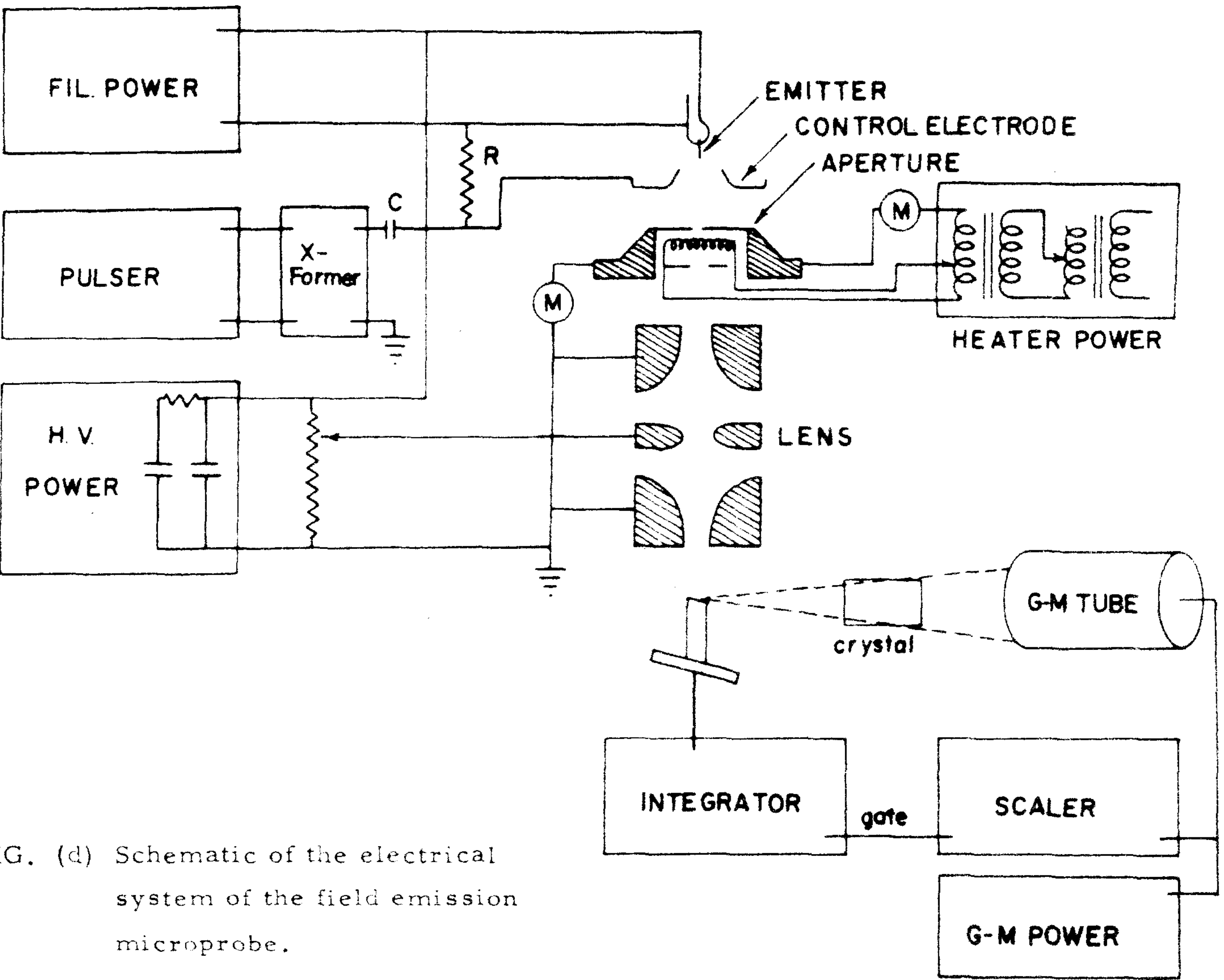

FIG. (d) Schematic of the electrical system of the field emission microprobe.

Appendix

B. Calculation of the Maximum Temperature Attained in the Target of the Microprobe with a Pulsed Electron Source

The differential equation for heat flow is

$$\frac{\partial u}{\partial t} = \frac{k}{c\delta} \nabla^2 u + \frac{p}{c\delta} \tag{9.1}$$

where

$u(t, \overline{r})$	is the temperature
t	is the time
k	is the thermal conductivity in cal/cm sec
c	is the specific heat in cal/gm degree
δ	is the density
$p(\overline{r})$	represents a heat source in cal/sec

In the case of a pulsed heat source, one cannot neglect $\frac{\partial u}{\partial t}$ Instead of solving the problem of a heat source which is uniform for $r < r_o$, zero everywhere else, and periodic in time, it is easier to solve the transient problem where there is no heat source for $t < -t_o$ and a uniform heat source which is on from $t = -t_o$ to $t = 0$ inside of a sphere of radius r_o. In this way, we can find the temperature after a heat pulse of any length, and if necessary, superpose solutions to find the effect of more than one such pulse occurring at a variable time later.

In spherical coordinates the homogeneous heat equation for spherical symmetry reduces to

$$\frac{\partial u}{\partial t} = \alpha^2 \left(\frac{\partial^2 u}{\partial r^2} + \frac{2}{r} \frac{\partial u}{\partial r} \right) \tag{9.2}$$

where

$$\alpha^2 = \frac{k}{c\delta} \tag{9.3}$$

This has the solution

$$u = \frac{A}{r\sqrt{t}} \exp\left(-\frac{r^2}{4\alpha^2 t}\right) \tag{9.4}$$

Another solution which does not blow up at the origin is

$$\frac{1}{r}\frac{\partial}{\partial r}(ru) = \frac{B}{t^{3/2}} \exp\left(-\frac{r^2}{4\alpha^2 t}\right) \tag{9.5}$$

And therefore, the general solution is

$$u = \frac{1}{(2\alpha\sqrt{t\pi})^3} \iiint \psi(\bar{r}') \exp - \frac{(\bar{r} - \bar{r}')^2}{4\alpha^2 t} \, d\tau' \tag{9.6}$$

In the case where the initial temperature $\psi(\bar{r}')$ depends only on the radius, one can write the element of volume, $d\tau'$, in spherical polar coordinates, $r'^2 dr' \sin\theta \, d\theta \, d\phi$, and by using the cosine law for $(r - r')^2$ the integration over ϕ and θ can be performed

$$u(r,t) = \frac{1}{2\alpha\sqrt{t\pi}} \int \phi(r') \left[e^{-\frac{(r-r')^2}{2\alpha\sqrt{t}}} - e^{-\frac{(r+r')^2}{2\alpha\sqrt{t}}} \right] r' \, dr' \tag{9.7}$$

where $\phi(r')$ denotes the initial temperature distribution. Now, let $\phi = 1$ for $r < r_o$ and zero elsewhere. Making the changes of variable,

$$x = \frac{r'-r}{2\alpha\sqrt{t}} \qquad \text{and} \qquad x' = \frac{r'+r}{2\alpha\sqrt{t}}$$

we have

$$u(r,t) = \frac{1}{\sqrt{\pi}\,r}\left[\int_0^{\frac{r_o-r}{2\alpha\sqrt{t}}} e^{-x^2}(r + 2\alpha\sqrt{t}\,x)dx - \int_0^{\frac{r+r_o}{2\alpha\sqrt{t}}} e^{-x'^2}(r + 2\alpha\sqrt{t}\,x')dx'\right]$$

$$= \frac{1}{2}\left\{\psi\left(\frac{r_o-r}{2\alpha\sqrt{t}}\right) + \psi\left(\frac{r_o+r}{2\alpha\sqrt{t}}\right)\right\} + \frac{\alpha\sqrt{t}}{\sqrt{\pi}\,r}\left\{e^{-\left(\frac{r_o+r}{2\alpha\sqrt{t}}\right)^2} - e^{-\left(\frac{r_o-r}{2\alpha\sqrt{t}}\right)^2}\right\} \tag{9.8}$$

where ψ is the error function:

$$(x) = \frac{2}{\sqrt{\pi}} \int_0^x e^{-\xi^2}\, d\xi$$

We are interested in the maximum temperature which is obviously attained at the origin so we desire the limit as $r \to 0$. The first term remains finite, and the behavior of the second can be obtained by expanding the exponential in a power series and retaining only the first two terms. Thus, the last term in (9.7) becomes

$$\frac{\alpha\sqrt{t}}{\sqrt{\pi}\, r}\left\{1 - \frac{r_o^2 + 2rr_o + r^2}{4\alpha^2 t} + \dots \quad -1 + \frac{r_o^2 - 2rr_o + r^2}{4\alpha^2 t} + \dots\right\}$$

which goes to the limit

$$\frac{-r_o}{\sqrt{\pi}\,\alpha\sqrt{t}} \qquad \text{as} \qquad r \rightarrow 0$$

Hence

$$u(r=0,t) = \psi\left(\frac{r_o}{2\alpha\sqrt{t}}\right) - \frac{r_o}{\alpha\sqrt{\pi}\, t} \tag{9.9}$$

This represents the temperature at time t after a heat pulse of infinitely short duration. If the initial temperature distribution corresponds to an energy, E, the result, given by equation (9.8) can be expressed in terms of this energy by multiplying by $E/Jc\delta V$, where J is the mechanical equivalent of heat in cal/erg, V is the volume which is initially at temperature $u = 0$, and c and δ are as defined earlier. To get the effect of a pulse of finite time, let $t = t + \xi$ (this represents a delta function heat source at $t = -\xi$) and replace E by $2p\, d\xi$ where p represents the power in the beam (the factor of 2 comes from the fact that the beam power goes into a hemisphere of radius r_o in the physical problem). Thus,

$$u(r=0,t) = \frac{2p}{c\delta VJ}\int_{t_o}^{0}\left[\frac{2}{\sqrt{\pi}}\int_0^{r_o/[2\alpha\sqrt{t-\xi}]} e^{-x^2}\,dx - \frac{r_o}{\alpha\sqrt{\pi}\,(t-\xi)}\right] d\xi \tag{9.10}$$

The integral can be simplified by a change in variable. Let

$$y = \frac{r_o^2}{4\,\alpha^2(t-\xi)}$$

Then

$$u = \frac{2p}{c\delta VJ}\int_{r_o/(4\alpha^2 t)}^{r_o^2/[4\alpha^2(t+t_o)]}\int_0^{\sqrt{y}}\left[\frac{2}{\sqrt{\pi}}e^{-x^2}dx - \frac{2\sqrt{y}}{\sqrt{\pi}}\right]\frac{r_o^2}{4\alpha^2 y^2}\,dy$$

Or, substituting for V and for α^2,

$$u = \frac{3p}{8Jr_o k\pi}\int_{r_o^2/[4\alpha^2(t+t_o)]}^{r_o^2/(4\alpha^2 t)}\left(\frac{2}{\sqrt{\pi}}\frac{\sqrt{y}}{y^2} - \frac{1}{y^2}\operatorname{erf}\sqrt{y}\right)dy$$

(9.11)

Now, this should reduce to the steady state case for t_o very large and t = 0 ; therefore, for this case,

$$u = \frac{3}{8}\,\frac{p}{r_o k\pi}\int_0^{\infty}\frac{2}{\sqrt{\pi}}\frac{\sqrt{y}}{y^2} - \frac{1}{y^2}\operatorname{erf}\sqrt{y}\,)\,dy \qquad (9.12)$$

It can be verified by numerical integration that the above integral is constant and equal to 2. Hence, in the steady state:

$$u = \frac{3}{4} \frac{p}{J r_o k \pi} \tag{9.13}$$

which is the same as the solution of the steady state problem (15).

Let us investigate the temperature after a pulse of 1 microsecond. For this case, $t = 0$, $t_o = 10^{-6}$, and the upper limit of the integral in (9.10) is infinity and the lower limit is

$$\frac{c\delta}{4k} \frac{r_o^2}{t_o}$$

Using the values for copper: $c \doteq 0.1$; $k \doteq 0.9$; $\delta = 8.9$ and a radius $r_o = 10^{-4}$ cm, we have

$$\frac{c\delta r_o^2}{4kt_o} = \frac{(0.1)(8.9)\, 10^{-8}}{(0.9)(4)\, 10^{-6}} \doteq \frac{10^{-2}}{4}$$

and using this value,

$$u = \frac{3}{4} \frac{p}{J r_o k \pi} \int_{1/4 \cdot 10^{-2}}^{\infty} \left(\frac{2}{\sqrt{\pi}} \frac{\sqrt{y}}{y^2} - \frac{1}{y^2} \operatorname{erf} \sqrt{y} \right) dy$$

or

$$u = \frac{3}{4} \frac{p}{J r_o k \pi} \left[2 - \int_0^{1/4 \cdot 10^{-2}} \left(\frac{2}{\sqrt{\pi}} \frac{\sqrt{y}}{y^2} - \frac{1}{y^2} \operatorname{erf} \sqrt{y} \right) dy \right] \tag{9.14}$$

We may expand $\operatorname{erf} \sqrt{y}$, since y is small:

$$\operatorname{erf} \sqrt{y} = \frac{2}{\sqrt{\pi}} \sqrt{y} \; 1 - \frac{y}{1!\, 3} + \frac{y^2}{2!\, 5} + \cdots$$

Retaining only the first two terms of the expansion, we get

$$u = \frac{3}{4\pi} \frac{p}{J r_o k} \left[2 - \int_0^{1/4 \cdot 10^{-2}} \left(\frac{2}{3\sqrt{\pi}\sqrt{y}} \right) dy \right.$$

$$= \frac{3}{4\pi} \frac{p}{J r_o k} \left[2 - \frac{4}{3} \frac{\sqrt{y}}{\sqrt{\pi}} \Bigg|_0^{1/4 \cdot 10^{-2}} \right]$$

$$= 2 - 0.037 \tag{9.15}$$

which differs by only 1.8% from the maximum temperature which would result from an infinitely long pulse. On the other hand, for a poor thermal conductor, e.g., for $k = 0.1$, the result is

$$u = \frac{3}{4\pi} \frac{p}{J r_o k} (2 - 0.119) \tag{9.16}$$

At first sight, the longer time to achieve maximum temperature for a substance of lower thermal conductivity seems unreasonable, but it must be remembered that the maximum temperature is higher since the steady state temperature is proportional to $1/k$.

In any case, it is apparent that at the center of the sample, the temperature becomes nearly equal to the maximum temperature in a very short period of time.

REFERENCES

(1) V. E. Cosslett and D. Jones, J. Sci. Instr. (1955), vol. 23, pp. 86-91.

(2) E. W. Mueller, Ergeb. Exak. Naturwiss. (1953), vol. 27, p. 290 ff.

(3) Zworykin et al, Electron Optics and the Electron Microscope, (Wiley, 1945), pp. 102-106.

(4) McMullen, Proc. Inst. Elect. Engrs. (1953), vol. 100, part II, pp. 245-259.

C. W. Oatley, Brit. J. Appl. Phys. (1955), vol. 6, p. 391.

(5) M. von Ardenne, Z. tech. Physik (1938), vol. 19, pp. 407-416.

Zworykin et al, loc. cit., pp. 100-102.

(6) V. E. Cosslett and P. Duncumb, Nature (1956), vol. 177, pp. 1172-1173.

(7) Private communication, 2 February, 1956.

(8) H. H. Pattee, Jr., Letter in J. Opt. Soc. Amer. (1953), vol. 43, pp. 61-62.

(9) V. E. Cosslett and W. C. Nixon, J. Appl. Phys. (1953), vol. 24, pp. 616-623.

V. E. Cosslett and H. E. Pearson, J. Sci. Instr. (1954), vol. 31, pp. 255-257.

(10) R. A. Schrack, R. C. Placious, and L. Marton, Bull. Amer. Phys. Soc. (1956), vol. 1, p. 167 (Abstract).

(11) Norton et al, A Representative Collection of X-Ray Micrographs (G. E. General Engineering Laboratory, 1954), Report No. R54GL259.

S. P. Newberry, J. Appl. Phys. (1954), vol. 25, p. 1454 (Abstract).

(12) B. M. Siegel and K. C. Knowlton, J. Appl. Phys. (1955), vol. 26, p. 1395 (Abstract).

(13) J. Hillier and R. F. Baker, J. Appl. Phys. (1944), vol. 15, p. 663.

J. Hillier, Phys. Rev. (1943), vol. 64, pp. 318-319.

(14) S. Rubin and V. K. Rasmussen, Phys. Rev. (1950), vol. 78, p. 83 (Abstract).

(15) R. Castaing, Ph.D. thesis, University of Paris (1952).

R. Castaing, La Recherche Aeronautique (1951), vol. 23, pp. 41-50.

(16) R. M. Fisher and J. C. Swartz, "Modification, an Electron Microscope for Micro-probe X-Ray Spectroscopy," paper presented at the fifth annual symposium on Industrial Applications of X-Ray Analysis sponsored by the Metallurgy Division of the Denver Research Institute, University of Denver, 9-10 August, 1956.

(17) L. S. Birks and E. J. Brooks, "An Inexpensive Electron Probe Instrument for X-Ray Spectroscopy," Ibid.

(18) R. Castaing and J. Descamps, J. de Phys. et le Radium, (1955), vol. 16, pp. 304-317.

(19) A. H. Compton and S. K. Allison, X-Rays in Theory and Experiment, (Van Nostrand, 1935), p. 76.

(20) P. M. Morse and H. Feshbach, Methods of Theoretical Physics II, (McGraw-Hill, 1953), p. 1592 ff.

(21) Ibid., p. 1632.

(22) P. B. Wagner, Phys. Rev. (1930), vol. 35, pp. 98-106.

(23) J. O. Brand, Ann. Physik (1936), vol. 26, pp. 609-624.

(24) P. Palluel, Comptes Rendus (1947), vol. 224, pp. 1492-1494 and pp. 1551-1553.

(25) B. F. J. Schonland, Proc. Roy. Soc. Lond. (1923), vol. 104 A, p. 235; (1925), vol. 108 A, p. 187.

(26) Private communication, 10 November, 1956.

(27) W. W. Hansen and K. B. Stoddard, Phys. Rev. (1933), vol. 43, pp. 701-706; (1935), vol. 48, p. 43.

K. B. Stoddard, Phys. Rev. (1935), vol. 48, pp. 43-46.

(28) J. Philibert and C. Crussard, J. Iron and Steel Inst. (1956), vol. 183, pp. 42-47.

(29) P. Lenard, Quantitatives über Kathodenstrahlen, (Heidelberg, 1918).

(30) Compton and Allison, loc. cit., p. 71.

(31) A. E. Ennos, Brit. J. Appl. Phys. (1953), vol. 4, pp. 101-106.

(32) R. Castaing and J. Descamps, Comptes Rendus (1954), vol. 238, pp. 1506-1508.

(33) A. E. Ennos, Brit. J. Appl. Phys. (1954), vol. 5, pp. 27-31.

(34) L. G. Parratt, C. F. Hempstead, and E. L. Jossem, Rev. Sci. Instr. (1952), vol. 23, pp. 1-7.

(35) W. Parrish and T. R. Kohler, Rev. Sci. Instr. (1956), vol. 27, pp. 795-808.

(36) J. Sharpe, Nuclear Radiation Detectors (Methuen & Co., London, 1955), p. 172.

(37) L. Marton, N.B.S. Circular 527 (1954), pp. 265-270 (Proceedings of the Symposium on Electron Physics, Washington, 1951).

(38) R. H. Fowler and L. Nordheim, Proc. Roy. Soc. Lond. (1928), vol. 119 A, pp. 173-181.

(39) W. P. Dyke, J. P. Barbour, J. K. Trolan, and E. E. Martin, Bull. Amer. Phys. Soc. (1954), vol. 29, p. 15 (Abstract).

(40) Frank and Mises, Differential Gleichungen der Physik, Vol. II, (Rosenberg, 1943), p. 542.

(41) Seitz, Modern Theory of Solids, (McGraw-Hill, 1940), p. 494.

(42) J. K. Trolan, J. P. Barbour, E. E. Martin, and W. P. Dyke, Phys. Rev. (1955), vol. 100, pp. 1646-1649.

(43) Private communication, December 1955.

(44) W. P. Dyke, J. K. Trolan, W. W. Dolan, and F. J. Grundhauser, J. Appl. Phys. (1954), vol. 25, pp. 106-112.

(45) D. B. Langmuir, Proc. I. R. E. (1937), vol. 25, pp. 977-991.

(46) Zworykin et al, Electron Optics and the Electron Microscope, (Wiley, 1945), p. 555.

(47) V. E. Cosslett and M. E. Haine, Proceedings of the International Conference on Electron Microscopy, London (1954), (Royal Microscopical Society, London, 1954), p. 639.

(48) D. B. Wittry, Rev. Sci. Instr. (1957), vol. 28, p. 58.

(49) G. Liebman and M. E. Grad, _Proc. Phys. Soc. Lond._ (1951). vol. B64, pp. 956-972.

G. Liebman, _Proc. Phys. Soc. Lond._ (1951), vol. B64, pp. 972-977.

(50) G. Liebman, _Proc. Phys. Soc. Lond._ (1952), vol. B65, pp. 448-458.

(51) T. Mulvey, _Proc. Phys. Soc. Lond._ (1953), vol. B66, pp. 441-447.

(52) Zworykin, et al, _loc. cit._, p. 754.

(53) E. Ingelstam, _Arkiv f. Math. Astr. och Fysik_ (1940-41), vol. 27B, paper no. 4.

(54) Compton and Allison, _loc. cit._, p. 640.